HIGH RESOLUTION MODELLING OF GLACIER FLOW

Alun Lloyd Hubbard

DOCTOR OF PHILOSOPHY
UNIVERSITY OF EDINBURGH
1996

DECLARATION

I hereby declare that this thesis has been composed by myself and the work within it is my own, except where otherwise referenced.

Alun Lloyd Hubbard

ABSTRACT

This thesis aims to develop and apply models of glacier flow at sufficiently high resolution to permit meaningful and accurate comparison with field data. At present there exists a discrepancy between the scales at which realistic simulations of glacier flow operate and the empirical data with which they are compared. This is true at a variety of spatial scales; from reconstructing the dynamics of past ice sheets constrained by geomorphological evidence to computing the stress/strain conditions acting alongside the processes of basal motion at the glacier bed. However, at finer scales of investigation, it becomes necessary to include more involved glaciological physics into models of glacier flow. This thesis is primarily concerned with one aspect of the quest for high resolution models; that is the inclusion of longitudinal stresses.

Three schemes for the solution of longitudinal stresses in glaciers are presented, tested against field data and their role on dynamics is investigated. The commonly utilised shallow ice approximation, which neglects longitudinal stresses, is also assessed within this framework in order to gauge if any significant improvement in predictive power has been made. In light of these experiments, the models are in turn, applied to three case studies in order to demonstrate the level of insight which high resolution modelling of glacier flow has the potential to provide. These case studies involve the detailed comparison of modelling results with empirical data to investigate: i) palaeoglacier and climate fluctuations in the Chilean Andes; ii) the dynamics and evolution of the Younger Dryas ice sheet in Scotland; and, iii) the three-dimensional stress/strain field of Haut Glacier d'Arolla.

Results indicate that longitudinal effects play a significant role in determining the dynamics of glaciers. Even though the solution of longitudinal stresses may require considerable computer overheads, their inclusion is crucial if we are to model glacier flow at high temporal and spatial resolutions with confidence. In doing so we equip ourselves with a powerful methodology for investigating a whole host of problems which exist in contemporary glaciology and ice sheet reconstruction.

ACKNOWLEDGEMENTS

I am indebted to my supervisor, David Sugden for his constant critical input, encouragement and inspiration without which this research would not have taken place, to Tony Payne for placing me soundly on the original track and to Heinz Blatter for more recent guidance through the numerical modelling jungle. I would also like to thank a number of people who I have known for long who have made substantial impact on my ideas, written work and to my enthusiasm for this subject: Bryn Hubbard, Peter Nienow, Andrew Kerr and Debbie Green. Others I wish to thank for more specific input include: Colin Ballantyne, Chalmers Clapperton and to the many at the Department of Geography who have been helped in the completion of this thesis, especially: Hermione Cockburn, Steve Dowers, Gavin Park and also Martin Siegert at the Institute of Earth Studies, Aberystwyth. On a similar note thanks also to Ann Peletier for her assistance in an hour (or two) of need during the final countdown. Thanks to all at Edinburgh who have made my time here so enjoyable and especially my family, chez Scots, various climbing mates, KB, IR, LW, MM, ML and CW for their support and companionship.

This work has been supported by the Natural Environment Research Council, and EISMINT for which I am grateful.

TABLE OF CONTENTS

Abstract page iii

Acknowledgements page iv

Chapter 1: page 1
INTRODUCTION

Chapter 2: page 6
THE DERIVATION, DESCRIPTION AND NUMERICAL SOLUTION OF THREE SCHEMES FOR THE COMPUTATION OF LONGITUDINAL DEVIATORIC STRESS GRADIENTS IN GLACIERS

Chapter 3: page 14
THE COMPARISON AND SIGNIFICANCE OF LONGITUDINAL STRESSES IN MODELLING GLACIER DYNAMICS OF HAUT GLACIER D'AROLLA

Chapter 4: page 27
MODELLING CLIMATE, TOPOGRAPHY AND PALAEO-GLACIER FLUCTUATIONS IN THE CHILEAN ANDES

Chapter 5: page 40
HIGH RESOLUTION MODELLING OF THE YOUNGER DRYAS ICE SHEET ADVANCE IN SCOTLAND

Chapter 6: page 61
COMPARISON OF A THREE-DIMENSIONAL MODEL FOR GLACIER FLOW WITH FIELD DATA FROM HAUT GLACIER D'AROLLA, SWITZERLAND

References page 77

Appendix A page 82

INTRODUCTION

MOTIVATION

This thesis is concerned with the modelling of glacier dynamics. The importance of studying glacier dynamics is threefold. First and foremost, is the key role which glaciers play in the global ocean-atmosphere system. Medium and long-term climate changes manifest themselves as variations in glacier mass balance, resulting in advance or retreat and the concomitant storage or release of waters into the world's oceans. Not only do glaciers represent a considerable amount of 'stored' global water, but also the release of this water may have considerable implications and knock-on effects for the operation of the North Atlantic Thermohaline Circulation system. This ocean current conveyor, the surface component of which is expressed as the Gulf Stream, supplies vast heat flux from low latitude, equatorial waters to higher latitudes of the North Atlantic. Recent evidence from the oxygen isotope record contained within deep sea ocean cores in conjunction with the GRIP/GISP analysis of Greenland ice cores strongly suggests that global climate has undergone large and rapid fluctuations in the recent past as a direct result of the switching of the North Atlantic Thermohaline Circulation system between different modes of operation. One mechanism by which this switching takes place is linked to the quantities and distribution of meltwater runoff from the land masses which surround the North Atlantic. Slight dilution of the saline current arriving in the North Atlantic appears to prevent the down-welling required to produce the counter-current in the deep Atlantic which returns waters to the equator. In light of these findings, study of the behaviour of ice sheets, for example at the last glacial/interglacial transition, is an important step in the understanding mechanisms of global climate change.

A second reason for studying glacier dynamics is that they provide good indicators of climate change. Because a glacier's mass balance is sensitive to small but persistent variations in temperature, precipitation and other meteorological quantities, their volume and length will tend to reflect medium and long term changes in these quantities. Thus, past glacier fluctuations, whether they be recorded in the geological/geomorphological record, from direct/indirect historical observation or even by direct measurement, can be used to identify regional climate trends over different time-scales. Thus, the rapid retreat of glaciers in the European and North American Alps over the last century, which may in itself have contributed significantly to sea-level rise, potentially provides a framework by which anthropogenic contribution to global warming may be assessed.

The third, and perhaps most interesting, motivation behind research into glacier dynamics is concerned with the elucidation of the complex processes which give rise to glacier flow. There are three components which contribute to the overall motion of a glacier; internal deformation of the ice, basal sliding and deformation of the underlying substrate. The latter two components describe 'basal motion', and represent the major unsolved problem in contemporary glaciology. Basal motion is often responsible for a significant proportion of the overall velocity of temperate glaciers and gives rise to large temporal and spatial variations in a glacier's flow regime. It is therefore a subject of vital importance in the dynamics of not just valley glaciers but also of ice sheets, where essentially similar processes are operating but on a considerably larger scale, giving rise to considerable temporal and spatial variations in flow of a much greater magnitude.

MODELLING

Numerical modelling of glacier dynamics has the potential to make substantial contributions in all three of these research areas. It provides a unique methodology capable of combining a variety of hypotheses involving both glacier and climate physics which, because of their complexity, have to be solved numerically. The predictions of the model can subsequently be tested against available empirical data, either adding to or subtracting from the credibility of the initial hypotheses used in its construction. In this way, one can model glacier dynamics at a variety of spatial and temporal scales depending on the focus of investigation. For

instance, the application of numerical ice sheet models in Quaternary studies enables predictions of variables such as ice extent and flow pattern over a glacier cycle to be made which subsequently can be compared with the glacial geomorphological record. At higher spatial and temporal scales, a combined glacier flow/climate model can be used to provide the complex process link between records of valley glacier fluctuations and the climate changes responsible. Finally, a modelling approach can provide insight into process studies of glacial dynamics. The latter approach may be illustrated more fully with reference to the search for a universal sliding law in contemporary glaciology.

Due to the dependency of basal motion on particular physical conditions at the glacier bed, namely the basal shear stress, the form/geometry of the bed and the local water pressure, the development of a generalised sliding law applicable to all ice masses is extremely difficult. A number of field based studies have been initiated world wide with the aim of investigating the processes of basal motion through detailed measurements of variations in surface velocity, down borehole inclinometry, basal water pressure fluctuations and other physical properties on which basal motion may depend. This thesis is mainly concerned with the solution of equations which govern the internal deformation component of glacier flow, and is significant since the processes of basal motion cannot be considered in isolation of the internal stress/strain pattern. The internal stress/strain distribution within an ice mass is constantly adjusting in response to temporal and spatial changes in basal motion. This adjusting pattern, in turn, determines the basal shear stress which drives basal motion. Thus, an understanding and solution of the internal stress/strain pattern within a glacier is an essential element in the isolation of the boundary conditions which frame these investigations into basal motion. This is particularly true since basal shear stress is a quantity which is extremely difficult, if not impossible, to measure empirically.

Accurate modelling requires an understanding of the mechanics governing glacier flow. For example, as outlined above, the processes of basal motion are not well understood. From a climate/glacier flow modelling perspective, sliding becomes a sub-grid process (for spatial resolutions currently practicable) which can only be broadly covered by an empirically based sliding law. This generalised sliding law is expected to give the contribution of all sub-grid processes to an average basal velocity as a function of some quantity calculated in the model, such as basal shear stress, and occasionally, effective pressure. The relevance of this to the modelling of medium and long term climate/glacier fluctuations is that it assumes that it is valid to spatially and temporally aggregate these sub-grid processes of basal motion through some empirically constrained law.

In contrast to the problem of generalising the indeterminate processes of basal motion, the mechanics operating within the body of a temperate glacier are fairly well understood. Ice mechanics are described by the Navier-Stokes equations based on Newton's laws of motion with acceleration terms neglected. Furthermore, laboratory experiments and field observations strongly suggest a constitutive relation that links strain rates to applied stresses in the form of what has come to be known as Glen's flow law. Although, the values of the two parameters in this law are only approximately known with no strong experimental basis, there appears to be general agreement over the form of this relation for anisotropic ice. Despite these relative certainties in the structure of a glacier's internal stress/strain field, theoretical studies of glacier flow are still relatively poor. This is because exact solutions of the Navier-Stokes equations are very difficult to obtain and involve either numerical techniques and/or the reduction of these equations by some sort of systematic approximation technique. A principal limitation arises from the non-linear rheology of ice. Put simply, for a given stress, the corresponding deformation rate not only depends on that particular stress, but on all other stresses. Previously, the simplifying assumptions used in the reduction of the field equations have been highly restrictive. For instance, the most commonly used approximation in contemporary glaciology derived by Nye (1957) is based on the driving stress concept, calculated on strictly local conditions of ice thickness

and surface gradient. The procedure by which this simplified solution is obtained involves the introduction of a small scaling parameter, the aspect ratio (defined as the ratio of thickness to length) into the field equations and the subsequent neglect of terms of order one and higher in the remainder of the analysis. The resulting shallow ice or zero-order approximation is derived for the idealised geometry of a parallel-sided slab in which the bottom and top surfaces deviate only slightly from straight lines. Such implicit assumptions are highly restrictive when applied to the complex boundary conditions which constrain glaciers. Despite this, many studies of valley glacier dynamics are based on this approximation with little or no regard to these strict assumptions which govern its application.

PROJECT SCOPE AND SUMMARY

The central aim of this thesis is to present a number of schemes for the solution of the above field equations governing the internal deformation of ice without invoking the restrictive, simplifying assumptions limiting their application to small, topographically constrained glaciers. This involves the computation of the first-order terms, that is longitudinal deviatoric stresses, and represents the next logical step in the systematic analysis of glacier deformation. Longitudinal stresses are the expression of the tensile and compressive forces acting within a glacier and are a direct result of large irregularities in the glacier bed and surface and/or large fluctuations in basal motion. They become increasingly important in glacier modelling at high resolution and are exhibited in nature in the glacio-tectonic features of crevassing and faulting and/or folding.

Computation of the first-order terms for realistic glacier geometries has only become a realisable research goal as a result of huge increases in computational power which have become readily available in recent years. Their computation represents a trade-off between the simplifying assumptions used in the solution of the field equations of ice motion and the practicality of the computation time taken in their numerical solution. In Chapter 2, the shallow ice approximation and three schemes for the computation of longitudinal stresses are presented; the full first-order approximation which is taken directly from Blatter (1995), a scheme adapted from van der Veen (1987) for the calculation of the stress/strain field at the grounding line of a calving ice-sheet, and a scheme which utilises the concept of ice surface stretching in order to provide a correction term for the driving stress equation. The rationale behind the presentation of three different schemes lies in the assumptions and simplifications used in their derivation. They represent a hierarchy, characterised by increasing numerical complexity and mathematical rigor; the first-order approximation representing the state of the art solution but requiring significant numerical and computational overheads at one end of the spectrum, with the shallow ice approximation which can be solved analytically lying at the other end.

Chapter 3 is concerned with the testing and sensitivity of the longitudinal stress schemes using a reference scenario constructed along the central flowline of Haut Glacier d'Arolla at 100 m resolution. These experiments provide a framework by which the three schemes and their effects on the modelled stress/strain field can be validated by comparison to field data and assessment made of any improvement. In the absence of actual measurements of the internal stress field of this glacier, the calculated surface velocities using the three schemes are compared with observed surface velocities from summer 1990. The calculated stress fields from the three schemes are similar and indicate that longitudinal stresses are of an equal order of magnitude to basal shear stress. These experiments reveal that the role of longitudinal stresses in glacier dynamics is significant with a substantial amount of longitudinal coupling taking place throughout the glacier. The results show a significant improvement over the shallow ice approximation in the prediction of the observed velocity field.

The remaining three Chapters are concerned with the application of these three longitudinal stress models to particular case studies; Chapters 4 and 5 investigate climate fluctuations and their relationship to past glacier dynamics, and Chapter 6 examines the three dimensional structure of the internal stress/strain field of a contemporary alpine glacier. Chapter 4 presents the

application of the modified van der Veen flowline model to two formerly glaciated valley basins in Southern Chile. By coupling this flow model to a net mass balance formulation through the continuity equation for mass conservation, the response and sensitivity of the two palaeo-glaciers to climate fluctuations is investigated and compared with geomorphological evidence. This study provides a number of insights into the dynamics of these palaeo-glaciers, the resulting depositional sequence and the nature of the climate forcing responsible.

Chapter 5 presents a quasi-three dimensional, high resolution model of an ice cap and its associated outlet glaciers. By coupling the ice surface stretching flow model to the continuity equation and a climate model the evolution of the Loch Lomond Stadial ice cap in Scotland is investigated at a grid resolution of 1 km. The high resolution of this modelling provides a framework by which the dynamics and sensitivity of the Loch Lomond Stadial ice cap can be studied. This enables detailed comparison of model results with empirical evidence from a variety of sources and through a process of primitive inverse modelling permits a number of climatic inferences about the nature of the Younger Dryas cooling event in Scotland to be made.

In Chapter 6, the full three dimensional, first order approximation of Blatter is applied to boundary conditions provided by Haut Glacier d'Arolla. Almost all previous models of glacier deformation have been carried out using one or two dimensional models in spite of the fact that the effect of the third dimension, through the influence of transverse stresses due to changes in the valley shape and direction and convergence of ice from tributary glaciers, may be large. Computation of the structure of the three dimensional internal stress/strain fields at 70 m horizontal resolution with 60 vertical levels gives extremely promising results. Modelled surface velocities display a high degree of fit when compared with observed winter velocities and computed eigenvectors giving the principal surface stresses predict the distribution and orientation of crevasses across the glacier as observed from aerial photography. The high level of accuracy in prediction obtained through the application of the first order approximation at this level of resolution to an alpine glacier offers huge scope for the further investigation of glacier process dynamics. Also, it has the potential to provide a framework by which the boundaries governing the processes of basal motion can be isolated for the first time.

CONCLUSIONS

In this thesis, three schemes for the computation of longitudinal stresses in ice masses are presented and offer significant improvements over the commonly utilised shallow ice approximation in the modelling of the internal stress/strain fields in glaciers. Application of the full stress schemes permits the modelling of glaciers at an accuracy and resolution that has been lacking in previous studies. In the past, this has largely been due to the lack of available computational resources for the numerical solution of the full stress/strain pattern. However, recent developments in numerical techniques and the constant advance of computer technology should mark the end of the application of the shallow ice approximation to scenarios where its restrictive assumptions place serious limitations on its predictive power. In contemporary glaciology there is an abundance of scenarios where this is the case and where application of models including longitudinal stresses have the potential to provide a considerably firmer basis on which to study glacier dynamics. This is true at all spatial and temporal scales; for instance from the modelling of the dynamics of Antarctic ice streams to the isolation of the basal stress patterns beneath a surging glacier.

THE DERIVATION, DESCRIPTION AND NUMERICAL SOLUTION OF THREE SCHEMES FOR THE COMPUTATION OF LONGITUDINAL DEVIATORIC STRESS GRADIENTS IN GLACIERS

ABSTRACT

A thorough understanding of the mechanics of ice flow is an essential element in the construction of models of glacier dynamics. Three approaches to the solution of longitudinal deviatoric stress gradients in glaciers are presented; the intention is to improve the representation of ice physics underpinning existing models of valley glacier flow dynamics based on the shallow ice approximation. The first, and most elaborate of these schemes is that of the first order approximation of the field equations governing ice motion in three-dimensions derived by Blatter (1995). The second is modified from a solution for the stress and velocity fields at the margins of calving ice sheets in plane-strain flow (van der Veen, 1987). The final scheme relates the longitudinal deviatoric stress to ice surface stretching, which has the advantage of having extremely low computational overheads in comparison with the other two schemes; it can be applied in two areal dimensions but involves the tenuous assumption of a negligible component of internal deformation in overall glacier motion. The three schemes offer a suite of approaches in which there is a trade-off between mathematical rigor and numerical complexity on the one hand and ease of application and computational overheads on the other.

INTRODUCTION

In the last decade a number of valley glacier flowline models have been based on the shallow ice approximation (Hutter, 1983). The glacier dynamics in these studies are based on the concept of a driving stress (τ_d) defined by:

$$\tau_d = -\rho g H \frac{\partial h}{\partial x} \qquad (1)$$

where is ρ the density of ice, g is acceleration of gravity, H is the ice thickness and $\frac{\partial h}{\partial x}$ is the surface gradient (Paterson, 1994). To satisfy the condition of force equilibrium, it is assumed that this stress is exactly balanced by the basal drag, that is the basal shear stress (τ_{xz}) across the bed of the glacier in the immediate vicinity. Thus, by assuming that the longitudinal deviatoric stresses are negligible compared to the driving stress the resulting components of glacier motion from internal deformation ($\dot{\varepsilon}_{xz}$) and basal sliding (u_b) can be subsequently calculated from Glen's flow law:

$$\dot{\varepsilon}_{xz} = \frac{\partial u}{\partial z} = 2A\tau_d^3 \qquad (2)$$

where A is the rate factor (also known as the flow parameter) and a generalised sliding law, respectively:

$$u_b = A_s H \tau_d^3 \qquad (3)$$

where A_s is the sliding parameter.

Paterson (1994) succinctly summarises the limitations of modelling glacier dynamics utilising this form of the field equations for ice motion based on the shallow ice approximation; although studies based on the standard equation 1 for the basal shear stress successfully predict the overall profile of an ice sheet or large glacier, it has been noted that they do not explain the details. Use of this equation implies that bed friction exactly balances the driving stress at every point along the glacier length. However, at high resolutions, as a result of bedrock bumps and hollows and spatial gradients in basal sliding, there are regions where the driving stress exceeds friction; such a region exerts a push down-glacier and pulls up-glacier ice. Similarly, regions where the friction is greater than the driving stress are pushed from up-glacier and pulled by down-glacier ice. The expression of the tensile and compressive forces due to longitudinal stresses result in important surface features such as crevassing and faulting and/or folding within a glacier (Nye, 1963). In such regions, the longitudinal stress component is significant and the equation 1 for the basal shear stress requires serious qualification.

These observations also raise the important question of the horizontal distance over which slope and ice thicknesses can be averaged in order to calculate the basal shear stress using the shallow ice approximation with confidence. When averaged over sufficiently large distances the irregularities in the bed profile and changes in the basal sliding rate which give rise to longitudinal stress gradients will eventually cancel each other out and render the term negligible, enabling a valid application of the driving stress concept through the shallow ice approximation.

The aim of this study is to present three schemes for the computation of longitudinal deviatoric stress

gradients in valley glaciers. Of these schemes, the first order approximation in three-dimensions has been fully derived and described by Blatter (1995) and only a synopsis of his derivation is presented here. The plane-strain scheme of van der Veen (1987) has been modified to account for three-dimensional transverse effects and significant improvements to its numerical solution have been made. The third scheme owed its origins to the physics of floating ice shelves and has been applied to grounded ice masses from scratch. These three schemes, as well as the approach based on the shallow ice approximation will be derived and described in detail along with brief details of their numerical solution.

FIELD EQUATIONS OF ICE MOTION

Assuming ice is an incompressible fluid, then its mechanical properties will depend on the physical properties such as temperature and stress. If the geometry of the glacier under analysis is defined by the upper surface S = S(x,y) and the bed B = B(x,y) in Cartesian coordinates (x,y,z) with the z-axis in the vertical plane, positive upwards, then the equation of mass continuity becomes:

$$\frac{\partial u}{\partial x}+\frac{\partial v}{\partial y}+\frac{\partial w}{\partial z}=0 \qquad (4)$$

where u, v, and w are the velocity components in the x, y, and z directions respectively. Assuming that glacier flow is sufficiently slow that the acceleration terms can be neglected, then the linear momentum equations reduce to:

$$\frac{\partial \tau_{xx}}{\partial x}+\frac{\partial \tau_{xy}}{\partial y}+\frac{\partial \tau_{xz}}{\partial z}=0 \qquad (5)$$

$$\frac{\partial \tau_{xy}}{\partial x}+\frac{\partial \tau_{yy}}{\partial y}+\frac{\partial \tau_{yz}}{\partial z}=0 \qquad (6)$$

$$\frac{\partial \tau_{xz}}{\partial x}+\frac{\partial \tau_{yz}}{\partial y}+\frac{\partial \tau_{zz}}{\partial z}=\rho g \qquad (7)$$

where ρ is the density of ice, g is gravity and τ_{ij} are the components of the Cauchy stress tensor.

Glen's flow law has commonly been used for a constitutive relation between stress and strain rates, although there are reasons to believe that it represents some, if not drastic, oversimplification of the rheological properties of ice. However, within the bounds of this study, glacier ice is assumed to behave as a non-Newtonian fluid (Paterson, 1994; Hutter, 1983) with a stress-strain relationship defined by Glen's flow law (Glen, 1958; Paterson, 1994):

$$\dot{\varepsilon}_{ij}=A\tau^{(n-1)}\tau_{ij} \qquad (8)$$

where $\dot{\varepsilon}_{ij}$ is the strain tensor, τ the effective stress (defined by the second invariant of the deviatoric stress tensor), **A** is the rate factor which is assumed to depend on temperature and n the flow law exponent which is most often set equal to 3 (Paterson, 1994; Hutter, 1983). Moisture content, ice fabric, ice composition, etc. affect the rheological properties of ice and since these properties may vary from one glacier to another the values of for **A** and **n** that are in some sense appropriate for one particular glacier may not necessarily be used with confidence for other glaciers.

Expanding equation 8 for the five components of stress yields:

$$\frac{\partial u}{\partial x}=A\tau^{(n-1)}\tau'_{xx} \qquad (9)$$

$$\frac{\partial v}{\partial y}=A\tau^{(n-1)}\tau'_{yy} \qquad (10)$$

$$\frac{1}{2}\left(\frac{\partial u}{\partial z}+\frac{\partial w}{\partial x}\right)=A\tau^{(n-1)}\tau'_{xz} \qquad (11)$$

$$\frac{1}{2}\left(\frac{\partial v}{\partial z}+\frac{\partial w}{\partial y}\right)=A\tau^{(n-1)}\tau'_{yz} \qquad (12)$$

$$\frac{1}{2}\left(\frac{\partial u}{\partial y}+\frac{\partial v}{\partial x}\right)=A\tau^{(n-1)}\tau'_{xy} \qquad (13)$$

where $\tau'_{ij}=\tau_{ij}-(\tau_{kk}\delta_{ij})/3$ is the deviatoric stress tensor and τ'_{xx} and τ'_{yy} are the normal deviatoric stress components.

Before proceeding, the boundary conditions at the the glacier surface need to be defined. For the upper free surface S=S(x,y), the boundary conditions for stress are:

$$n_x\tau_{xx} + n_y\tau_{xy} + n_z\tau_{xz} = -n_x P \quad (14)$$

$$n_x\tau_{xy} + n_y\tau_{yy} + n_z\tau_{yz} = -n_y P \quad (15)$$

$$n_x\tau_{xz} + n_y\tau_{yz} + n_z\tau_{zz} = -n_z P \quad (16)$$

where $n_x = -\frac{\partial S}{\partial x}$, $n_y = -\frac{\partial S}{\partial y}$ and $n_z = 1$ and are the components of the normal vector **n** pointing outward from the ice and **P** is the pressure of the outward side of the surface.

These equations or partial variations on them, known as the field equations of ice motion (Hutter, 1983), form the foundation on which many general analyses of ice motion are derived, for example, Hutter (1983), Huybrechts (1986), van der Veen and Whillans (1990) and Blatter (1995). One way of proceeding to derive a consistent simplified set of equations, is to estimate the order of magnitude of the various terms. Since the extent of a glacier is usually much larger than its thickness, the aspect ratio ε, defined as vertical extent {H} divided by horizontal extent {L} is introduced (Hutter, 1983; Blatter, 1995). In this way, the three spatial dimensions of the cartesian coordinate system represented by x, y, z and the glacier surface (S) and bed (B) domains can be scaled according to the method of Blatter (1995):

$$(x, y, z, S, B) = \{L\}(\tilde{x}, \tilde{y}, \varepsilon\tilde{z}, \varepsilon\tilde{S}, \varepsilon\tilde{B}),$$

along with the three dimensional velocity components:

$$(u, v, w) = A_0\{H\}(\{\rho g\{H\}\varepsilon)^n(\tilde{u}, \tilde{v}, \varepsilon\tilde{w}),$$

the stress components and the pressure **P**:

$$(\tau_{ij}, \tau'_{kk}, P) = \rho g\{H\}\varepsilon(\tilde{\tau}_{ij}, \tilde{\tau}'_{kk}, \tilde{P}),$$

and the rate factor:

$$A = A_0\tilde{A},$$

where A_0 is a typical rate factor, and the ~ subscript denotes the corresponding dimensionless scaled variables of order unity.

Substituting equations 9 and 10 into the continuity equation 4 and scaling this and the stress equations 5 - 7 and the constitutive equations 9 - 13 yields:

$$\varepsilon\frac{\partial\tilde{w}}{\partial\tilde{z}} = -\tilde{A}\tilde{\tau}^{(n-1)}(\tilde{\tau}'_{xx} + \tilde{\tau}'_{yy}), \quad (17)$$

$$\varepsilon\frac{\partial\tilde{\tau}_{xx}}{\partial\tilde{x}} + \varepsilon\frac{\partial\tilde{\tau}_{xy}}{\partial\tilde{y}} + \frac{\partial\tilde{\tau}_{xz}}{\partial\tilde{z}} = 0, \quad (18)$$

$$\varepsilon\frac{\partial\tilde{\tau}_{xy}}{\partial\tilde{x}} + \varepsilon\frac{\partial\tilde{\tau}_{yy}}{\partial\tilde{y}} + \frac{\partial\tilde{\tau}_{yz}}{\partial\tilde{z}} = 0, \quad (19)$$

$$\varepsilon^2\frac{\partial\tilde{\tau}_{xz}}{\partial\tilde{x}} + \varepsilon^2\frac{\partial\tilde{\tau}_{yz}}{\partial\tilde{y}} + \varepsilon\frac{\partial\tilde{\tau}_{zz}}{\partial\tilde{z}} = 1, \quad (20)$$

$$\varepsilon\frac{\partial\tilde{u}}{\partial\tilde{x}} = \tilde{A}\tilde{\tau}^{(n-1)}\tilde{\tau}'_{xx} \quad (21)$$

$$\varepsilon\frac{\partial\tilde{v}}{\partial\tilde{y}} = \tilde{A}\tilde{\tau}^{(n-1)}\tilde{\tau}'_{yy} \quad (22)$$

$$\frac{\partial\tilde{u}}{\partial\tilde{z}} + \varepsilon^2\frac{\partial\tilde{w}}{\partial\tilde{x}} = 2\tilde{A}\tilde{\tau}^{(n-1)}\tilde{\tau}'_{xz}, \quad (23)$$

$$\frac{\partial\tilde{v}}{\partial\tilde{z}} + \varepsilon^2\frac{\partial\tilde{w}}{\partial\tilde{y}} = 2\tilde{A}\tilde{\tau}^{(n-1)}\tilde{\tau}'_{yz}, \quad (24)$$

$$\varepsilon\left(\frac{\partial\tilde{u}}{\partial\tilde{y}} + \frac{\partial\tilde{v}}{\partial\tilde{x}}\right) = 2\tilde{A}\tilde{\tau}^{(n-1)}\tilde{\tau}'_{xy}. \quad (25)$$

and the surface boundary conditions for stress in scaled form become:

$$-\varepsilon\frac{\partial\tilde{S}}{\partial\tilde{x}}\tilde{\tau}_{xx} - \varepsilon\frac{\partial\tilde{S}}{\partial\tilde{y}}\tilde{\tau}_{xy} + \tilde{\tau}_{xz} = \varepsilon\frac{\partial\tilde{S}}{\partial\tilde{x}}\tilde{P}_{air} \quad (26)$$

$$-\varepsilon\frac{\partial\tilde{S}}{\partial\tilde{x}}\tilde{\tau}_{xy} - \varepsilon\frac{\partial\tilde{S}}{\partial\tilde{y}}\tilde{\tau}_{yy} + \tilde{\tau}_{yz} = \varepsilon\frac{\partial\tilde{S}}{\partial\tilde{y}}\tilde{P}_{air} \quad (27)$$

$$-\varepsilon\frac{\partial\tilde{S}}{\partial\tilde{x}}\tilde{\tau}_{xz} - \varepsilon\frac{\partial\tilde{S}}{\partial\tilde{y}}\tilde{\tau}_{yz} + \tilde{\tau}_{zz} = -\tilde{P}_{air} \quad (28)$$

Since the aspect ratio (ε = {H}/{L} << 1) in all but exceptionally steep glaciers is significantly smaller than unity, then it is possible to neglect terms in the above scaled field equations of order $O(\varepsilon)$or $O(\varepsilon^2)$ depending on the discernment of the analysis in question.

THE SHALLOW ICE APPROXIMATION

The shallow ice approximation, which is strictly the zero-order approximation, is defined by deleting all terms of order $O(\varepsilon)$ and higher and retaining terms only of unity. Deleting terms of order $O(\varepsilon)$ in equations 18 and 19, and integrating the truncated equations from the bed to the surface and recovering the unscaled version of the equations by substituting ε for the local surface gradient (assuming that the glacier bed is horizontal) yields the common from of the equation for driving stress (τ_d) without longitudinal stresses:

$$\tau_{xz} = -\rho g H \frac{\partial S}{\partial x} \tag{29}$$

$$\tau_{yz} = -\rho g H \frac{\partial S}{\partial y}. \tag{30}$$

Furthermore, the recovered constitutive relations yield:

$$\frac{\partial u}{\partial z} = 2A\tau^{(n-1)}\tau_{xz}, \tag{31}$$

$$\frac{\partial v}{\partial z} = 2A\tau^{(n-1)}\tau_{yz} \tag{32}$$

where the effective stress is given by:

$$\tau^2 = (\tau_{xz}^2 + \tau_{yz}^2). \tag{33}$$

In two-dimensional, plane strain the origins of equation II based on the driving stress concept become immediately evident where $\tau_{yz} = 0$ in equation 33 and the result is substituted into equation 31:

$$\frac{\partial u}{\partial z} = 2A\tau_{xz}^n \tag{34}.$$

The resulting reduced equations of ice motion are straight forward to apply to any ice mass or glacier with defined bed and surface geometry and require no numerical solution but a careful regard to the assumptions used in their derivation.

THE FIRST ORDER APPROXIMATION

The First Order Approximation of Blatter (1995) represents the most elaborate finite-difference solution to the field equations of ice motion to date. The first order approximation is defined by deleting terms of order $O(\varepsilon^2)$ but retaining terms of unity and order $O(\varepsilon)$ in the above scaled field equations. It can be applied in three-dimensions or to problems of planar flow in two-dimensions. Furthermore, it is flexible and can be applied to any boundary conditions provided by a grounded ice mass. The algorithm is based on an original two-dimensional derivation developed by Muller (1991) and has been extended to three-dimensions and demonstrated on a simple synthetic ice-sheet geometry by Blatter (1995). The following synopsis of the scheme is adapted from Blatter (1995).

In order to eliminate the normal Cauchy stresses in equations 18 - 20, the term of order $O(\varepsilon^2)$ in equation 20 is deleted and the truncated equation is integrated from $\tilde{z}$ to the surface $\tilde{S}$ and the result is applied to equation 18 and 19. Further integration yields:

$$\tilde{\tau}_{zz} = \tilde{\tau}_{zz}(\tilde{S}) - \frac{1}{\varepsilon}(\tilde{S} - \tilde{z}) \tag{35}$$

Using equation 28 and the relation between Cauchy stresses and deviatoric stresses in the form:

$$\tilde{\tau}_{zz} = \tilde{\tau}_{xx} - \tilde{\tau}'_{yy} - 2\tilde{\tau}'_{xx} - \tilde{\tau}_{yy} - \tilde{\tau}'_{xx} - 2\tilde{\tau}'_{yy} \tag{36}$$

in equation 35 and deleting terms of order $O(\varepsilon^2)$ yields:

$$\tilde{\tau}_{xx} = \tilde{\tau}'_{yy} + 2\tilde{\tau}'_{xx} - \frac{1}{\varepsilon}(\tilde{S} - \tilde{z}) - \tilde{P}_{air} \tag{37}$$

$$\tilde{\tau}_{yy} = \tilde{\tau}'_{xx} + 2\tilde{\tau}'_{yy} - \frac{1}{\varepsilon}(\tilde{S} - \tilde{z}) - \tilde{P}_{air} \tag{38}$$

Differentiating these two equations and substituting the result into 18 and 19 respectively gives:

$$\varepsilon\left(2\frac{\partial \tilde{\tau}'_{xx}}{\partial \tilde{x}} + \frac{\partial \tilde{\tau}'_{yy}}{\partial \tilde{x}} + \frac{\partial \tilde{\tau}_{xy}}{\partial \tilde{y}}\right) + \frac{\partial \tilde{\tau}_{xz}}{\partial \tilde{z}} = \frac{\partial \tilde{S}}{\partial \tilde{x}} \tag{39}$$

$$\varepsilon\left(2\frac{\partial \tilde{\tau}'_{yy}}{\partial \tilde{y}} + \frac{\partial \tilde{\tau}'_{xx}}{\partial \tilde{y}} + \frac{\partial \tilde{\tau}_{xy}}{\partial \tilde{x}}\right) + \frac{\partial \tilde{\tau}_{yz}}{\partial \tilde{z}} = \frac{\partial \tilde{S}}{\partial \tilde{y}} \tag{40}$$

Similarly, eliminating $\tilde{\tau}_{xx}$, $\tilde{\tau}_{yy}$ and $\tilde{\tau}_{zz}$ in the boundary conditions in equations 26 - 28 and dropping terms of order $O(\varepsilon^2)$ gives the corresponding first order boundary conditions (Morland and Shoemaker, 1982; Morland, 1984):

$$\tilde{\tau}_{xz} - \varepsilon\frac{\partial \tilde{S}}{\partial \tilde{x}}(2\tilde{\tau}'_{xx} - \tilde{\tau}'_{yy}) + \varepsilon\frac{\partial \tilde{S}}{\partial \tilde{y}}\tilde{\tau}_{xz} = 0 \tag{41}$$

$$\tilde{\tau}_{yz} - \varepsilon \frac{\partial \tilde{S}}{\partial \tilde{y}} (2\tilde{\tau}'_{yy} - \tilde{\tau}'_{xx}) + \varepsilon \frac{\partial \tilde{S}}{\partial \tilde{x}} \tilde{\tau}_{xy} = 0 \qquad (42)$$

Finally, we have arrived at eight independent equations, 39, 40, 17, and 21 to 25 for the eight unknown field variables of the basal shear stress, longitudinal stress and the velocity vector. These reduced equations for ice motion represent a well posed problem; however their numerical solution is complex. The following summary of the numerical procedure is based on Blatter (1995).

Introducing a discrete, three-dimensional finite difference array and approximating the x and y derivatives by centred differences, the eight equations take the form of three algebraic and five ordinary differential equations. The full three-dimensional algorithm computes the stress/strain field throughout the glacier domain by first solving the three algebraic equations 23 to 25 across the glacier bed using an initial estimate of the basal shear stress based on the Shallow Ice Approximation (equations 29 and 30) and the prescribed basal velocity field. Using the Newton-Raphson method (Press et al., 1986) the algebraic equations are solved and the resulting stresses are used to calculate the stress/strain pattern at the next vertical level up through a second order Runge-Kutta integration (Press et al., 1986). This procedure, known as vertical shooting is repeated at all subsequent levels until the stress/strain field has been calculated at the top level, that is the glacier upper surface. This procedure is repeated forming the iteration cycle where subsequent basal stress values are amended so as to satisfy the upper surface boundary condition which supports zero (or negligible) shear traction. To this end, the following simple fixed point iteration scheme is used:

$$\hat{\tau}_b^{new} = \hat{\tau}_b^{old} - \beta \hat{\tau}_s^{old} \qquad (43)$$

where the subscripts **b** and **s** refer to the basal and surface shear tractions $\hat{\tau}$, respectively. Convergence of the iteration procedure is deemed to have been satisfied when the maximum absolute single value of the surface shear traction becomes sufficiently small (< 1.0×10^{-3} bars).

THE PLANE-STRAIN APPROXIMATION

The plane-strain scheme is based on van der Veen's (1987) derivation of longitudinal-stress gradients along a flowline of a calving ice sheet and is based on Glen's flow law and the equilibrium of forces. An approximation often used in glaciology is that of the plane flow, where all flow is supposed to take place in a vertical plane (Hindmarsh, 1993; Paterson, 1994). There are only two space dimensions considered, and the equations of linear momentum and conservation of mass can be rewritten as:

$$\frac{\partial \tau_{xz}}{\partial z} + 2\frac{\partial \tau'_{xx}}{\partial x} + \frac{\partial^2 \int_z^s \tau_{xz} dz}{\partial x^2} = \rho g \frac{\partial S}{\partial x}. \qquad (44)$$

Integrating this equation from the surface S to the base B and replacing τ'_{xx} by its vertical mean $\overline{\tau'_{xx}}$ yields:

$$\tau_{xz} = -\rho g H \frac{\partial h}{\partial x} + 2\frac{\partial}{\partial x}(H\overline{\tau'_{xx}}) + T, \qquad (45)$$

which bears a strong resemblance to the shallow ice approximation of the basal shear stress but with two correction terms. The term T, referred to as 'bridging effects' is rather complex and represents the terms of order $O(\varepsilon^2)$ in the previous three-dimensional scaled analysis (i.e. a second order approximation). It is not considered in van der Veen's (1987) scheme. Although limited to the two-dimensional plane flow approximation, this analysis can potentially be applied to valley glaciers in quasi three-dimensions through the introduction of a shape factor (S_f) into the basal shear stress equation, which accounts for the effects of side wall support and transverse stresses due to changes in valley shape down flowline (Paterson, 1994).

Derivation of the longitudinal stress deviator follows directly the method described by van der Veen (1987). Essentially the two constitutive equations and the reduced force balance equations are taken in the following form:

$$\frac{\partial u}{\partial x} = A_d \left[\tau'^2_{xx} + \tau^2_{xz}\right] \tau'_{xx} \qquad (46)$$

$$\frac{\partial u}{\partial z} = 2A_d \left[\tau'^2_{xx} + \tau^2_{xz}\right] \tau_{xz} \qquad (47)$$

$$\tau_{xz} = -\rho g H \frac{\partial h}{\partial x} + 2\frac{\partial}{\partial x}(H\overline{\tau'_{xx}}) \qquad (48)$$

Equation (48) is substituted into equations (46) and (47) and after a number of integrations and substitutions yield two equations containing two unknowns, **u** and $\overline{\tau'_{xx}}$ (Appendix A). By eliminating **u** the following expression for $\overline{\tau'_{xx}}$ is derived:

$$\overline{\tau'_{xx}}^{3}\left\{2\frac{\partial h}{\partial x}\left(\frac{\partial H}{\partial x}-\frac{\partial h}{\partial x}\right)+H\frac{\partial^2 h}{\partial x^2}+\frac{1}{2}\right\}+$$

$$+\ \overline{\tau'_{xx}}^{2}\left\{\tau_1\left(\frac{2}{3}\frac{\partial H}{\partial x}-\frac{3}{2}\frac{\partial h}{\partial x}\right)+\frac{1}{6}D_1+\frac{3}{2}D\frac{\partial h}{\partial x}\right\}+$$

$$+\ \overline{\tau'_{xx}}\left\{\tau_1^{\,2}\left[3\frac{\partial h}{\partial x}\frac{\partial H}{\partial x}+\frac{3}{2}H\frac{\partial^2 h}{\partial x^2}-2\left(\frac{\partial h}{\partial x}\right)^2-\frac{1}{6}\right]+\right.$$

$$\left.+\tau_1\left(\frac{1}{3}D+\frac{3}{2}D_1\frac{\partial h}{\partial x}\right)\right\}+\tau_1^{\,3}\left\{\frac{2}{5}\frac{\partial H}{\partial x}-\frac{1}{4}\frac{\partial h}{\partial x}\right\}+$$

$$+\ \tau_1^{\,2}\left\{\frac{3}{4}D\frac{\partial h}{\partial x}+\frac{3}{10}D_1\right\}+\frac{1}{2A}\frac{\partial u_s}{\partial x}=0 \qquad (49)$$

where $\tau_1 = \tau_d + D$, $D = 2H\frac{\partial}{\partial x}\left(\overline{t'_{xx}}\right)$, $D_1 = 2H\frac{\partial \tau_1}{\partial x}$ and $\tau_d = -\rho g H\frac{\partial h}{\partial x}$ and u_s is the prescribed basal sliding.

Equation 49 can be solved numerically using a Newton-Raphson root-finding iteration (*Press et al.*, 1986). Significant improvements to this numerical method have been investigated in this thesis since the Newton-Raphson method proposed by van der Veen (1987) often ran into stability and convergence problems when dealing with the steeper gradients of valley glacier profiles. Solving the discretised partial derivatives on a tridiagonal matrix results in an algorithm that reduces the convergence time of the original Newton-Raphson iteration by a factor of between 10 and 150 times, dependent on the operating resolution and glacier profile being analysed.

The solution and subsequent modification of the shear stress (τ_{xz}) through equation 49 can be used to compute the surface deformation velocity. A necessary assumption implicit in the plane-strain flowline approach is that the transverse, cross valley deviatoric stress ($\overline{\tau'_{yy}}$) does not significantly influence the stress field. Strictly speaking, this assumption is not consistent with this particular application to valley glacier analysis. However, as alluded to above, by introducing the shape factor (S_f) into equation 48:

$$\tau_{xz} = -S_f\rho g H\frac{\partial h}{\partial x}+2\frac{\partial}{\partial x}(H\overline{\tau'_{xx}}), \qquad (50)$$

transverse stress as well as the support of the glacier on the valley walls can be accounted for (Nye, 1965; Paterson, 1994). Typically values of S_f vary from between 0.45 for a parabolic straight valley cross-section with a width double the local ice thickness, to 0.65 for the same shape with a width four times the local ice thickness; a value of unity describes an infinitely wide valley, which represents the idealised shape to which the plane-strain approximation applies (Nye, 1965).

ICE SURFACE STRETCHING

The third scheme relates ice surface stretching (the Jacobian component of surface velocity (U_s)) to the longitudinal stress deviator ($\overline{\tau'}$) based on an initial assumption of negligible internal deformation compared to basal sliding ($\varepsilon_{xz} \to 0, \therefore \tau_{xz} \to 0$). If a further assumption of plane-strain flow is made then the effective stress (τ) in equation 9 reduces to:

$$\tau^2 = \overline{\tau'_{xx}}^{2} \ . \qquad (51)$$

Under these assumptions it is possible to rearrange equation 9 in order to derive a value for vertically averaged longitudinal deviatoric stress from the rate of ice surface stretching:

$$\overline{\tau'} = \left(\frac{1}{A}\frac{\partial U_s}{\partial x}\right)^{\frac{1}{n}}. \qquad (52)$$

The resulting value for the longitudinal stress deviator ($\overline{\tau'}$) is then used to modify the driving stress (τ_d) based on the shallow ice approximation:

$$\tau_d = \rho g H\frac{\partial h}{\partial x}+2\frac{\partial(H\overline{\tau'})}{\partial x} \qquad (53)$$

where ρ is the density of ice, g is acceleration of gravity and **h** is the surface elevation. Equations 53 and 54 are finally closed through re-evaluation of the surface velocity using Glen's flow law:

$$U_s = \varepsilon_{xz} = 2A.(\tau')^{n-1}.\tau_d + U_b \qquad (54)$$

where τ' is the effective stress calculated from the second invariant of the stress tensor and U_b is the basal sliding component from equation 3:

$$u_b = A_s H\tau_d^3.$$

On computation of an initial estimate for longitudinal stress, the above three equations can be numerically relaxed using a straightforward iteration procedure.

When sufficiently relaxed, the scheme solves the vertically integrated stress/velocity field across the ice sheet for the given ice sheet geometry.

DISCUSSION AND CONCLUSIONS

Three schemes for the computation of longitudinal deviatoric stresses and their associated strain fields have been presented along with an analysis of the shallow ice approximation through which the driving stress is derived. Each scheme involves different initial assumptions and as a consequence displays varying degrees of sophistication and complexity. A summary of the defining characteristics of the schemes, based on their application at Haut Glacier d'Arolla, is shown in Table 1. Together they represent a hierarchy of approaches of increasing numerical complexity, sophistication and rigor. The first order approximation of Blatter (1995) is at the most elaborate and exhaustive end of the spectrum offering a solution of the full, three-dimensional stress/strain field but requiring considerable computational overheads in order to achieve this end. The scheme based on van der Veen's (1987) analysis for two-dimensional, plane-strain flow, has been adapted in this thesis to account for the quasi three-dimensional nature of valley glaciers through the shape factor (S_f). Furthermore, considerable numerical improvements to the computational efficiency of this scheme have been made possible by replacing the original Newton-Raphson root-finder with a partial derivative root finder solved on a tridiagonal matrix (Press et al. 1986). The resulting flow model computes longitudinal and basal shear stresses down the central flowline efficiently, making it an ideal choice for valley glacier/climate fluctuation type investigations, as illustrated, for example in Chapter 4. The final scheme calculates a correction term to the driving stress equation of the shallow ice approximation and involves the tenuous assumption of a negligible internal deformation component to overall glacier motion, but requires little computational effort over and above that of the shallow ice approximation. This scheme lacks the mathematical rigor of the other two solutions but has the potential to provide a fairly well specified correction term to plan-form, quasi three-dimensional ice flow models which are integrated forward in time through a continuity equation and where computation time is therefore at a premium.

Scheme	Assumptions	Dimensions	Numerical Complexity	Computation Speed*
First Order Approximation (Blatter, 1995)	Terms of order $O(\varepsilon^2)$ and higher are neglected. i.e. no bridging effects.	Three-dimensional solution of the stress/strain field	Solution involves Newton-Raphson Root Solving at the bed, Runge-Kutta upward shooting and surface to bed iteration.	Slow, ~10^2 seconds: requires the re-evaluation of all equations at all levels for each surface to bed iteration.
Plane-Strain Approximation (van der Veen, 1987)	No transverse flow. That τ'_{xx} can be replaced by its vertical mean $\overline{\tau}'_{xx}$.	Quasi three-dimensional in flowline models through introduction of S_f.	Solution requires root-finding through solution of partial derivatives on a tridiagonal matrix.	Moderately fast, ~10^1 seconds: involves iteration procedure over one level.
Ice Surface Stretching	Negligible internal deformation. τ'_{xx} can be replaced by its vertical mean $\overline{\tau}'_{xx}$.	Two-dimensions in plan, areal extent.	Solution involves single evaluation of terms and numerical relaxation.	Fast, ~10^0 seconds: no iteration procedure required.
Shallow Ice Approximation	Terms of order $O(\varepsilon)$ and higher are neglected. i.e. no longitudinal effects.	Three-dimensions.	Can be solved without recourse to numerical techniques.	Fast, -10^0 seconds: straight evaluation of equations.

Table 1: *Summary of the main characteristics of three schemes for the computation of longitudinal stresses and the shallow ice approximation. * Results based on the application to the long profile geometry of Haut Glacier d'Arolla at 100 m resolution on a Pentium 100 PC (Chapter 3).*

THE COMPARISON AND SIGNIFICANCE OF LONGITUDINAL STRESSES IN MODELLING GLACIER DYNAMICS OF HAUT GLACIER D'AROLLA

ABSTRACT

Three schemes for the computation of longitudinal stresses have been applied to the central flowline of Haut Glacier d'Arolla at 100 m resolution. Comparison of the modelled velocity patterns reveal a good fit with the observed velocities for the summer season, 1990. The computed stress fields show consistency, and, in the absence of actual stress measurements, give some indication that the three independent schemes are functioning correctly. Furthermore, experiments based on changing the prescribed basal motion boundary condition reveal that there is also significant longitudinal coupling taking place throughout the glacier. These characteristics are not modelled on application of the shallow ice approximation to identical boundary conditions, which results in erratic fluctuations in the computed stress and velocity fields down glacier which neither agree with the observed pattern nor are realistic from mass continuity considerations. A series of experiments suggest that the shallow ice approximation can only be applied when gradients are averaged over about 20 ice thicknesses, a conclusion in agreement with Paterson (1994). The implication is that longitudinal stresses play a significant role in determining the internal deformation component of glacier flow and, therefore must be included in models of glacier dynamics at high resolutions.

INTRODUCTION AND STUDY AREA

This study aims to test the three independent approaches for the computation of longitudinal deviatoric stress gradients in glaciers described in Chapter 2. In the absence of direct field measurements of these stresses, this is mainly achieved through the comparison of the computed stress fields with each other. In addition, the computed surface velocity field which is a direct expression of these computed stresses, is compared to the observed surface velocity pattern which is directly accessible by standard surveying techniques. Central to this study is the comparison of the modelled stress and velocity fields using these three schemes with those derived using the shallow ice approximation. This is to gauge whether there is any significant improvement in predicting the observed pattern of surface velocity as a result of including longitudinal stresses in the analysis.

The three schemes are applied in two-dimensions to the central flowline of Haut Glacier d'Arolla, a small, self-contained glacier situated in the western Pennine Alps, Valais, Switzerland (Fig. 1). This glacier has an area of 6.3 km^2, is about 4 km long and from 2600 m a.s.l. at the snout to 3100 m a.s.l. is characterised by low surface gradients (< 0.125). The glacier is bounded by high mountains, and the upper accumulation area contains a series of steep ice falls on the north face of Mont Brulé up to an elevation of over 3500 m a.s.l. Haut Glacier d'Arolla provides the ideal site on which to conduct this case study as it has been investigated thoroughly in the field and all the relevant glaciological data required are readily available. If particular, the glacier displays large temporal variations in surface velocity on both diurnal and seasonal timescales, which suggests that there is a large component of basal sliding in the overall pattern of glacier motion (Nienow, 1995). Furthermore, detailed surface elevation surveys which have been conducted at 5 m horizontal resolution (Willis et al., *in press*) and radio-echo sounding data (Sharp et al., 1993) indicate that the surface and bed topography are irregular. All these observations imply that longitudinal deviatoric stress gradients should be playing a significant role in the dynamics of the glacier. Therefore, it provides a good case study on which to test and investigate the proposed models. Specifically, the model will be tested against winter and summer observed surface velocity measurements made between 1990 and 1991 along the central flowline (Fig. 2).

RESEARCH DESIGN

This study can be broken down into three specific objectives: 1) to apply all four models to a reference scenario in order to compare results with each other and with observed velocities; 2) to assess the degree to which longitudinal coupling due to variations in basal motion make a significant contribution to the glacier's flow dynamics, and; 3) to assess the horizontal resolution over which longitudinal effects tend to cancel out. These three objectives are achieved through five steps. The first three concern the construction of the reference scenario for Haut Glacier d'Arolla. The latter two investigate the effects on the computed stress/strain regime of, firstly, perturbing the prescribed basal motion boundary condition of the reference scenario, and secondly, systematically increasing the horizontal resolution of the reference scenario. These five steps establish:

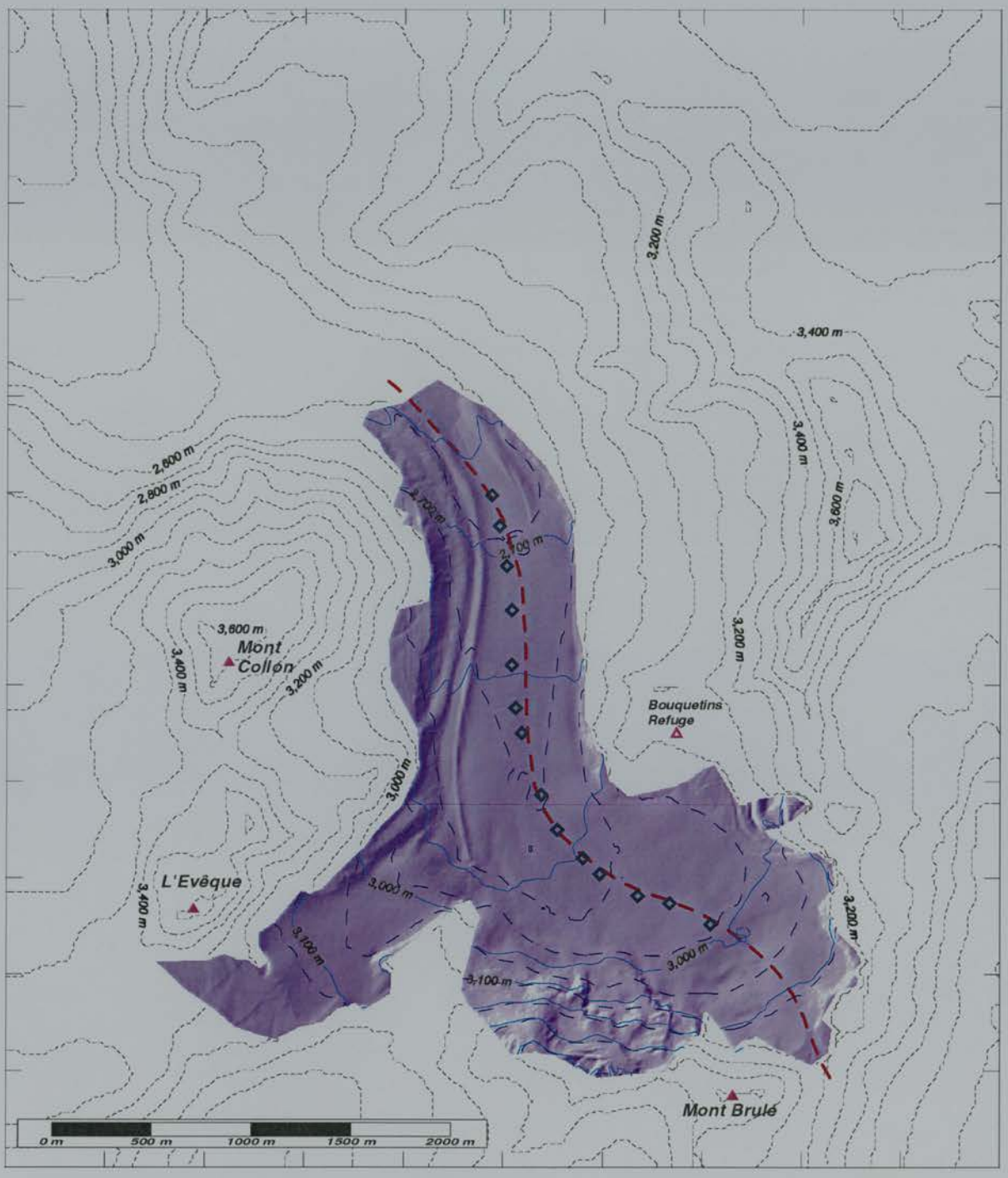

Fig. 1. *Surface and bed topography of Haut Glacier d'Arolla and its catchment showing the main summits, the velocity survey stake network and the central flowline to which the models were applied.*

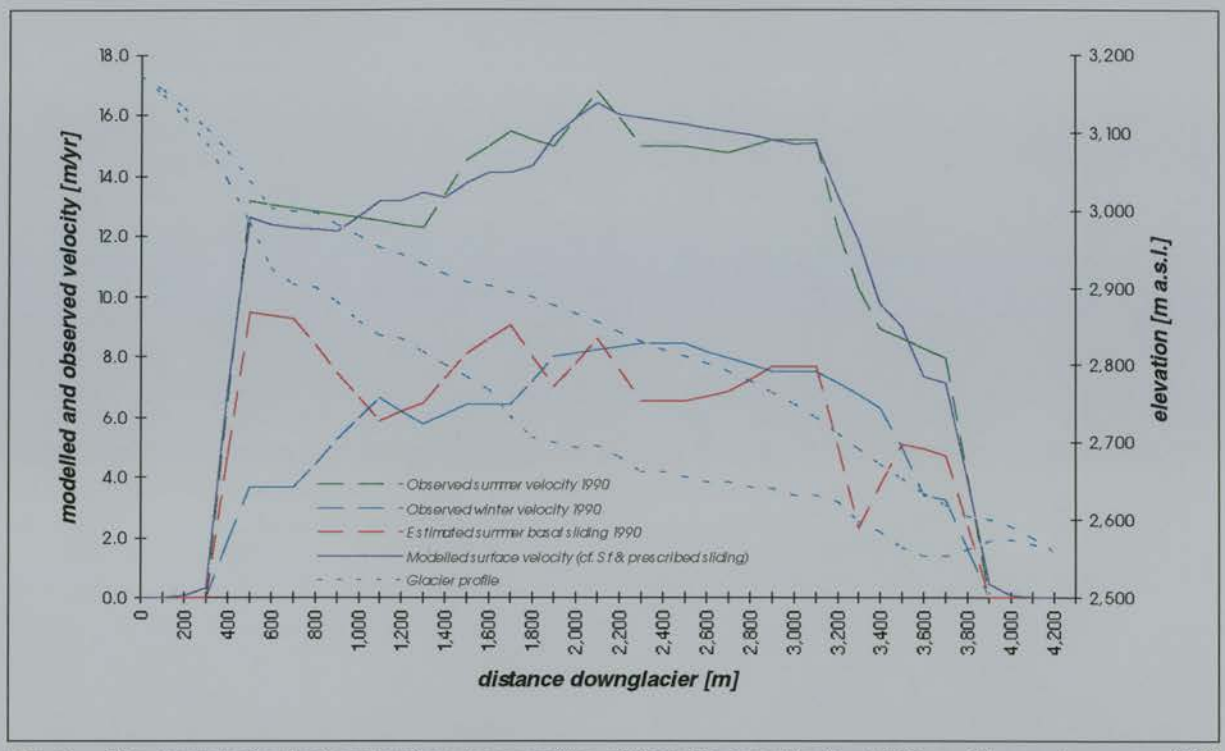

Fig. 2. The downglacier bed and surface long profiles of Haut Glacier d'Arolla at 100 m. Observed summer 1990 and winter 1990 - 1991 surface velocities, the estimated basal motion component (based on the subtraction of winter from summer surface patterns) and the two-dimensional first order modelled surface velocity pattern (with prescribed basal motion and the calculated downglacier variation of S_f).

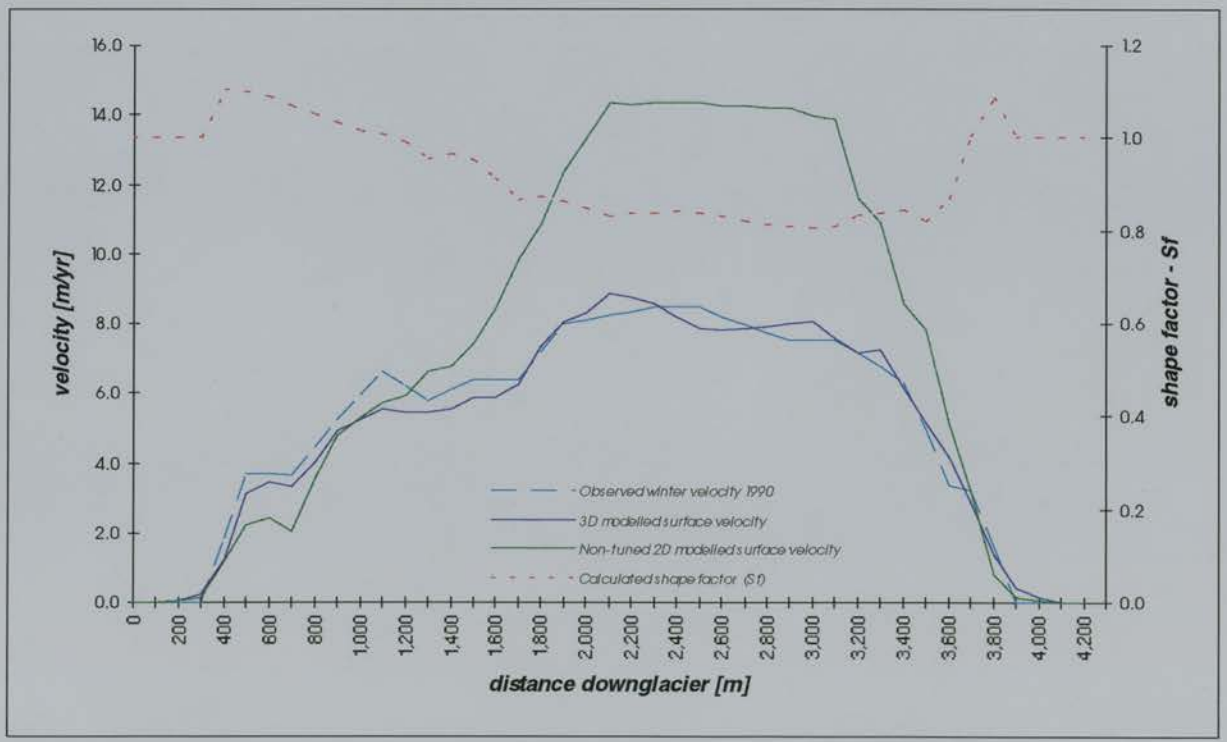

Fig. 3. The downglacier patterns of three-dimensional first order modelled surface velocity, two-dimension first order modelled surface velocity (without S_f and no basal motion), observed summer 1990 surface velocity and the calculated shape factor (S_f).

- The shape factor (S_f) which enables the two-dimensional flowline models to operate in three-dimensions. This takes account of different cross-section shapes of the valley and their variable contribution to transverse stresses and resistive drag along the glacier. In this study, these effects are isolated down the central flowline by direct comparison of the computed stress and velocity fields of the first order approximation flowline model with those extracted from the same flowline but computed using a three-dimensional first order model (Chapter 6).
- An initial estimate of the average summer sliding component which is calculated by subtracting observed summer surface velocities from those observed over the winter season, 1990. Two assumptions here are that winter flow involves negligible basal motion and that internal deformation does not alter significantly with the imposed summer basal motion pattern. Although, on first impression both of these assumption are tenuous, as will be discussed and investigated later they appear to give reasonable estimates.
- A reference scenario for independently testing and comparing the four models. This is based on bed and surface profiles taken from the centre flowline of Haut Glacier d'Arolla at 100 m resolution, the derived shape factor and the estimated summer basal sliding pattern. The resulting computed stress and velocity patterns can then be compared with each other, with the observed summer velocity pattern and with results from the shallow ice approximation in order to investigate the efficacy of the various schemes.
- A means of investigating the role of longitudinal coupling across Haut Glacier d'Arolla as a result of changes in basal motion. To achieve this the first order model will be applied to the reference scenario with a perturbed pattern of prescribed basal motion. This perturbation will take the form of: 1) setting basal sliding to zero across the length of the glacier bed, and, 2) increasing the basal velocity boundary condition in a 300 m zone in the ablation area of the glacier. Although the second approach may appear crude, it does have some physical grounding as a 'velocity event' was observed at Haut Glacier d'Arolla between June 19 and June 29, 1994. Furthermore, it appears to have been initiated from a small zone within the ablation area. During this event observed surface velocities exceeded their summer means by over 400% for over five days (Nienow, 1995).
- The horizontal resolution at which longitudinal effects tend to cancel out and the shallow ice model becomes valid. To achieve this the resolution of the reference run is increased from 100 m to 900 m. The computed longitudinal and basal shear stresses and associated velocity patterns using the first order approximation flowline model are compared with both observed velocities and the stress and velocity pattern computed using the shallow ice approximation. This provides an indication of the horizontal resolution over which slope and ice thickness need to be averaged in order to apply the shallow ice approximation with confidence.

THE SHAPE FACTOR

To construct the reference scenario on which the models can be investigated, the shape factor (S_f) needs to be calculated. S_f was derived by comparing the extracted computed basal shear stress and surface velocity patterns generated by a first order three-dimensional model (Chapter 6) with that of a first order two-dimensional flowline model. The surface velocities predicted by the two models are compared with the observed winter velocities (Fig. 3). The high level of coincidence between the pattern of extracted three-dimensional velocity with the observed winter pattern along the flowline implies that the three-dimensional model is predicting winter deformation successfully. It follows that the three-dimensional model is also successfully calculating the internal stress field. As both models were run with an identical rate factor (**A**) of 0.063 bar^{-1} a^{-3}, computed from a linear regression of modelled against observed winter 1994 velocities, (Chapter 6) then the differences in the modelled results can be directly attributed to the combined effects of support from the valley sides and transverse stresses. These effects can be accounted for in the plane-strain approximation by amending the computed basal shear stress through a multiplier, the shape factor (S_f).

Down glacier variability in S_f was calculated by dividing the three-dimensional modelled shear stress by the two-dimensional modelled shear stress (Fig. 3). The result is extremely encouraging and lends strong support to Nye's (1965) analytical analysis of shape factors for hypothetical valley shapes. Values of S_f fall between 0.8 and 1.1. The bulk of the glacier flowline has a S_f value of <0.9, which is in general agreement with Nye's prediction for a parabolic cross-section valley shape

with a width of the order of 10 times the maximum ice thickness (Paterson, 1994). There is little variability in these values down glacier, indicating that the effects of transverse strain may be negligible. The two zones where the S_f values depart from the expected are at the snout and head of the glacier, where S_f increases to around 1.1. This is contrary to Nye's (1965) analysis. However, calculated shear stresses are very low in these marginal areas and the calculated S_f, based on the division of two small numbers, gives a correspondingly disproportionate value. Furthermore, one may speculate that in these marginal areas where ice thickness and shear stresses are small, transverse strain effects may come into play with the steep convex valley sides affecting the flow.

SUMMER BASAL SLIDING

Isolation of the of the basal sliding component for summer 1990, was calculated by subtracting the observed winter surface velocity pattern in 1990 - 1991 from that observed over the summer 1990 (Fig. 2). This estimate is based on two premises: 1) that the winter velocity pattern has no basal sliding component and, 2) that the component of internal deformation remains relatively constant despite changes in the basal sliding condition. In the absence of detailed inclinometry measurements both of these premises are highly questionable. However, regression of three-dimensional modelled surface velocities without basal sliding against observed winter velocities (Chapter 6), reveals a good fit with an R^2 value of 0.74. Comparison of the extracted three-dimensional modelled surface velocity without basal motion with observed winter 1990 values down glacier also display a good similarity (Fig. 3). In light of these observations and in the absence of empirical data, premise 1 can be tentatively accepted.

The second premise is less plausible; the processes of basal motion do not operate independently of the internal deformation component of glacier flow. The internal stress/strain distribution within an ice mass is constantly adjusting in response to temporal and spatial changes in basal motion. This adjusting pattern, in turn, determines the basal shear stress which drives basal motion. However, the question to be posed regards the temporal scale at which the internal stress/strain component responds to changes in basal conditions and whether these are significant when averaged over a whole season. The internal stress/strain pattern within a glacier responds to the spatial derivative of basal motion, i.e. changes in basal friction/resistance, not in the prescribed component of basal motion itself. The calculated pattern of basal motion (Fig. 2), apart from a region c. 3,300 m downglacier which corresponds to a basal topographic hollow, does not fluctuate excessively except at the margins. Thus, the internal stress/strain distribution of the glacier will not be overly perturbed when the prescribed basal motion pattern is imposed. This conclusion is further substantiated by the simulation of the first order two-dimensional modelled surface velocity (constrained with S_f and the calculated sliding pattern) with the observed summer pattern (Fig. 2).

COMPARISON OF FOUR FLOW MODELS UNDER THE REFERENCE SCENARIO

The three longitudinal stress models along with the shallow ice model are applied to the boundary conditions provided by the central flowline of Haut Glacier d'Arolla at 100 m spatial resolution and constrained by the shape factor (S_f) and the pattern of basal motion derived above. The rate factor (**A**) in all of these runs is set at 0.063 bar^{-1} a^{-3} (Chapter 6). The aim of these reference runs is to provide a realistic framework with which the models can be compared under identical boundary conditions.

The three full stress models reveal that the longitudinal deviatoric stresses are significant and are of an equal order of magnitude to the computed shear stress for the whole length of the glacier (Fig. 4a). Furthermore, at the glacier margins, particularly at the snout, longitudinal stresses exceed shear stress values and therefore, in these regions dominate the resulting strain pattern. Computed values of basal shear stress fluctuate to a maximum value of 1.5 bars which is well within the bounds of the 0.5 - 2.0 bars quoted for 'normal glacier flow' (Paterson, 1994). What is significant is that the downglacier pattern of computed basal shear stress and longitudinal stress using the three full stress models all exhibit a strong resemblance to each other and all result in considerably 'smoother' variations in basal shear stress than that predicted using the driving stress equation (Chapter 2.1) derived from the shallow ice approximation. An exception to this general smoothness is observed 700 m downglacier in the transition zone at the base of the Mont Brulé ice fall where large variations in glacier gradient and thickness occur over short distances. Otherwise all three full stress schemes show a good similarity in computed values of τ_{xz} and τ'_{xx} which appear to offer significant

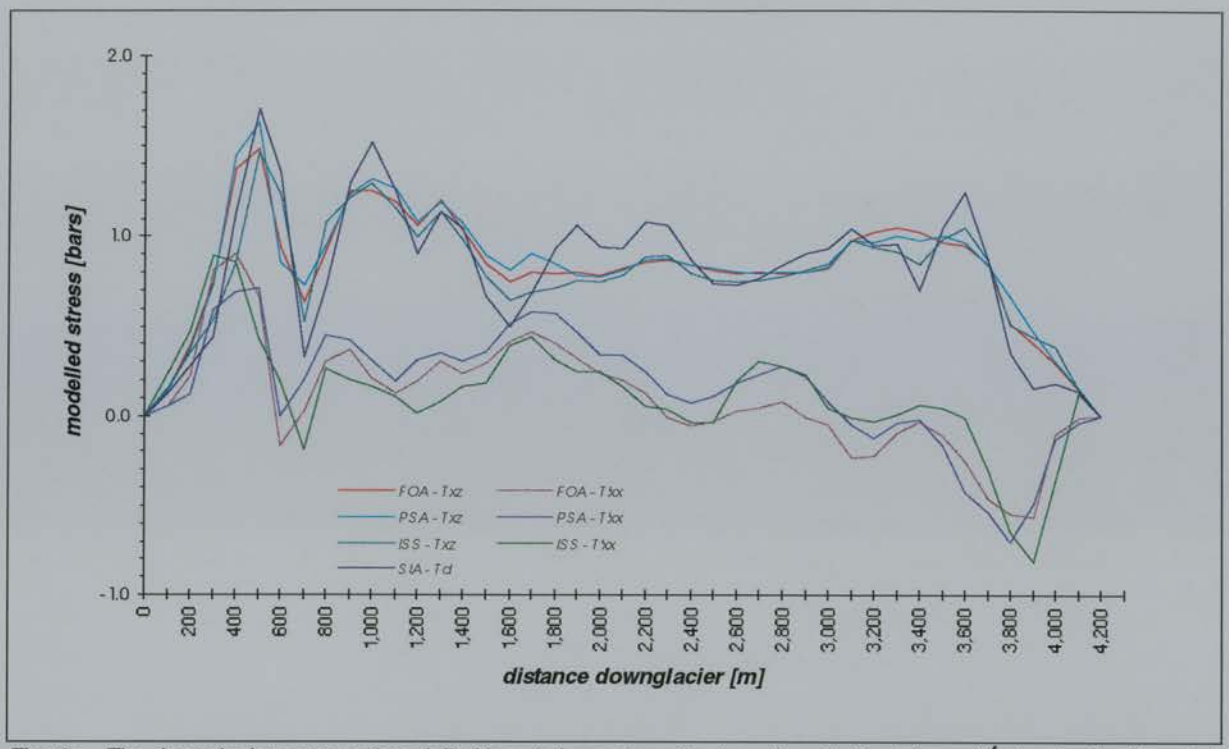

Fig. 4a. *The downglacier pattern of modelled basal shear stress (τ_{xz}) and longitudinal stress (τ'_{xx}) using the three full stress schemes compared with the pattern of driving stress (τ_d) computed from the shallow ice approximation. These results indicate that the full stress schemes are giving similar patterns of modelled τ_{xz} and τ'_{xx} and that τ_d displays large fluctuations over the whole length of the glacier. (key:* ***FOA*** *– first order approximation,* ***PSA*** *– plain strain approximation,* ***SIA*** *– shallow ice approximation and* ***ISS*** *– ice surface stretching).*

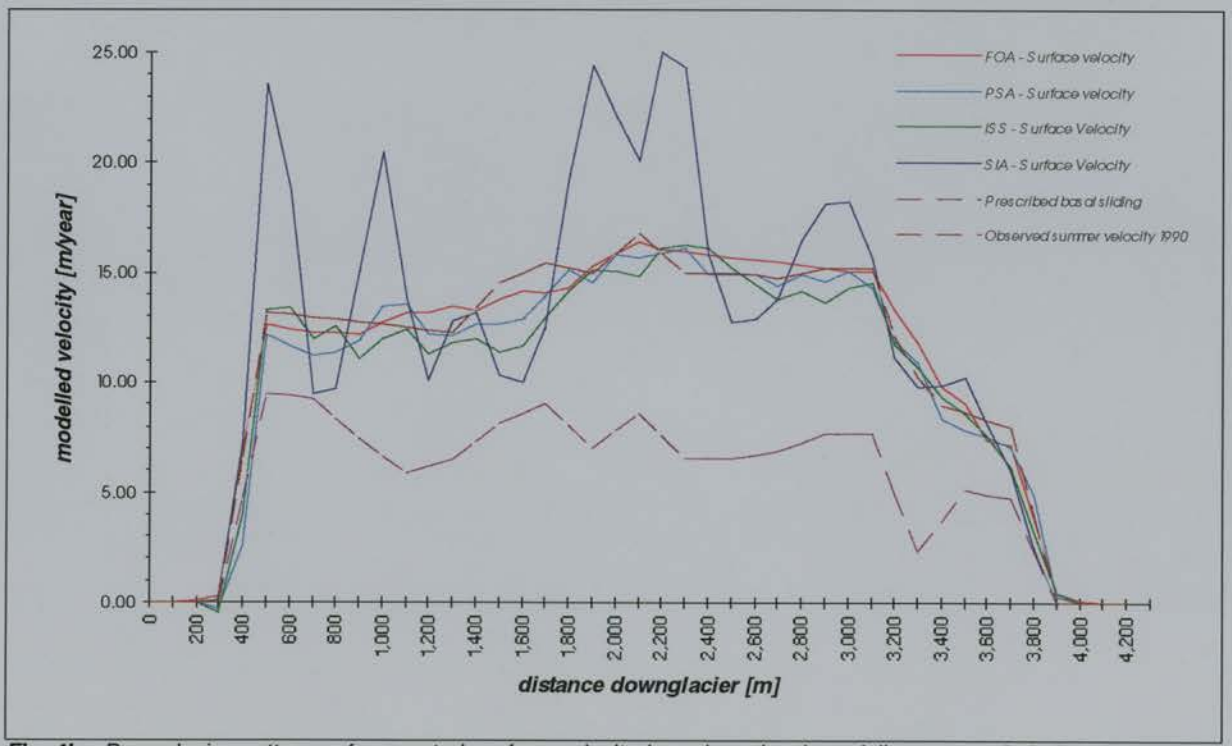

Fig. 4b. *Downglacier patterns of computed surface velocity based on the three full stress and shallow ice models compared with the observed summer 1990 velocity pattern. The full stress models show a good level of coincidence with observed velocities whilst the shallow ice model displays large fluctuations. (key:* ***FOA*** *– first order approximation,* ***PSA*** *– plain strain approximation,* ***SIA*** *– shallow ice approximation and* ***ISS*** *– ice surface stretching).*

improvements to the corresponding computed value of τ_d which tends to fluctuate more wildly.

In the absence of direct observations of the stresses experienced by Haut Glacier d'Arolla, a degree of validation of the full stress schemes can be achieved by comparing the computed surface velocities, the direct expression of τ_{xz} and τ'_{xx} with the observed summer velocity pattern (Fig. 4b). The comparison reveals a smooth downglacier pattern of computed surface velocity using the full stress schemes, which agrees well with the observed summer 1990 pattern. The resemblance is considerably better than that of the shallow ice modelled surface velocity. The latter velocity pattern shows large spatial fluctuations which are not only unrealistic but impossible to sustain from mass continuity considerations. These large and artificial fluctuations in the shallow ice modelled velocity are a direct consequence of defining the driving stress (τ_d) by the strictly local conditions of ice thickness and surface gradient. The limitation can be attributed to the neglect of inherited longitudinal stress gradients in the shallow ice approximation. Transfer of tensile and compressive forces between areas of high and low velocity effectively 'smooth out' velocity variations across the glacier surface, resulting in the considerably dampened velocity pattern which is observed in reality.

LONGITUDINAL COUPLING ACROSS HAUT GLACIER D'AROLLA

The purpose of the next series of experiments is to determine the sensitivity and extent of longitudinal coupling across Haut Glacier d'Arolla by applying the first order model to the reference scenario but with a perturbed pattern of imposed basal velocity. As discussed previously, the internal stress/strain distribution within a glacier is sensitive to the basal boundary condition. However, from force balance considerations, it is the spatial derivative of basal motion reflecting changes in the resistance and shear traction exerted by the bed that affect the basal shear stress over and above the absolute component of basal motion. In order to investigate how changes in the basal boundary condition manifests itself on the internal stress/strain distribution, two model runs are initiated based on the above reference run but with a different pattern of imposed basal velocity: 1) zero velocity component is prescribed along the length of the glacier, and, 2) a small 300 m zone within the ablation area is 'decoupled' from its bed.

Experiment 1, with a prescribed basal boundary condition of zero velocity is relatively straightforward to justify since it is the scenario that has been assumed to apply in winter. Experiment 2 is initiated by doubling the prescribed basal motion boundary condition in a 300 m zone, c. 3,000 m down glacier. Although, this experiment may appear crude, it does have some physical justification. Nienow (1995) observed a major high velocity event at Haut Glacier d'Arolla between June 19 and June 29, 1994. This 'velocity event' was characterised by observed surface velocities of 65 ma^{-1} in the ablation zone, representing a 500% increase over their summer mean (Nienow, 1995). Although, no precise mechanism has been postulated to account for the observed 'velocity event' it is likely that it is linked to a sudden increase in meltwater input into a relatively inefficient, distributed hydrological system leading to localised decoupling associated with rapid increases in basal water pressures. What is pertinent to the present experiment, is that although the velocity event was observed over the whole of the glacier, it appears to have been initiated on 20 June from a small zone lying within the ablation area (Nienow, 1995).

Experiment 1, where the prescribed basal velocity pattern was set to zero, reveals that the computed stress field does not change substantially even with large imposed changes in the actual magnitude of basal sliding (Fig. 5a & b). This shows that the internal stress/strain distribution is in fact reacting to the derivative of basal motion, which is a direct expression of the changing force balance experienced at the glacier bed, and not to the actual magnitude of the imposed velocity change. Zones of basal shear stress and longitudinal stress down glacier which appear to differ slightly from the reference run coincide with zones where there has been a change in the spatial derivative of basal motion as a result of the new imposed pattern, for example, at 3,300 m downglacier a sharp decrease in the prescribed summer basal motion from c. 7 ma^{-1} either side of this zone to c. 3 ma^{-1} results in a computed basal shear stress increase of c. 0.1 bar compared to the no basal motion case.

Experiment 2 reveals that there is considerable longitudinal coupling taking place around the decoupled zone. In the immediate vicinity of the perturbation, both τ'_{xx} and τ_{xz} fluctuate rapidly by c. 1 bar (Fig. 5a). Within the decoupled zone itself, a much reduced value for the basal shear stress (τ_{xz}) is experienced, dropping from 0.9 bars upglacier to less than 0.3 bars. The

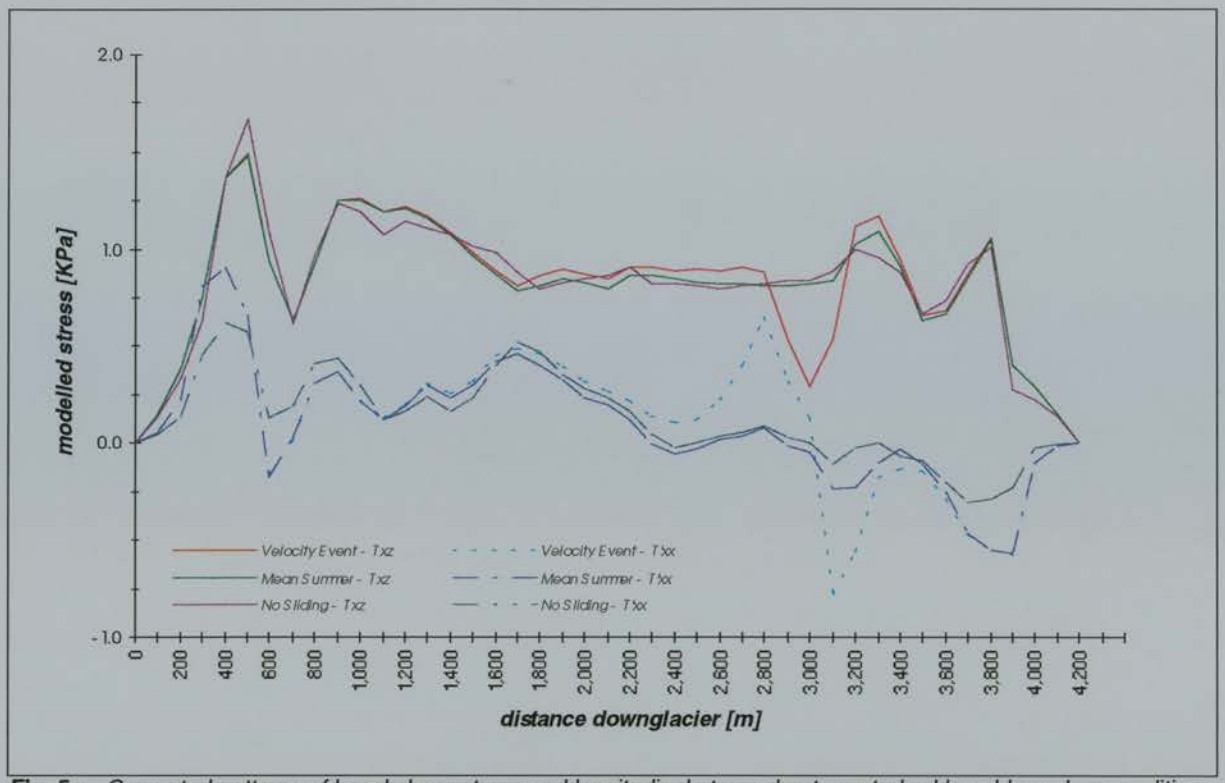

Fig. 5a. *Computed patterns of basal shear stress and longitudinal stress due to perturbed basal boundary conditions: no basal motion, mean summer and the velocity event. The modelled stress pattern is significantly effected in the zone of basal decouping where basal shear stress decreases substantially and longitudinal stresses dominate.*

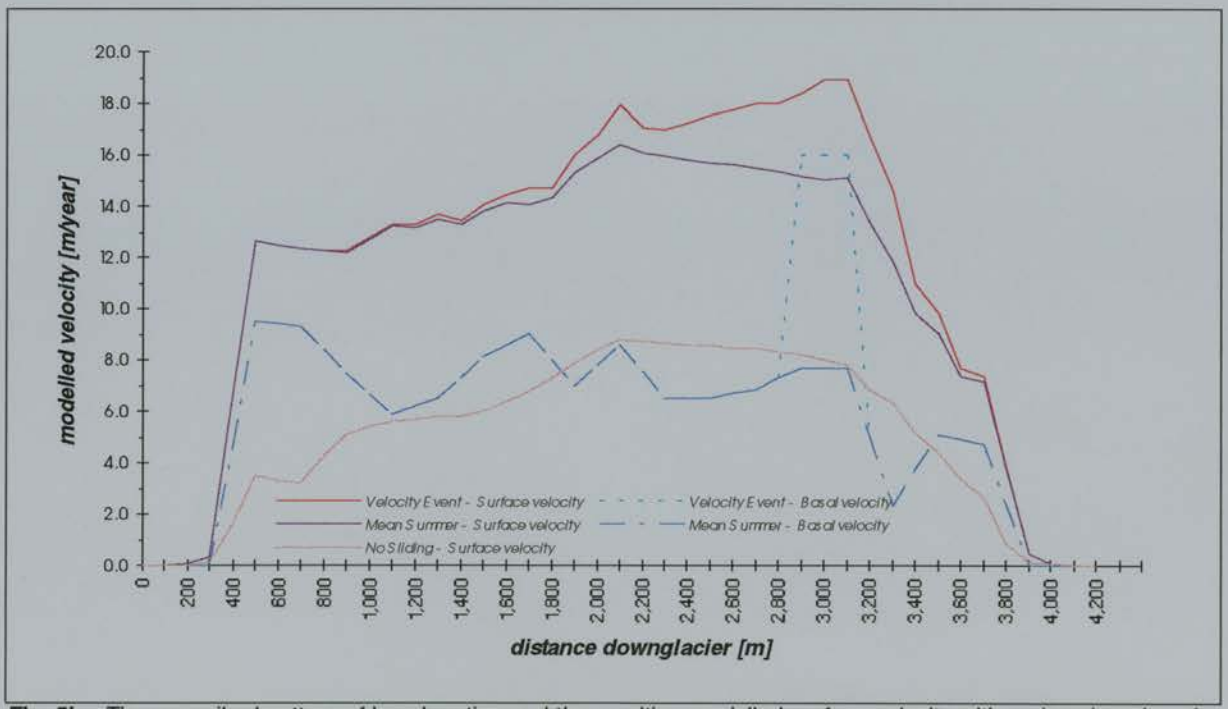

Fig. 5b. *The prescribed pattern of basal motion and the resulting modelled surface velocity with no basal motion, the mean summer basal motion and the velocity event. Significant longitudinal coupling is taking place throughout the glacier as the effects of decoupling a small region of the bed downglacier are experienced some c. 1,700 m upglacier.*

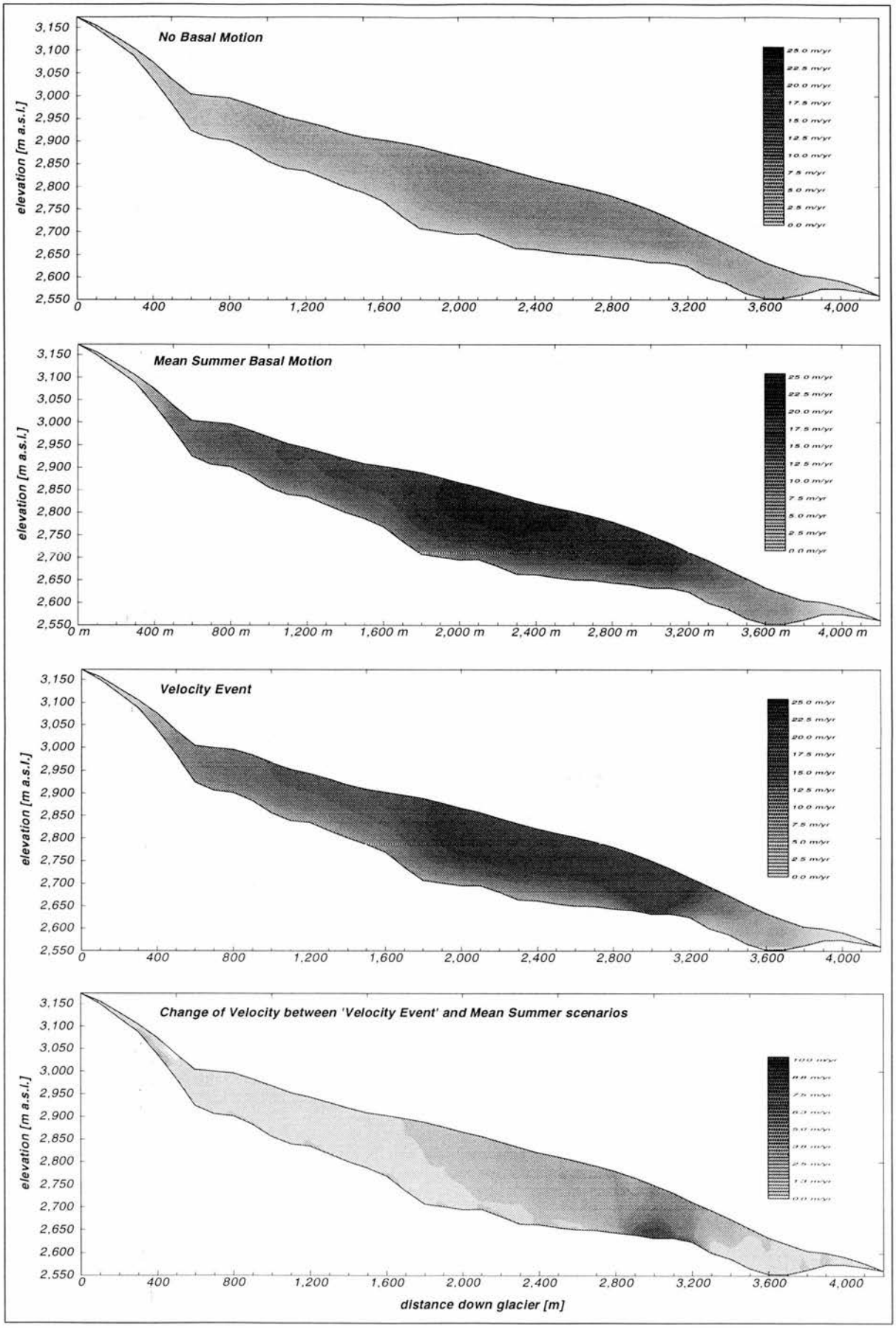

Fig. 6. *The two-dimensional modelled velocity pattern along the central flowline of Haut Glacier d'Arolla as a function of three different prescribed basal motion scenarios; no sliding, mean summer and the velocity event. The forth panel illustrates the change in velocity between the mean summer reference run and the velocity event and indicates the degree of longitudinal coupling taking place throughout the glacier as a result of 'decoupling' a small section of the bed.*

longitudinal deviatoric stress (τ'_{xx}) fluctuates from a much increased value of +0.75 bars upglacier (indicating tensile extension) to -0.8 bars immediately downglacier of the decoupled zone indicating a zone of strong compression. The transfer of stresses is also reflected in the modelled basal shear stress values in the region downglacier which increase by 0.2 bars, reflecting the additional resistance/shear traction that the bed has to support in this area as a result of additional stress from the decoupled zone.

Modelled surface velocities in experiment 2, reveal that the effects of locally decoupling a small zone of the bed manifest themselves over a large proportion of the glacier surface (Figs. 5a & 6). In the immediate vicinity of the decoupled zone, surface velocities increase by about 3.0 ma^{-1}. This represents a considerable dampening of the original basal velocity perturbation of 8.0 ma^{-1} as it is transmitted through the main body of the glacier (Fig. 6). However, the dampened signal is actually experienced across a considerable portion of the glacier surface up to 800 m downglacier and a slight perturbation of the surface velocity some c. 1,700 m upglacier (Figs. 5b & 6). These observations lend strong support to the importance of longitudinal coupling in valley glaciers and imply that inferences on glacier dynamics based on empirical studies of temporal changes in surface velocity cannot be made independently of the internal stress/strain field.

HORIZONTAL RESOLUTION

The significance of longitudinal stresses in determining valley glacier dynamics raises the important issue of the optimal horizontal distance over which slope and ice thickness are to be averaged in order to calculate the driving stress (τ_d) using the shallow ice approximation. If the quantities of slope and thickness are averaged over sufficiently long distances it is likely that the effects of longitudinal stresses will cancel out (Paterson, 1994). In order to test this assertion, the first order and shallow ice models were applied to the reference scenario at successively larger horizontal resolutions and their computed stress and velocity fields were compared with each other and to the observed pattern of velocity for summer 1990. The glacier long profile, S_f and the pattern of prescribed basal velocity were averaged at horizontal resolutions of 100 m (reference scenario), 200 m, 300 m, 600 m and 900 m. Horizontal resolutions larger than 900 m would be meaningless in this case study, resulting in less than four discrete points for Haut Glacier d'Arolla.

The results indicate that up to 900 m the computed longitudinal stress does not significantly cancel out (Fig. 7). Since the bed topography of Haut Glacier d'Arolla, even at 900 m resolution, represents an inclined plane, then longitudinal stresses are always going to be generated as the glacier is always going to be in tensile extension in the accumulation area where velocities tend to increase, and will always be in compression in the ablation area where velocities are reducing. Hence, at the coarser resolutions, the down glacier pattern of computed longitudinal stress approximates a sinusoidal curve but its magnitude does not diminish significantly.

At successively coarser resolutions, the computed pattern of driving stress (τ_d) from the shallow ice approximation does appear to converge on the computed pattern of basal shear stress (τ_{xz}) including longitudinal stress gradients. Even so, the computed surface velocity pattern using the shallow ice approximation is still substantially wide of the mark, varying by up to 40% above and below the observed pattern. This is due to the non-linear nature of the constitutive flow relation used. Even though the pattern of driving stress (τ_d) converges on the computed pattern of basal shear stress (τ_{xz}), small differences are magnified when cubed in Glen's flow law. Thus, the neglect of longitudinal stress gradients in the shallow ice approximation, even at 900 m resolution, leads to an erroneous pattern of surface velocity. Even though it is not possible to test the hypothesis that longitudinal effects become negligible when averaged over horizontal distances of about 20 ice thicknesses (Paterson, 1994), the present study indicates that when considering valley glaciers this is not necessarily the case. Valley glaciers, by their nature will always have inclined long profiles, and thus will experience acceleration and deceleration and therefore tensile and compressive stresses at whatever resolution they are analysed, although the pattern of computed driving stress may in fact well approximate to the basal shear stress. However, it is likely that at horizontal resolutions of the equivalent of 20 ice thicknesses then valley scale topography may very well become averaged to that of a non-inclined plane and hence longitudinal gradients in this case may well cancel out.

DISCUSSION

The significance of these experiments are threefold. Firstly, the three schemes described in Chapter 2 for the computation of longitudinal stresses in glaciers appear

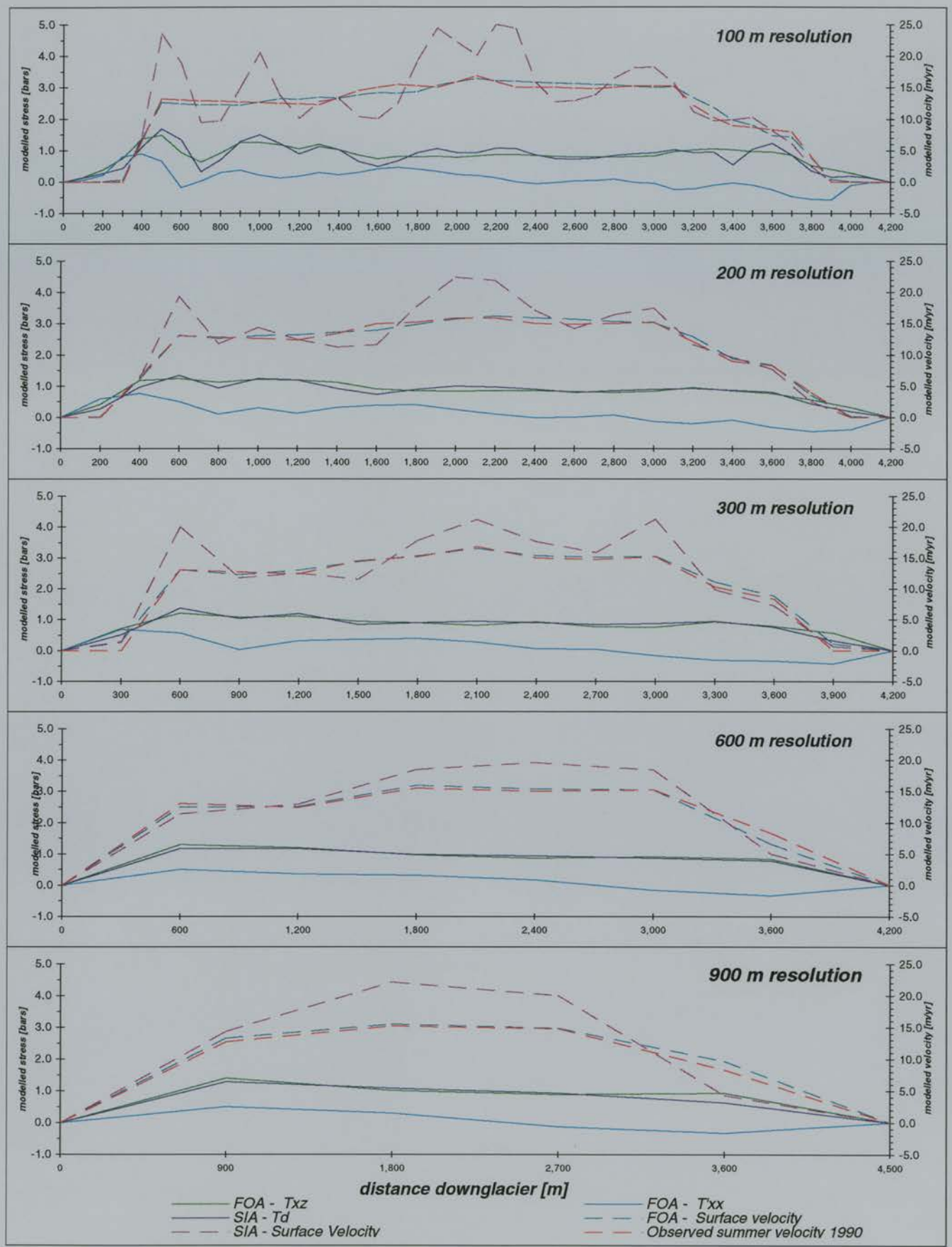

Fig. 7. *Computed and observed patterns of surface velocity and modelled stress using the first order and shallow ice models at a variety of horizontal resolutions.(key: FOA: first order approximation and SIA: shallow ice approximation).*

to function correctly, resulting in realistic stress patterns with associated surface velocities which successfully predict the observed summer pattern. Secondly, longitudinal stresses play a significant role in the dynamics of valley glaciers. Considerable longitudinal coupling is experienced throughout the glacier as a result of perturbing the basal motion boundary condition in a way which appears to be reflected in nature. Thirdly, the shallow ice approximation is not successful in modelling the dynamics of Haut Glacier d'Arolla, resulting in a computed stress and velocity patterns which fluctuate considerably as a direct consequence of only taking into account local surface slope and ice thickness in its derivation.

Although, at first appraisal the form of these experiments may appear circular, at no point have the models been 'tuned' to the observed velocity patterns with which they have been compared. The rate factor (**A**) of 0.063 m^{-1} a^{-3} for Haut Glacier d'Arolla, is derived through the regression of three-dimensional modelled surface velocities with a completely different data set, which was observed over a short winter period, 1994 (Nienow, pers. com.). The derivation of the downglacier values of the shape factor (S_f) necessary to account for three-dimensional valley shape effects in the flowline models involves only the division of two modelled stress fields without any reference the observed velocity data. That the three-dimensional modelled velocity pattern shows good coincidence with the winter 1990 - 1991 observed pattern reflects the high level of prediction achieved using the full three-dimensional, first order approximation. Finally, the isolation of the summer basal velocity boundary condition for the reference scenario is made without any recourse to the models tested, and involves the simple subtraction of the observed mean winter surface pattern from the mean summer pattern of surface velocity.

CONCLUSIONS

- Three schemes for the computation of longitudinal stresses have been applied to boundary conditions of Haut Glacier d'Arolla in plane-flow at 100 m resolution. Results reveal that longitudinal stresses are significant in influencing flow along the length of the glacier. Moreover, they are of an equal order of magnitude as the basal shear stress and even exceed it at the glacier margins.
- The computed surface velocity patterns using the full stress models display a good likeness and fit with the observed summer 1990 pattern. This is encouraging since it provides an empirical validation for this modelling.
- The pattern of surface velocity and driving stress modelled using the shallow ice approximation does not yield a good likeness with either of the three full stress models or with observed velocity. Moreover, it is characterised by large fluctuations, a symptom of it being based on purely local glacier conditions. This implies that the shallow ice approximation is not effective in modelling valley glacier dynamics.
- Decoupling a 300 m zone of the glacier bed results in significant changes in the computed stress and velocity patterns across the glacier. Furthermore, the relationship between basal motion and the internal stress/strain field is complex and considerable longitudinal coupling is taking place across the glacier.
- Systematically increasing the horizontal resolution of the analysis implies that longitudinal effects are significant at all resolutions in typical valley glaciers. Although the computed driving stress pattern using the shallow ice approximation does converge on the basal shear stress pattern at resolutions of 600 m and above, the resulting computed surface velocity pattern still shows variations of up to 40% from the observed pattern.

MODELLING CLIMATE, TOPOGRAPHY AND PALAEO-GLACIER FLUCTUATIONS IN THE CHILEAN ANDES

ABSTRACT

A one dimensional flowline model has been constructed, tested and applied to two formerly glaciated valley basins within the Chilean Lake District. The vertically integrated ice flow model is similar to those used to study historical fluctuations of European Alpine glaciers and includes terms for internal deformation and basal sliding. In addition, longitudinal deviatoric stresses are computed and velocity terms are correspondingly adjusted. The model is driven through a mass balance term forced by a stepped lowering of the equilibrium line altitude (ELA) through time.

Experiments, based on generating equilibrium glacier surface profiles corresponding to various ELAs, indicate that a lowering of at least 1000 m of the ELA from its present day position is required to simulate the glacial maximum. Furthermore, the specific geometry of the two valleys provides an important control on the extent of the two glaciers, effectively decoupling them from further climatic deterioration once they have advanced beyond the constraining influence of their valleys into the piedmont zone. The tight nesting of terminal moraine loops provides evidence for this topographical control on palaeo-glacier extent.

The modelled response and sensitivity of the two palaeo-glaciers to climate change differ markedly as a result of contrasting valley geometry. Glaciers resting on steeper gradients tend to have thinner profiles, faster mass turnover times and correspondingly shorter volume time-scales. Puyehue glacier has a response time of c. 1000 years whereas the Rupanco glacier has a response time of c. 2000 years. Hence, Puyehue is more sensitive to climatic fluctuations occurring on a time scale of 500 - 1000 years. Furthermore, the Rupanco glacier may lag or even fail to respond at all to climatic fluctuations at these time-scales, a conclusion substantiated by field evidence.

INTRODUCTION

Hindmarsh (1993) identifies several steps in the technical process of modelling: (1) the identification of the physical processes to be modelled and their formulation into a system of equations; (2) simplification and solution of these equations often requiring numerical techniques; and (3) comparison of the solution with data in order to validate models, infer parameters and make predictions. The value of ice sheet and glacier modelling to Quaternary reconstruction lies in its ability to link evidence of past glacier fluctuations (which may be expressed in depositional sequences) to the climatic changes responsible for producing them. The model may be applied to specific glacier boundary conditions and driven by assumed climatic changes and the results then compared with the glacial geomorphology and geology in the area concerned. The purpose of such comparisons lies in a combination one or more of the following:

- a verification procedure for the model and its parameterisation,
- an insight into the palaeoclimatic forcing,
- an aid in explanation of the observed glacial geomorphology and geology.

Over the last two decades, coinciding with progress in computing technology and numerical techniques, there has been an explosion in the use of ice sheet models for Quaternary reconstruction. For example: the evolution of the East Antarctic ice sheet (Huybrechts and Oerlemans, 1988) and an assessment of its stability (Huybrechts, 1992); the Laurentide ice sheet (Hughes, 1987; Roberts, 1991) and its sensitivity to insolation fluctuations (Oerlemans, 1993); the Younger Dryas (Loch Lomond Stadial) ice sheet in Scotland (Payne and Sugden, 1990); the Fenno-Scandian ice sheet (Holmlund and Fastook, 1995) and associated ice streams (Arnold and Sharp, 1992; Holmlund and Fastook, 1993; Payne, 1995). Of specific relevance to this study is Hulton et al.'s (1994) reconstruction of the

late glacial maximum and associated climate in Patagonia. There is, however, a discrepancy between the scale of operation of these models and the glacial geomorphology against which they are compared and tested. Whereas ice sheet models typically operate at grid resolutions greater than 10 km, glacial sequences are investigated from aerial photography and field study at a significantly higher resolution (Alley, 1996). Hence, ice sheet models, as a result of limitations imposed by the assumptions used in their construction, are only compared against field evidence at the broadest scale and consequently overlook the complexity revealed by detailed field-based investigations. There is a requirement therefore, for a high resolution approach which can address this imbalance of scale between simulation and the empirical record. Inclusion of a computed longitudinal stress field within the flow model goes some way towards overcoming one important aspect of the limits to a higher resolution which constrain ice sheet simulations.

In this paper, a one-dimensional flowline model driven by ELA lowering is used to investigate the effect of basin geometry on the dynamics of two palaeo-glaciers which occupied adjacent valleys in southern Chile. Model results are compared with the glacial geomorphology of the areas concerned. Specifically the following are investigated:

- the amplitude of the climatic deterioration necessary to reproduce the glacial maximum position of the two palaeo-glaciers;
- the effect of valley geometry on the sensitivity and response of the palaeo-glaciers;
- the varying response of the two palaeo-glaciers as expressed in the depositional sequence.

THE STUDY AREA

The Puyehue and Rupanco valley basins are located on the westward side of the Andean massif, at latitude 40°30´S within the Chilean Lake District (Figure 1a). The area has been subject to repeated advances of locally-derived piedmont glaciers throughout the Quaternary resulting in an abundance of over-deepened lake basins (*Clapperton*, 1993). Since the onset of the Holocene, glaciers in the region have retreated, and largely disappeared, in response to a combination of warmer temperatures and reduced precipitation (*Heusser*, 1974, 1989). Glaciers lying between 40°S and 41°S are now limited to areas of highland, and isolated peaks lying above 1600 m.

The Puyehue and Rupanco lake basins are considerably over-deepened and elongated east-west relative to other lakes in the area. These lakes occupy well defined valleys that are 62 km and 50 km long respectively, and up to 15 km wide (Figure 1b). Their source lies within a relatively low-lying, volcanically-active section of the Andes to the east, with the highest peak of Volcan Puyehue rising to 2240 m. Throughout the Holocene the region has experienced steady volcanic activity. However, within the study area this has been superficial (Moreno and Varela, 1985). Therefore, we assume no major post-glacial modification of topography. The valleys open into a large, gentle westward-sloping outwash plain, 100 m asl, which extends some 110 km to the Pacific coastal mountain range.

The glacial geomorphology of the Lago Puyehue and Rupanco basins has been the subject of recent aerial and field investigation (Bentley, 1996). The area is also adjacent to the Llanquihue basin, which represents one of the most intensively ^{14}C dated sets of moraines in the Southern Hemisphere (Clapperton, 1993; Denton, 1993). The salient points to be noted in Figures 1b and 2 are as follows:

- Even though both valleys have well-defined margins and constrained ablation zones, their accumulation areas are sufficiently different to provide a potentially large variability in mass balance response to initial climatic perturbation. Despite this, the last glacial terminal moraines are concentrated and tightly nested in similar positions at the westward ends of each lake. There appears to have been a restriction to further glacier advance beyond this zone.
- In comparison with Rupanco, the westward end of Puyehue is characterised by a significantly more developed and elaborate terminal moraine sequence that suggests a more complex re-advance or standstill history relative to Rupanco.

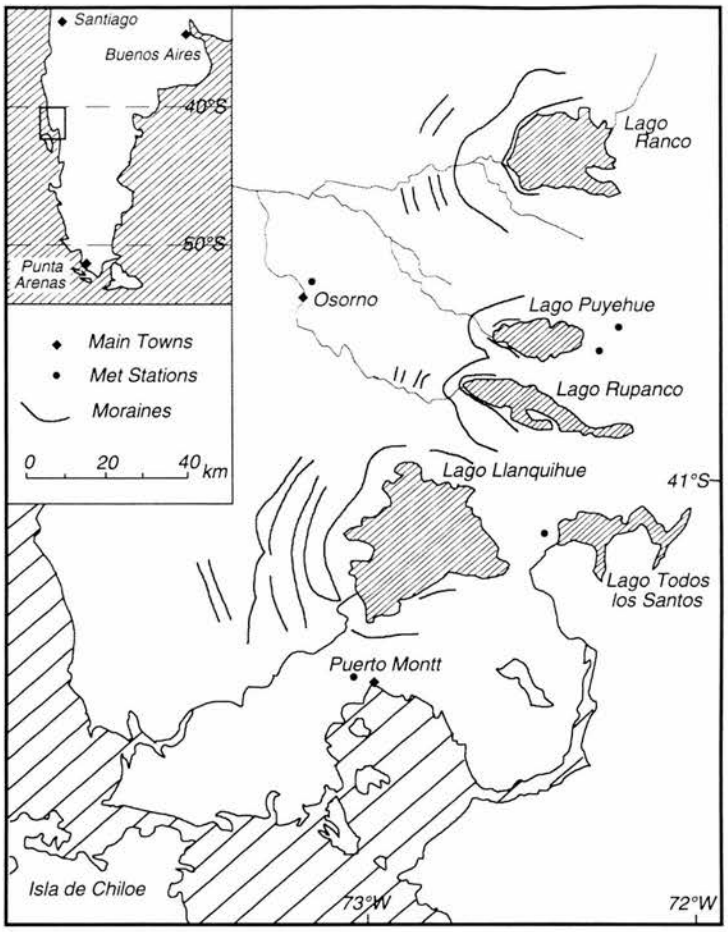

Fig. 1a. *Location map of the southern Chilean Lake District showing the position of the main lakes and position of the moraine belts associated with the last glaciation (from Mercer, 1976).*

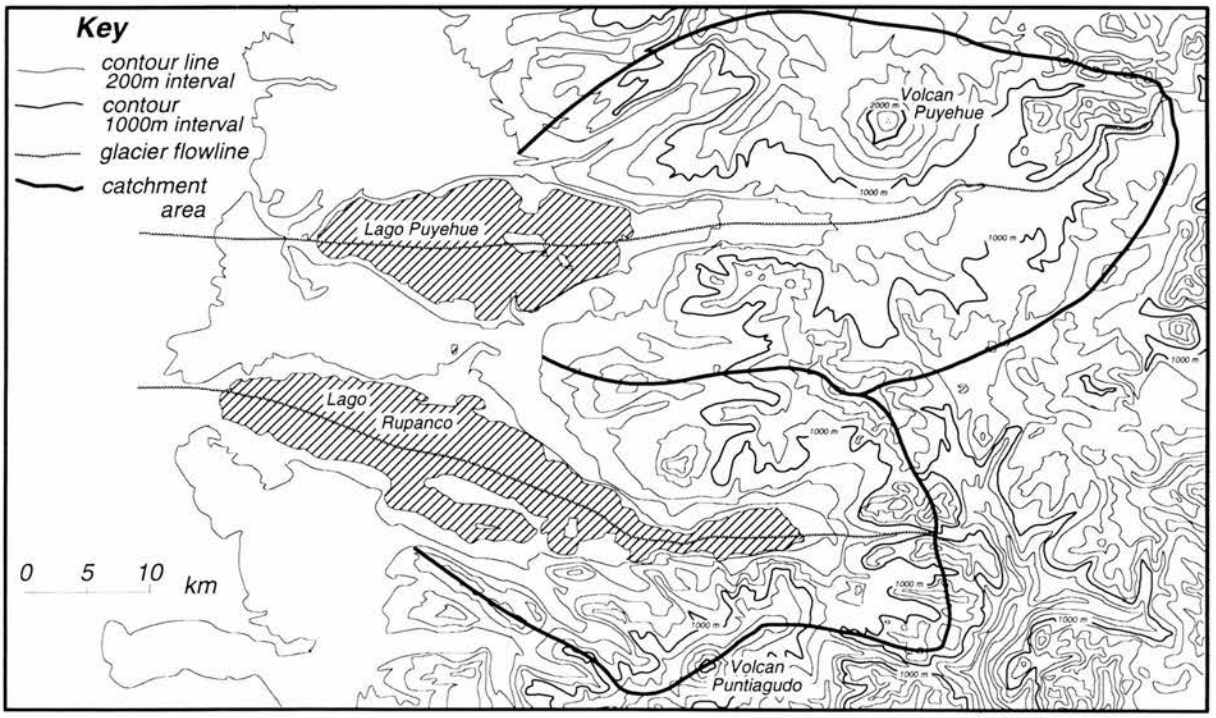

Fig. 1b *The topography of the Puyehue and Rupanco valleys showing the flowlines used in the model and catchment for each glacier.*

- A complex lateral moraine sequence exists between the two lakes, north of Laguna Pichilifaquen. This must have been formed by the Rupanco glacier at its last maximum extent but is well within the limits of the Puyehue glacier at its maximum. It follows therefore, that during final deglaciation Rupanco ice was, at some stage, at its most westward extent while Puyehue ice had retreated to some position to the east. The deposition of this moraine sequence is most likely to have occurred during final deglaciation since the deposits would have been destroyed by any subsequent re-advance.

GLACIER SENSITIVITY & RESPONSE

Valley glaciers are considered to be sensitive indicators of medium and long term climatic change (Häberli, 1994). However, individual glacier response can be extremely complicated due to the many feedbacks that are in operation and may vary as a function of a number of controls (Oerlemans, 1989). These include:

- the nature of the climatic forcing;
- the mechanics of glacier flow;
- the role of basal hydrology;
- the role of valley geometry, both on: the elevation - mass balance feedback, and the flow response to a given mass balance change.

These two valleys were selected for glacial modelling as they permit the effect of valley geometry on palaeo-glacier response to be isolated. The other controls listed which affect glacier response can to some degree be held constant since both valleys:

- are adjacent and similarly aligned and have therefore been subject to roughly the same general climatic changes through time;
- are bounded by similar geologic materials, hence similar flow mechanisms and basal conditions may be expected.

Response time, broadly defined as the time taken for a glacier to complete its adjustment to climatic change, is central to any discussion on the link between past glacier fluctuations and climatic history. Although response time is one of the most important physical variables characterising the dynamics of a glacier it has been difficult to define analytically and as a consequence has been the focus of much research (Nye, 1960, 1963, 1965; Lliboutry, 1971; Paterson, 1994; Hutter, 1983). However, Jóhannesson et al. (1989a,b) find a strong link between the response time and the volume time scale of a glacier and show previous derivations of the response time using kinematic wave theory (Nye, 1963) to be unnecessarily complicated and limited due to involvement with terminus dynamics. Van de Wal and Oerlemans (1995) in their flowline modelling study of kinematic waves further this criticism and conclude that the strong simplifications used in the linear theory developed by Nye (1960, 1963) give misleading results. Jóhannesson et al. (1989a) provide a simpler and more robust estimate of the response time ($\mathbf{T_m}$) independent of terminus dynamics with the following:

$$\mathbf{T_m \sim h/(-b_t)} \qquad (1)$$

where h is the thickness scale for the glacier and $\mathbf{-b_t}$ is the mass balance rate at the terminus. Using this analysis Jóhannesson et al. (1989a,b) calculate a response time for contemporary mountain glaciers to be 10^1 - 10^2 years, substantially less than that estimated by previous methods. However, they note that the above equation should be regarded only as a very crude measure of the temporal and spatial response of a glacier to mass balance perturbations. Furthermore, the estimate is based on a single, specified mass balance perturbation, constant in time. The existence of a positive mass balance feedback, whereby the net mass balance across a glacier tends to increase as its surface elevation increases, makes this assumption unrealistic and will tend to extend response time.

The role of valley geometry on glacier dynamics has been investigated in the theoretical treatment of Oerlemans (1989). Oerlemans emphasises the importance of the longitudinal bed profile on glacier sensitivity and response and introduces a simple analytical solution for the steady state length ($\mathbf{L}$) of a

hypothetical glacier with uniform bed slope (γ), width and basal stress:

$$L = \frac{2(\Lambda / \gamma + b_0 - E)}{\gamma} \quad (2)$$

where Λ is a constant, b_0 is the elevation of the glacier divide and E is the ELA. This expression illustrates that the height-mass balance feedback, reflected in the term Λ / γ, becomes increasingly effective when the bed slope is smaller. Furthermore, the sensitivity of glacier length to ELA change is inversely proportional to the bed slope. Hence, glaciers with a gentle bed slope are more sensitive in terms of terminus position to climatic change but will also have longer response times as they maintain a greater ice thickness (h in equation 1).

Evaluation of the geometrical differences between the Puyehue and Rupanco valleys (Figure 1b) which may be of significance to any differential response between the palaeo-glaciers to climatic forcing, reveals that:

- Specific evaluation of the response time (T_m) for each of the glaciers is difficult as there are no trimlines or proxy data indicating a value for the thickness scale (**h**) in equation 1. However, assuming for typical glaciers of this length and bed slope a thickness scale (**h**) ~ 500 - 1500 m (Hambrey and Alean, 1992) and applying Kerr and Sugden's (1994) estimated ablation rates ($-b_t$) at sea level for the last glacial maximum of 1 - 5 m a^{-1}, gives a response time (T_m) of ~ 10^2 - 10^3 years.
- Puyehue has a larger catchment/accumulation area at high elevation; hence a faster initiation and advance from ice-free conditions may be expected with initial climatic deterioration relative to Rupanco.
- Puyehue has a more uniformly constant and steeper bed slope (γ); hence may experience a more linear and predictable front advance or retreat to climatic forcing and consequently may have a shorter response time since a thinner ice profile (**h**) would be expected on a steeper slope.
- Rupanco is dominated by its over-deepened lake basin characterised by a very gentle, almost horizontal slope (γ), hence its glacier front will tend to be more sensitive to climatic change and is likely to have a somewhat longer response time than Puyehue, due to an subsequently thicker profile (**h**).

MODEL CONSTRUCTION

The main components to the model may be depicted schematically (Figure 3a). The model is similar to those used to investigate historical glacier fluctuations in the European Alps (e.g. Huybrechts et al., 1989; Oerlemans, 1988, 1989; Greuell, 1989, 1992) with the exception of the inclusion of longitudinal stresses. The model is time dependent and calculations were made on a centred, finite difference array at fixed (1000 m) intervals along the glacier flowlines (Figure 1b).

CONTINUITY AND VALLEY PARAMETERISATION

The development of the glacier form through time (t) is governed by the continuity equation assuming ice density remains constant:

$$\frac{\partial H}{\partial t} = m_s - \frac{1}{b_s}\frac{\partial (H\bar{u} b_s)}{\partial x} \quad (3)$$

where m_s is net mass balance, b_s is the glacier width at the surface, $\bar{u}$ is vertically-averaged horizontal velocity and **H** is the ice thickness at each point along the flowline (**X**). Even though this type of model approximates ice flow in one dimension down the valley flowline, the three-dimensional geometry of the valley is implicitly accounted for within the continuity equation through the changing width distribution (b_s). The width distribution is dependent on the local ice thickness and a parabolic approximation of the valley cross section at each point down flowline relates these two variables (Figure 3a). It is taken from Huybrechts et al. (1989) and takes the form:

$$b_s = b_{ref}\left[\frac{H}{H_{ref}}\right]^{\frac{1}{2}} \quad (4)$$

where b_{ref} and H_{ref} are the reference width and height parameters respectively used to define the parabola from which the valley cross-section is approximated and are generated from 1:50,000 scale maps using a

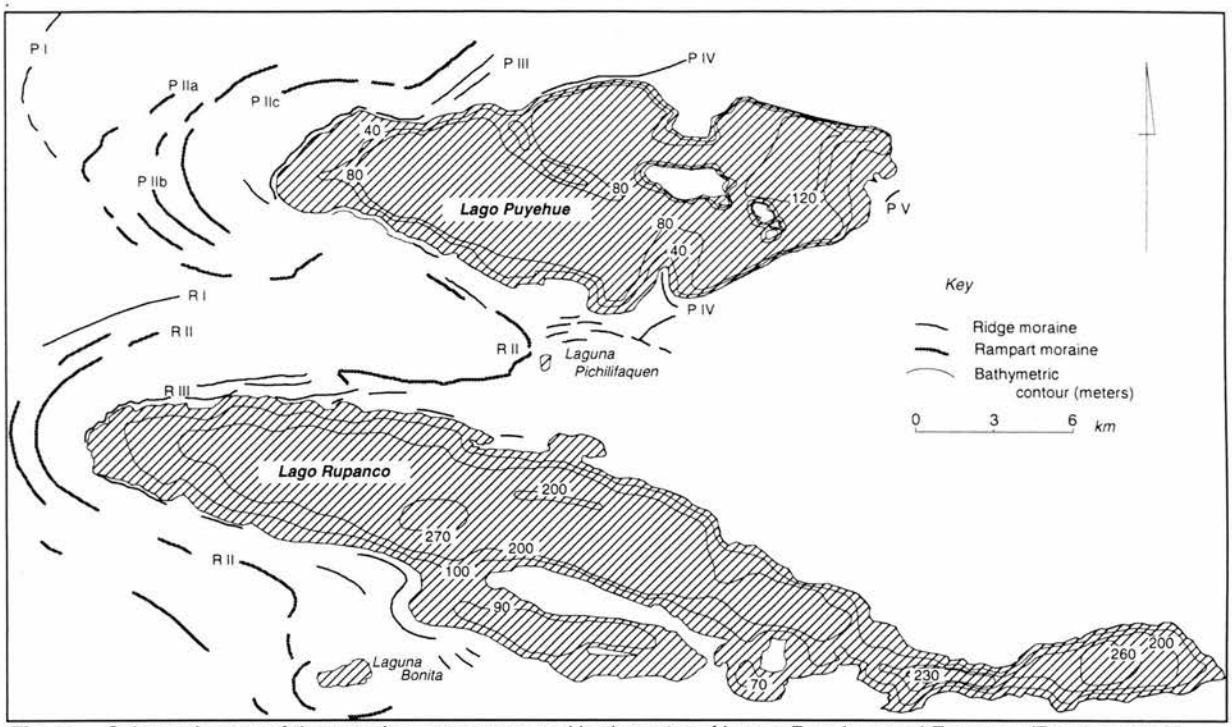

Fig. 2. *Schematic map of the moraine sequences and bathymetry of Lagos Puyehue and Rupanco (Bentley, 1996).*

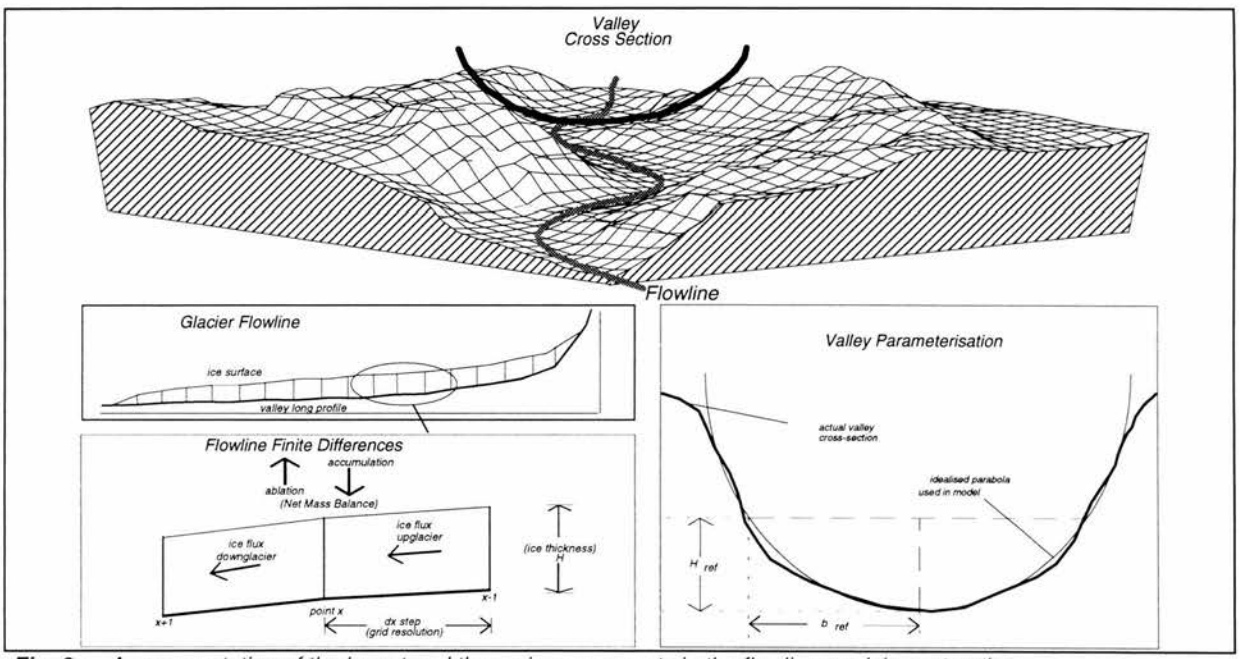

Fig. 3a. *A representation of the layout and the main components in the flowline model construction.*

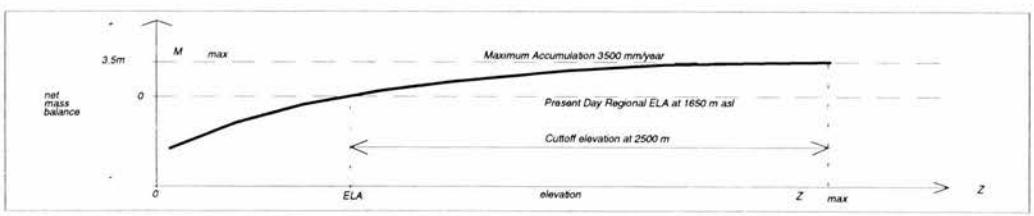

Fig 3b. *Plot of Oerlemans (1980) mass balance formulation. Net mass balance is a parabolic function of elevation, crossing the x-axis at the ELA and levelling out at elevation* $\mathbf{Z}_{\max}$ *with a corresponding maximum accumulation of* $\mathbf{m}_{\max}$.

nominal H_{ref} of 400 m. Changes in the local ice thickness through time therefore occur as a result of a change in balance between ice accumulation and ablation at each finite difference cell (expressed as net mass balance), and the ice flux from adjacent cells up and down the glacier flowline, expressed as horizontal ice divergence - convergence.

LONGITUDINAL STRESSES AND FLOW

The vertically-averaged horizontal velocity is composed of terms for both internal deformation (u_d) and basal sliding (u_s). The modelled stress field is adapted from a numerical scheme developed for the derivation of longitudinal deviatoric stresses at the margin of calving ice sheets by van der Veen (1987). Essentially, at scales where local bedrock irregularities are of a comparable order of magnitude to local ice thickness (Paterson, 1994), the simplified physics used in ice sheet modelling becomes unstable. Local irregularities in the upper and lower glacier boundaries, or high basal water pressures giving rise to hydraulic jacking and basal sliding, introduce longitudinal stresses throughout the glacier profile. These stresses are equivalent to the transfer of extensive and compressive forces up and down the ice mass and when large enough express themselves in crevassing and over-thrusting at the surface.

Derivation of the longitudinal stress deviator follows directly the method described by van der Veen (1987). Essentially the following three equations are solved:

$$\frac{\partial u}{\partial x} = A_d\left[\tau'^2_{xx} + \tau^2_{xz}\right]\tau'_{xx} \qquad (5)$$

$$\frac{\partial u}{\partial z} = 2A_d\left[\tau'^2_{xx} + \tau^2_{xz}\right]\tau_{xz} \qquad (6)$$

$$\tau_{xz}(z') = -\rho g(h-z')\frac{\partial h}{\partial x} + 2\frac{\partial}{\partial x}\int_{z'}^{h}\tau'_{xx}\,dz \qquad (7)$$

where u is the depth-dependent horizontal ice velocity, A_d is a temperature-dependent flow parameter, z' is the vertical ordinate positive upwards, τ'_{xx} is the depth dependent longitudinal deviatoric stress, τ_{xz} is the shear stress, ρ is the mean density of ice, g the gravitational constant, h is the surface elevation of the glacier and H is ice thickness. Equation (5) is substituted into equations (6) and (7) and it is assumed that $\tau'_{xx}(z)$ can be replaced by its vertical mean $\overline{\tau'_{xx}}$. After a number of integrations and substitutions two equations containing two unknowns, u and $\overline{\tau'_{xx}}$ are arrived at. By eliminating u the following expression for $\overline{\tau'_{xx}}$ is derived:

$$\overline{\tau'_{xx}}^3\left\{2\frac{\partial h}{\partial x}\left(\frac{\partial H}{\partial x}-\frac{\partial h}{\partial x}\right)+H\frac{\partial^2 h}{\partial x^2}+\frac{1}{2}\right\}+$$

$$+\ \overline{\tau'_{xx}}^2\left\{\tau_1\left(\frac{2}{3}\frac{\partial H}{\partial x}-\frac{3}{2}\frac{\partial h}{\partial x}\right)+\frac{1}{6}D_1+\frac{3}{2}D\frac{\partial h}{\partial x}\right\}+$$

$$+\ \overline{\tau'_{xx}}\left\{\tau_1^2\left[3\frac{\partial h}{\partial x}\frac{\partial H}{\partial x}+\frac{3}{2}H\frac{\partial^2 h}{\partial x^2}-2\left(\frac{\partial h}{\partial x}\right)^2-\frac{1}{6}\right]+\right.$$

$$\left.+\ \tau_1\left(\frac{1}{3}D+\frac{3}{2}D_1\frac{\partial h}{\partial x}\right)\right\}+$$

$$+\ \tau_1^3\left\{\frac{2}{5}\frac{\partial H}{\partial x}-\frac{1}{4}\frac{\partial h}{\partial x}\right\}+\tau_1^2\left\{\frac{3}{4}D\frac{\partial h}{\partial x}+\frac{3}{10}D_1\right\}+$$

$$+\ \frac{1}{2A}\frac{\partial u_s}{\partial x}=0 \qquad (8)$$

where $\tau_1 = \tau_d + D$, $D = 2H\frac{\partial}{\partial x}\left(\overline{t'_{xx}}\right)$, $D_1 = 2H\frac{\partial \tau_1}{\partial x}$ and $\tau_d = -\rho g H\frac{\partial h}{\partial x}$.

This equation is solved iteratively for each time step in the flow model using the Newton-Raphson method (*Press et al.*, 1986). The solution and subsequent modification of the shear stress (τ_{xz}) through equation 8 is used to compute the components of velocity from internal deformation and basal sliding. A necessary assumption implicit to van der Veen's flowline approach is that the transverse, cross valley deviatoric stress ($\overline{\tau'_{yy}}$) does not significantly influence the stress field. Strictly speaking, this assumption is not consistent with this particular application to valley glacier analysis.

However, on the basis that there are no rapid changes in valley cross section or orientation one can speculate that the cross valley stresses are not significant when compared to τ_{xz} and $\overline{\tau'_{xx}}$. For this reason, and for the sake of simplicity, their influence is ignored.

Greuell (1992) incorporated *van der Veen*'s scheme into his flowline model of the Hintereisferner, Austria but found in sensitivity tests that the resulting glacier dynamics were not significantly altered to justify the considerable computational time necessary for their inclusion into his main experiments. The computed longitudinal deviatoric stress for the Puyehue and Rupanco glaciers is of the same order of magnitude as the basal shear stress, and even exceeds it at the ice margins and divide (Figure 4). Hence, the inclusion of the longitudinal deviatoric stress in this experiment does appear to have a significant effect on modelled ice dynamics through the modification of the shear stress (τ_{xz}) and is justified on this basis. A full description of the scheme and its derivation along with the results of sensitivity analyses and testing falls beyond the scope of this paper.

Other details of the model are relatively straight forward. In view of the altitude and latitude of the area, the glaciers are assumed to be warm based and isothermal, and no variability in basal hydrology is taken into account. Sliding is given by the following expression taken from Oerlemans (1989):

$$u_s = A_s H \tau_{xz}^3 (z_0) \qquad (9)$$

where A_s is a sliding parameter and $\tau_{xz}^3(z_0)$ is the basal shear stress, calculated from equation 7.

MASS BALANCE

A realistic estimate of the net mass balance was achieved through accumulating mass on a three-dimensional elevation model with predefined catchment areas (Figure 1b). The 1 km grid was digitised from 1:50,000 maps and total accumulation for each column was fed directly into the corresponding point in the flowline.

The net mass balance was computed using a elevation/mass balance formulation developed by Oerlemans (1980):

$$m = aZ - bZ^2 \qquad (7)$$

where m is net mass balance, Z is point elevation and a and b are parameters. The resulting plot of net mass balance as a function of elevation which tends to level off at a pre-defined elevation (Z_{max}) where accumulation rate (m_{max}) becomes constant (Figure 3b). The parameterisations for these curves are taken from Kerr and Sugden (1993) who used meteorological data from Puerto Montt and Valdivia to drive an energy balance model in order to reconstruct the regional mass balance curve. Local maximum accumulation is calibrated with rainfall data from two meteorological stations located to the east of Lago Puyehue and set at 3500 mm a^{-1} (*CONAF*, pers. comm., 1993).

MODEL RESULTS AND DISCUSSION

Climatic deterioration within the model is simulated through a stepped ELA lowering from the present day altitude of 1600 m. A set of steady-state surface profiles have been assembled corresponding to ELA depressions ranging from 400 m to 1100 m in 100 m intervals (Figure 5). These experiments reveal a number of interesting points.

Both glaciers require at least 1000 m of ELA lowering to obtain their maximum positions beyond the west end of the lakes. An independent corroboration of this result is provided by Moreno's (in press) palynological analysis of a peat core from a spillway of Lago Llanquihue. Moreno used the altitudinal displacement of modern species to derive an estimated local cooling of 7°C and an annual total precipitation in excess of 4000 mm in the region at c. 21,000 years BP during the last glacial maximum. Together, they represent an ELA lowering equivalent to c. 1000 m. This result is further supported by Porter's (1981) estimation of the regional ELA lowering for the late glacial maximum using a simple elevation analysis of the reconstructed Llanquihue moraines.

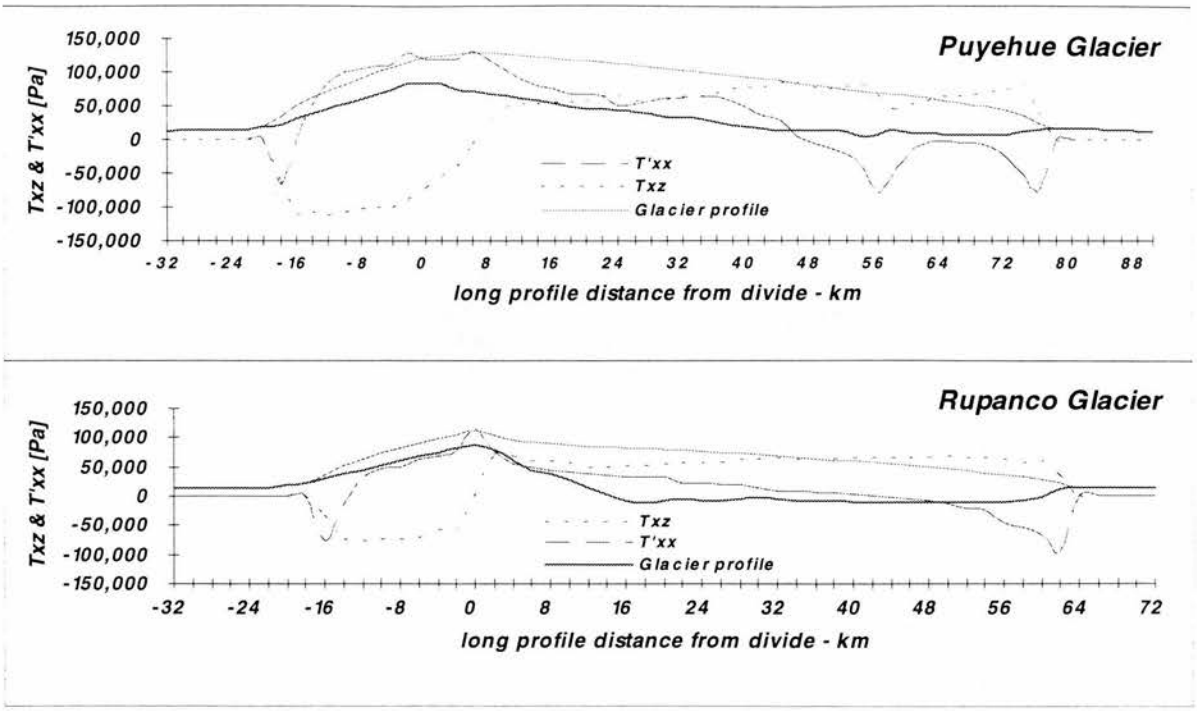

Fig. 4. *Comparison of the computed driving stress (τ_{xz}) and vertically-averaged longitudinal stress deviator ($\overline{\tau'_{xx}}$) for the Puyehue and Rupanco glacier profiles.*

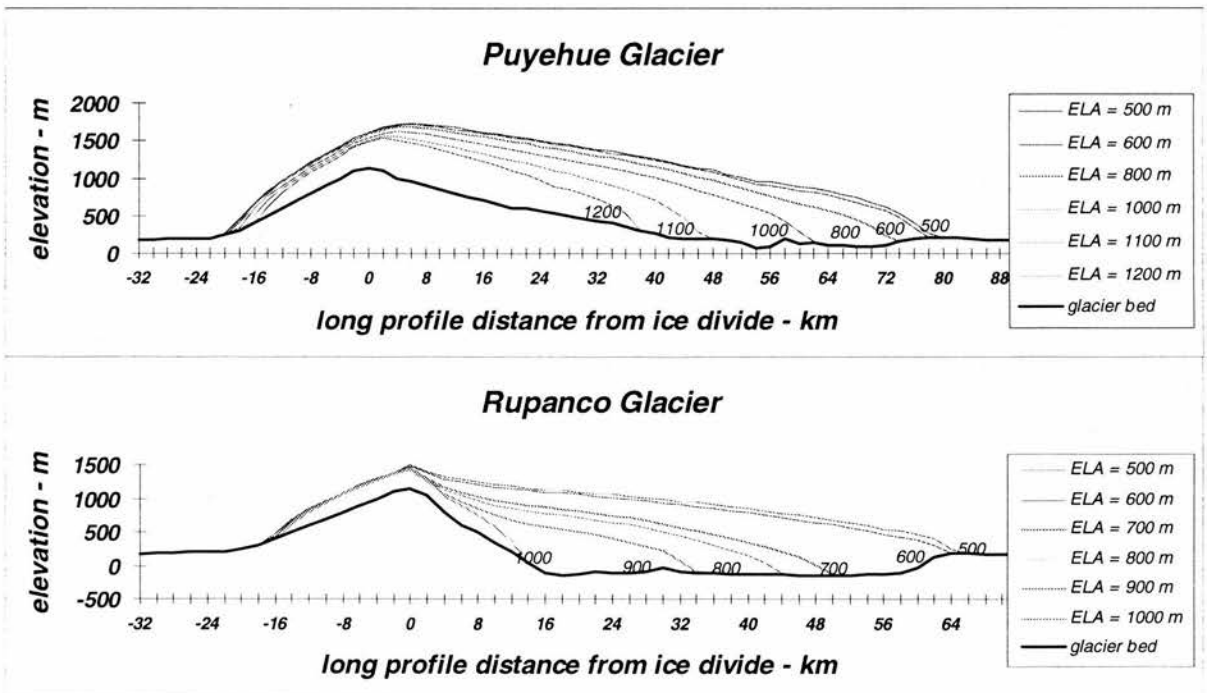

Fig. 5. *Equilibrium surface profiles of the modelled Puyehue and Rupanco glaciers as a function of an incremental lowering of the ELA from 1100 m to 400 m.*

It is worth noting that this lowering is markedly greater than that presented by Hulton et al. (1994) in their modelling investigation of the whole of the late glacial Patagonian ice cap. This discrepancy can be attributed to the grid spacing of 20 km which is adopted in their study and illustrates the general problem of resolution associated with ice sheet modelling as mentioned earlier. Essentially, the relief and mass balance smoothing required for their two dimensional ice sheet model of Patagonia and Tierra del Fuego fails to pick out any of the topographic details associated with the individual valley basins in the area. This scale of model cannot accommodate local build up of independent alpine type valley glaciers and as a consequence any comparison with the local glacial geomorphology is meaningful only at a very crude scale.

With respect to individual glacier dynamics, as expected from qualitative analysis, the Rupanco glacier is indeed more sensitive to ELA lowering than the Puyehue glacier. For example, the Rupanco glacier advances some 14 km (50 to 64 km from ice divide) when the ELA is lowered by 100 m from an altitude of 700 m to 600 m (Figure 5). In comparison, the Puyehue glacier behaves relatively linearly in response to a uniform slope, and a difference in front position of some c. 6 km occurs for each 100 m stepped change in ELA.

In addition, these results suggest that both glaciers appear to decouple from climatic forcing under certain conditions. For example, there is only a 1 km advance in the frontal position of both glaciers when the ELA is dropped from an altitude of 600 m to 500 m (Figure 5). There is a critical length beyond which glacier advance is negligible despite further climatic deterioration. This critical length corresponds with the westward end of the valleys and is related to unconfined spreading of the glaciers over the outwash plain, where high ablation rates render the ice unsustainable. Hence, once the glaciers have extended beyond the confines of the valleys they become increasingly insensitive to further ELA lowering and are effectively decoupled from further climatic forcing. As a consequence of such decoupling the glaciers are likely to stand at these positions for much of their history, hence leading to the formation of the nested sequences of terminal moraines found across the west end of each of the lakes.

A further set of dynamic experiments have been initiated in order to assess the response and sensitivity of the glaciers to climatic forcing. These results suggest that Puyehue is more responsive to climatic change than Rupanco in a number of ways. First, there is the time taken to achieve equilibrium, that is their response time. The Puyehue glacier requires 1000 years to obtain equilibrium, whereas Rupanco requires 2000 years (Figure 6). This contrast is directly related to differences in longitudinal bed profile described by Oerlemans (1989) and is fully consistent with the derivation of $\mathbf{T_m}$ by Jóhannesson et al. (1989a). Hence, Puyehue with an overall steeper, uniform bed slope is more responsive to short term climatic fluctuations than Rupanco, even though the elevation - mass balance feedback enables Rupanco ice to show a greater overall sensitivity in terms of its frontal position.

Second, there is the response to small, short term climatic perturbations. The response of the two glaciers has been modelled as a function of a series of stepped ELA changes through time (Figure 7). In the first 3000 years of simulated time there are three square wave oscillations of the ELA of amplitude 375 m to 500 m with a period of between 300 and 700 years. There is a significantly larger geometric response of Puyehue ice in comparison to Rupanco ice. What is significant here is that although Rupanco may be more sensitive, in terms of its frontal position, to climatic forcing, its response time as a whole is so much slower than Puyehue that it fails to react sufficiently to the fluctuating climatic signal. This prediction is born out by the geomorphic contrasts between the two depositional sequences. As indicated in Figure 2, Puyehue has a suite of terminal moraines at its west end indicating a more sensitive response to climate fluctuations, which are quite different to the simpler, broader ridges that lie west of Rupanco

Finally, there is the differential response of the two glaciers to climatic fluctuations. This is illustrated in Figure 7 from 6,000 to 6,500 years. Puyehue responds to a 300 year period of climatic amelioration by

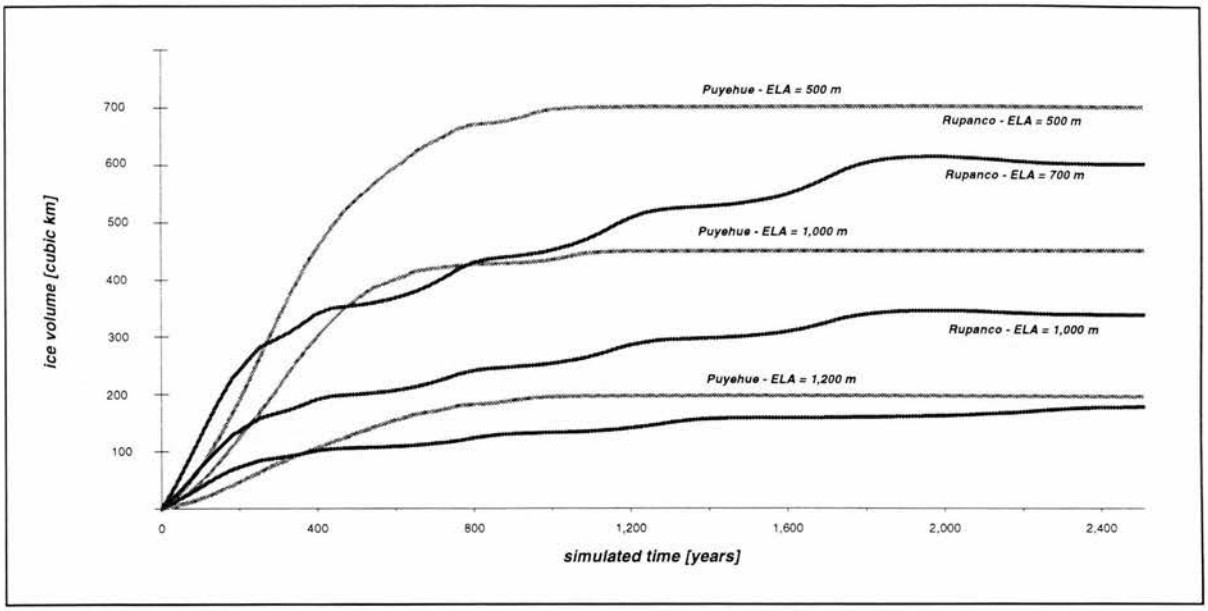

Fig 6. *The evolution of the Puyehue and Rupanco glacier surfaces in 50 year time-slices as they advance to equilibrium positions corresponding to a single stepped ELA depression of 1000 m.*

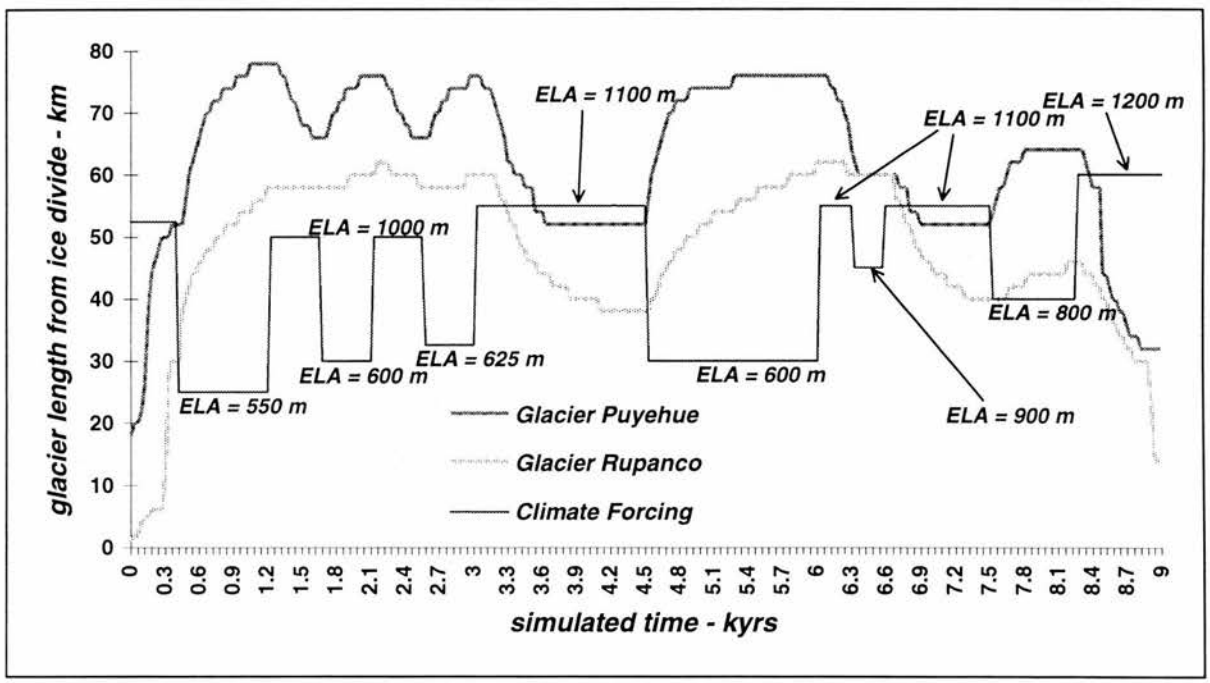

Fig. 7. *Modelled Puyehue and Rupanco glacier front position as a function of a set of stepped ELA changes of different amplitude and duration through time. The frontal plots show the contrasting response of the two glaciers to climatic forcing. Although Rupanco shows greater overall sensitivity to climatic forcing, its response time is so much larger than Puyehue that many of the short term climatic fluctuations fail to significantly effect its position.*

retreating some 20 km from its maximum position whilst Rupanco remains within 2 km of its maximum position. A short period of standstill or re-advance at this point would give rise to a small re-advance of the expanded Rupanco glacier with the potential for depositing ice marginal moraines in the area previously occupied by the Puyehue glacier. Interestingly, it is this type of scenario that could lead to the pattern of the lateral deposits mentioned earlier that lie between the two lakes which were left by Rupanco ice before final climatic amelioration and total deglaciation took place (Figure 2).

It is worth noting that many factors may lead to a differential response between two adjacent glaciers. Specifically, the existence of a saturated bed with high basal water pressures is a possibility as these glaciers were warm based with an abundance of meltwater. A resulting deforming sediment layer or surge-type event could explain the observations in the moraine sequence noted above. Bentley (1996) investigates the possibility of such events on the basis of the glacial geomorphology of the area. Such is the nature of Quaternary reconstruction that it is impossible to discount these mechanisms. However, it must be noted that, in this study, an attempt has been made to isolate and qualify the effect of valley geometry on the palaeo-glaciers' behaviour. Numerical modelling of these glaciers reveals that valley geometry does have a significant effect and that under a hypothetical sequence of climatic fluctuations, which are not too removed from contemporary ideas about late Quaternary climate changes, these glaciers fluctuate in a way which provides both explanation and insight into the glacial record.

CONCLUSIONS

1. A simple model has been constructed and shown to help in the interpretation of the glacial depositional record.

2. In the Lakes District of southern Chile a local ELA lowering of at least 1000 m must be introduced in order to simulate the late glacial maximum positions of these glaciers as indicated by the outer set of nested terminal moraine loops.

3. Valley geometry has a significant impact on the sensitivity and response of valley glaciers. Glaciers that appear to be broadly similar may respond in different ways to the same climatic stimuli.

4. The contrasting response of Puyehue and Rupanco, as indicated by the morainic landforms, may be explained in terms of the different geometries of the valleys in which these two glaciers flow. Other factors may also play a role, but it is important to appreciate that the two valleys are different and that this must influence glacier response to some extent.

5. This research reaffirms that the links between glacier form and climate change are complex, and that caution should therefore be taken when attempting to derive regional glacial chronologies on the basis of a restricted number of depositional sequences. It also illustrates the utility and the benefits to be gained by applying a simple flow model to areas which are subject to intensive glacial geomorphological field study.

CHAPTER 5

HIGH RESOLUTION MODELLING OF THE YOUNGER DRYAS ICE SHEET ADVANCE IN SCOTLAND

ABSTRACT

A two-dimensional, plan-form finite difference ice flow model is coupled to a climate model and applied to a 1 km digital elevation model of Scotland. The flow model is based upon an algorithm for the computation of shear and longitudinal stresses within an ice mass from which the components of internal deformation and basal sliding are calculated. The flow model is coupled to a mass balance formulation where temperature depression and precipitation distribution are specified. Mass loss through ice calving using a depth dependent empirical relationship is also included. The distribution of ice through time is governed by a mass continuity equation which is integrated using the alternate direction implicit method. The Younger Dryas (Loch Lomond Stadial) ice sheet in Scotland is modelled using climate forcing based on the GRIP temperature curve locally adjusted for amplitude using palaeo-ecological temperature data. Time-slice distributions of the ice sheet are qualitatively compared with ice limits generated from field-based reconstructions. These experiments indicate that a significant ice sheet has the potential to build up in the Lochaber massif based on Ben Nevis with an annual temperature depression of as little as 2.5°C, assuming a present day precipitation regime. The 'optimum-fit' simulation requires the introduction of enhanced west-east and south-north precipitation gradients of 25% and 50% respectively, compared to the present day and a July temperature depression of 8°C. The model is constrained by the distribution of glaciers in Skye and Mull in the west, and Lochnagar in the east. Ice advances rapidly, allowing the development of substantial independent and regional ice centres after 550 simulated years, which closely resemble those from field reconstructions. However, the modelled ice sheet is not in equilibrium with the 'optimum-fit' climate after 550 years and continues to expand after this time. This result is at odds with conclusions based on empirical reconstructions which indicate a sustained period of stability of ice for some 200 years at the Loch Lomond Stadial maximum. The discrepancy may be explained by the onset of extreme arid conditions which may have prevailed across Scotland after ca. 400 years associated with the migration of the Polar Front, which effectively starved the ice sheet of precipitation and prevented further expansion.

INTRODUCTION

This paper attempts to link both theoretical and empirical approaches to palaeo-environmental reconstruction by using a numerical coupled ice flow and climate model to reconstruct the evolution of the Loch Lomond Stadial (Younger Dryas) ice sheet in Scotland along with the palaeo-climatic envelope responsible for it. Current knowledge about environmental conditions during the Loch Lomond Stadial in Scotland comes primarily from two sources: glacial geomorphology and palaeoecology. Glacial geomorphological fieldwork is concerned with depositional evidence left primarily during the maximum extent and retreat stages of the ice sheet, and erosional features which may have formed at any point and time when the ice sheet was wet based. Since much of this evidence lacks chronological control, and as several ice flow directions may be represented at a given locality, time-dependent reconstructions of ice flow patterns cannot be made from the geomorphological record alone (Kleman, 1995; Roberts, 1991). In addition, retreating ice can destroy or disrupt evidence of previous flow and extent; hence little is known about the pattern of ice growth and flow during the build-up of the ice sheet. Palaeoecological reconstruction is also limited. By making assumptions about fauna and flora species abundance and distribution, an approximate amplitude of a climatic deterioration during the stadial is possible, but again these data often lack tight chronological control, are spatially generalised and are limited to areas remote from glaciers.

Coupled glacier and climate modelling experiments provide one method of addressing the problem of palaeo-environmental investigation. Modelling can assist in understanding the growth and retreat of the Loch Lomond Stadial ice sheet by providing chronological reconstructions of ice thickness and flow directions for the entire evolution of the ice sheet. Furthermore, modelling provides the link between form

and process. It is possible to specify particular palaeo-climatic boundary conditions within a modelling experiment, thus enabling a coherent combination of lines of disparate field data constraining ice sheet form to be tested critically. In the present study this procedure enables reconstructed temperature series, maximum ice limits and ice sheet geometry derived from geomorphological mapping to bracket other unknowns, such as precipitation pattern, which are required to generate a particular configuration.

Essentially deductive, this procedure utilising empirical evidence to constrain glacier-climate models appears to be relatively simple and aims at an ideal 'optimum-fit' simulation. However, in practice, the approach is inherently complicated; based on repetitive, non-systematic model re-runs, where testing requires the 'qualitative' comparison of data in four dimensions against a numerical experiment in which there are a number of rheological and climatic degrees of freedom involved. In addition, the approach involves a number of assumptions regarding the modelling of ice flow and climate as well as the accuracy and interpretation of field mapping. However, palaeo-ice sheet reconstruction by its nature is an inexact science; it is multi-disciplinary and an approach where there is no single answer, but where a range of scenarios have to be investigated and refined as more data and techniques emerge. This paper presents a first step in developing a model at sufficiently high resolution to provide an effective link between theoretical and empirical methods of investigation. It is hoped that it will demonstrate the potential that such modelling has in the role of Quaternary ice sheet reconstruction.

Specifically the aims are to:

- provide a series of time-slices of ice-thickness and extent of the reconstructed Loch Lomond Stadial ice sheet during its cycle of growth which closely fit available field-evidence;
- investigate the behaviour and dynamics of the ice sheet throughout its evolution, identifying key thresholds in the system;
- isolate the palaeo-temperature and precipitation envelope which gives rise to this 'optimum-fit' ice sheet.

APPROACH

In order to achieve these aims it is necessary to model ice sheet behaviour at a sufficiently high spatial resolution to enable a meaningful and accurate comparison with the available field evidence. Previous ice sheet modelling studies in Scotland (Payne and Sugden; 1990, Kerr; 1993) illustrate a discrepancy between the scale of the models and the glacial geomorphology against which they are compared and tested. Whereas these models operate at grid resolutions of at least 5 km, the depositional landforms against with which they are constrained occur in the field at a scale of 100s of meters. This imbalance of scale is addressed in the present study by constructing an ice flow model which operates on a finite difference areal grid of 1 km resolution. Whilst this is still not perfect for the interpretation of specific geomorphological landforms, reconstructions of individual outlet glaciers and other small ice sheets are possible. This high resolution is made possible by including some important glaciological physics ignored in previous ice sheet models, namely deviatoric longitudinal stresses. Computation of these stresses modifies the velocity terms within the model and helps overcome the main obstacle of scale imposed on previous ice sheet simulations.

The Younger Dryas has attracted a lot of attention and can be viewed as the last 'flip' in the north Atlantic thermohaline circulation which has been identified as a possible mechanism for the initiation and transfer of a ice-age signal around the world. The intensity and rapidity of the shift into cold conditions which characterised this period has significant consequences for contemporary ideas regarding global environmental and climatic change. It represents a short, sharp return to glacial and periglacial conditions in the northern Atlantic between 11,000 and 10,000 radiocarbon years BP which was terminated abruptly by a period of rapid climatic warming by c. 10,000 yrs BP (Atkinson et al., 1987; Dansgaard et al., 1989; Bennett and Boulton,

1993). During this intense cold phase small ice-fields and corrie glaciers formed in highland Britain and an ice sheet accumulated in the Scottish Highlands (Sissons, 1979; Gray, 1982; Thorpe, 1986; Ballantyne, 1989). This Lateglacial readvance in the Scottish Highlands, called the Loch Lomond Advance, has been the focus of considerable field research for the last 30 years with the central theme focusing on the reconstruction of the surface form of the ice sheet and of the valley glaciers associated with it (Ballantyne and Gray, 1984; Gray and Coxon, 1991; Bennett, 1991). These ice limits have been continually refined in numerous small-scale studies but are still ambiguous is many areas (Gray and Coxon, 1991).

Although there has been much interest in the Younger Dryas event there are sparse local palaeo-climatic data with which to constrain the model. A curve of estimated mean July temperatures, based on fossil coleopetera assemblages, indicate a steady decline from 12,500 years BP, when mean annual temperatures were similar to the present day, to c. 8°C by 10,000 years BP, after which there was rapid warming and recovery within 300 years (Coope, 1975; Fig. 1a). Although the estimated amplitude of this reconstruction is not in dispute, the shape and duration of the curve is at odds with recent findings from deep sea ocean cores and the Greenland ice cores. Bond et al., (1993) oxygen isotope analysis of the GRIP ice core gives a high resolution record of the frequency, duration and magnitude of the temperature fluctuations throughout the period (Fig. 1b). These data indicate that the Younger Dryas event was characterised at the summit of the Greenland Ice Sheet by an extremely rapid annual mean temperature depression of the order of 20°C. The timing and intensity of this deterioration has been closely correlated with temperatures reconstructed for north Atlantic sea surface temperatures from foram analysis (Bond et al., 1993). Furthermore, the GRIP data indicate that this 'epoch-defining event' was much shorter than previously believed (Dansgaard et al., 1989). Isotope analyses indicate that the initiation of the event at c.11,000 yrs BP is consistent with previous estimates (CLIMAP, 1984; Ruddiman and McIntyre, 1981). However, they show that at 10,700 yrs BP, in a period of less than 20 years, air temperatures over the North Atlantic region warmed and the climate had fully recovered within 50 years.

The amplitude of this fluctuation from the GRIP core may not regionally transferable. However, the timing and frequency of fluctuations are likely to be tele-connected across the North Atlantic due to the rapid response time of the ocean-atmosphere system. In this study it is assumed that the temperature time series for Scotland during the Younger Dryas is qualitatively similar to that of GRIP isotope analysis. However, the curve is modified and locally calibrated for amplitude using model climate sensitivity analysis which is in strong agreement with Coope's (1975) estimate of maximum July temperature depression of 8°C (Fig. 1c).

The overall problem can thus be posed in terms of using fieldwork reconstructions of ice extent and sparse palaeo-climatical data indicating the amplitude and duration of the stadial in order to constrain the boundaries of a time-dependent numerical experiment. In turn, the model has the potential to elucidate the gaps that exist in knowledge over the evolution, behaviour and extent of the ice sheet and the palaeo-climatic forcing. The limits and ice surface reconstructions used to constrain the model are based on a number of regional studies (Fig. 2). For the purposes of this study, they have been broadly divided into two separate groups based on location; those which investigate parts of the main ice sheet and associated outlet glaciers and those which investigate smaller, outlying isles and areas not affected by the main ice sheet. The strategy behind this division is that the outlying, smaller glaciers located to the north, west and east provide an experiment by which the precipitation pattern for the stadial can be constrained. They include the Isle of Skye (Ballantyne, 1989, 1994; Benn et al., 1992); the Cairngorms (Sugden, 1970; Brazier et al., 1996) and the Isle of Mull (Thorp, 1984, pers. comm., 1996). It is assumed in these outlying areas that localised climate modification through ice build-up/mass-balance feedback was minimised. The second group of studies are then used for a qualitative comparison and validation of the modelled ice sheet. These cover field studies of the ice sheet north of the Great Glen (Bennett and Boulton,

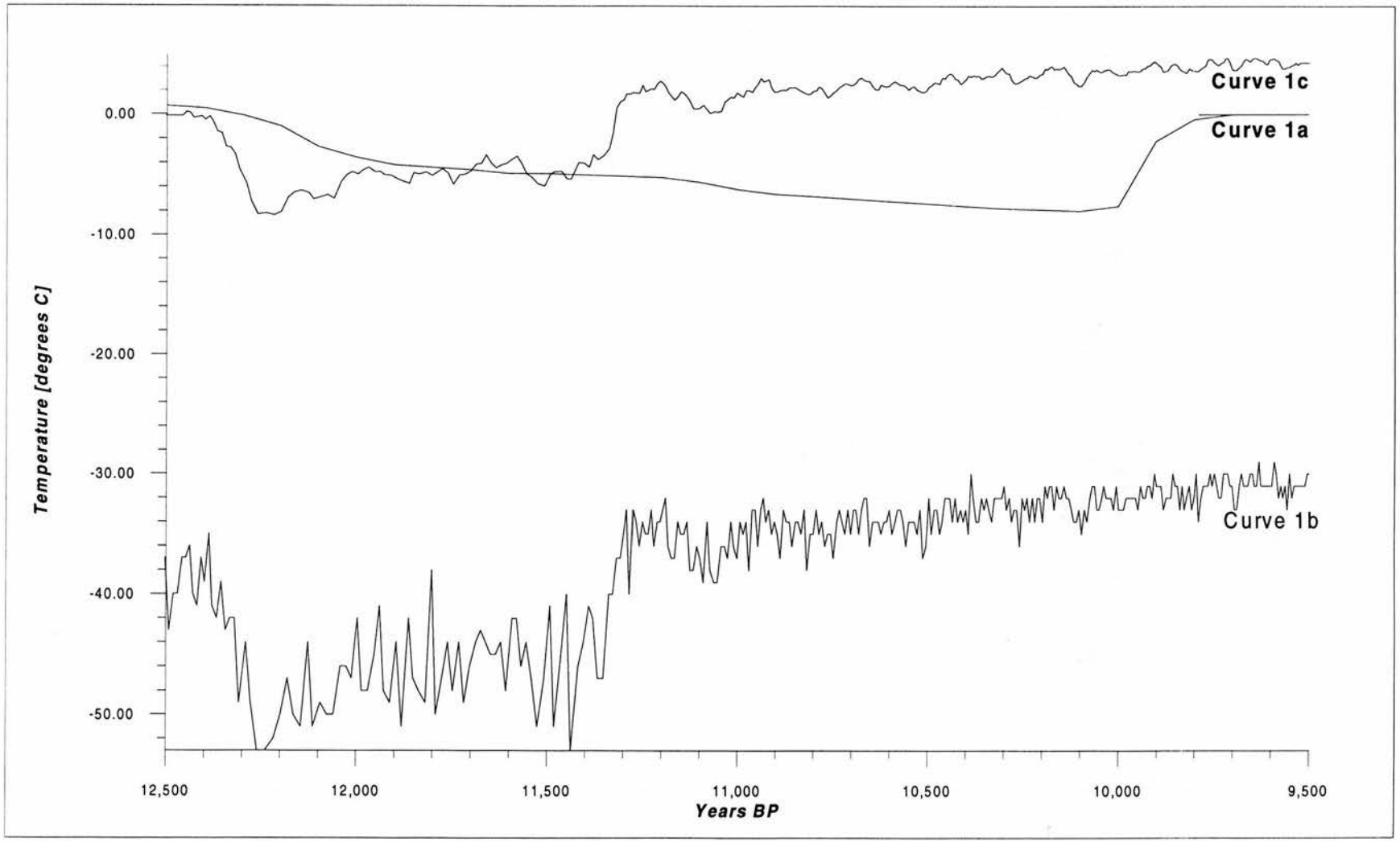

Figs. 1a. *July temperature depression for the Loch Lomond Stadial derived from Coleoptera assemblages (Coope, 1975)*

Figs. 1b. *Absolute temperature for the Younger Dryas at the summit of Greenland derived from the GRIP oxygen isotope record (Bond, Broecker and Dansgaard, 1983)*

Figs. 1c. *The temperature curve used to drive the model based on the locally calibrated GRIP curve with a maximum July temperature depression of 8 degrees C.*

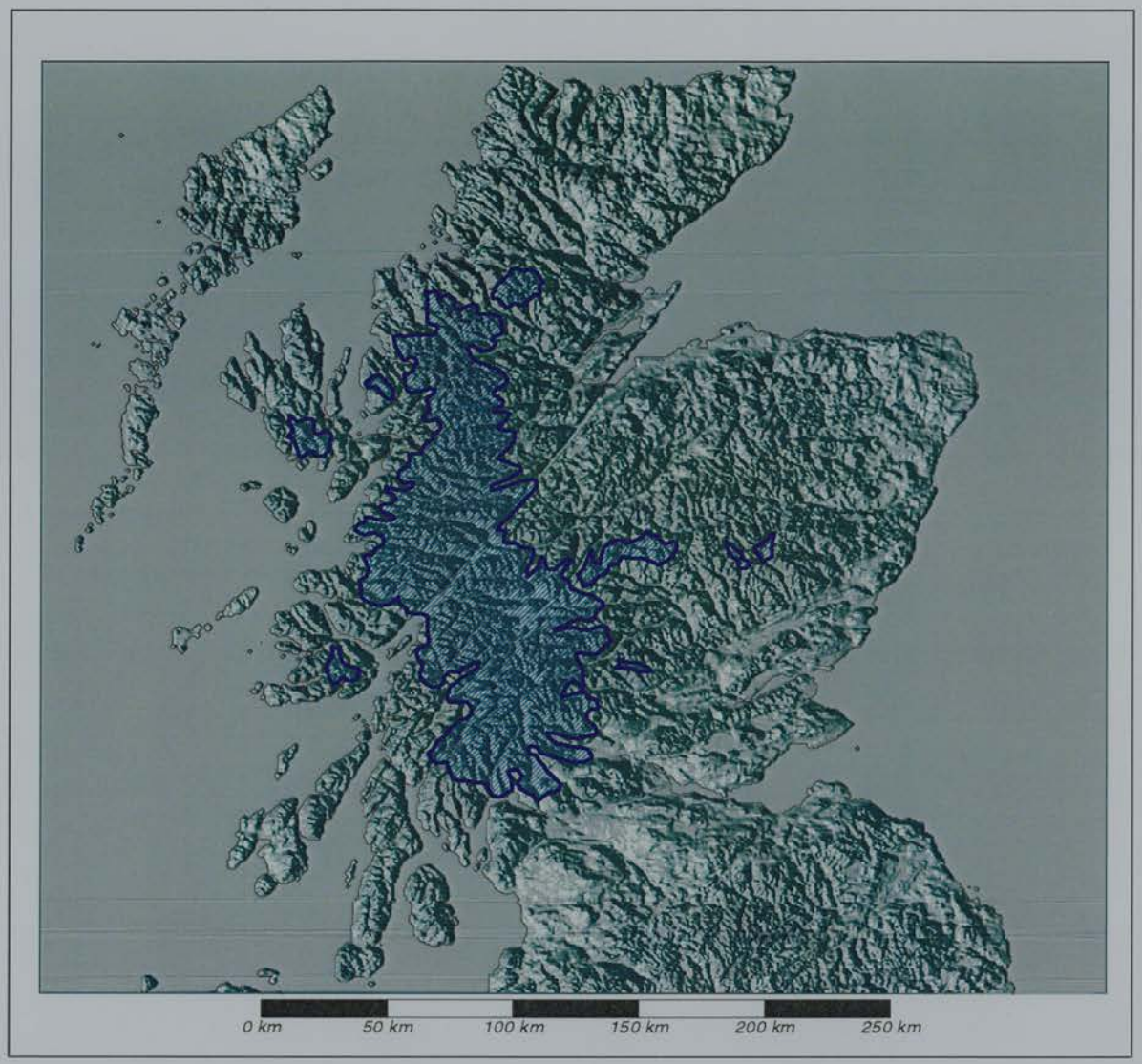

Fig. 2. *The extent of the Younger Dryas ice cap over Scotland as derived from a number of empirical reconstructions based on the field mapping and interpretation of glacial depositional and erosional features. Sources: Ballantyne, 1989; Bennett, 1991; Gray, 1975; Sissons, 1967; Sutherland, 1984; Thorp, 1986 and Green, 1995.*

1993); the ice sheet south of the Great Glen (Thorp, 1984, 1991, pers. comm., 1996) and western Lochaber (Green, 1995).

THE MODEL

Apart from computation of longitudinal stresses, the physics and numerics of the model are documented elsewhere (Mahaffy, 1976, Huybrechts and Oerlemans, 1988, Huybrechts, 1986, Payne and Sugden, 1990 and Hubbard, 1996). Time-dependent calculations are made on a 250 x 200 centred, finite difference grid at 1 km resolution. The main Inputs are: values for glacier sliding ($\mathbf{A_s}$) and flow ($\mathbf{A_d}$) parameters, basal topography (Fig. 3) and the net mass balance (**b**) averaged onto the central difference node of each cell. Assumptions used in the model's construction and application include:

- ice is isothermal;
- basal sliding is decoupled from hydrology;
- there is no variability in the basal hydrological system;
- the subglacial bed does not deform;
- the Loch Lomond Stadial topography has not changed substantially from the present day;
- little (< 10 m) relative isostatic or eustatic compensation took place during the Loch Lomond Stadial.

The evolution of the ice sheet thickness over time is given by the continuity equation:

$$\frac{\partial H}{\partial t} = b - \nabla (H\bar{u}) \qquad (1)$$

where **b** is net mass balance, $\bar{u}$ is vertically averaged horizontal velocity and **H** is ice thickness at each node. Changes in the local ice thickness through time therefore occur as a result of a change in balance between ice accumulation/ablation (expressed as net mass balance) and the vertically integrated ice flux from adjacent grid points, expressed as horizontal ice divergence/convergence. By replacing the horizontal flux term in equation (1) with a diffusion term, the above equation is numerically formulated and integrated using the Alternate Direction Implicit (ADI) method and solved on a Gaussian tridiagonal matrix (Press et al., 1986). Computation time and stability of the scheme are key factors in the applicability of ice sheet models; on a 250 x 200 km grid using a time step of 0.025 years, the model required c. 12.5 hours on a DEC Alpha workstation to integrate a simulation of 1,000 years.

Longitudinal Stresses and Flow

The vertically integrated horizontal velocity ($\bar{u}$) is composed of terms for both internal deformation ($\mathbf{U_d}$) and basal sliding ($\mathbf{U_b}$). Longitudinal stresses are computed using a numerical scheme developed for the derivation of the deviatoric stress gradients at the grounding zone of calving ice sheets. At high resolutions local bed undulations approach an order of magnitude comparable to the local ice thickness. This means that surface and bed gradients become large thus rendering the shallow ice approximation, on which most ice sheet models are based, inapplicable (Hutter, 1983; Paterson, 1994, Hubbard et al., 1996). Large changes in local surface and bed slope induce longitudinal stress gradients within the ice mass (tensile and compressive forces) which in the extreme case are expressed as crevassing and faulting and/or folding. The present modelling scheme relates ice surface stretching, the Jacobian component of surface velocity ($\mathbf{u_s}$) to the longitudinal stress deviator ($\bar{\tau}'$) based on an assumption of negligible internal deformation compared to basal sliding:

$$\bar{\tau}' = \left(\frac{1}{A} . \frac{\partial U_s}{\partial x} \right)^{\frac{1}{n}} \qquad (2)$$

where $\mathbf{A} = 0.081$ bar^{-1} a^{-3} the flow parameter, and **n**, the power exponent is set at 3. The resulting value for the longitudinal stress deviator ($\bar{\tau}'$) is then used to modify the driving stress (τ_d) based on a correction term to the shallow ice approximation:

$$\tau_d = \rho . g . H . \frac{\partial h}{\partial x} + 2 . \frac{\partial (H . \bar{\tau}')}{\partial x} \qquad (3)$$

where ρ is the density of ice, **g** is acceleration of gravity and **h** is the surface elevation. Equations II and III are finally closed through re-evaluation of the surface velocity using Glen's flow law:

$$U_s = \varepsilon_{xz} = 2A . (\tau')^{n-1} . \tau_d + U_b \qquad (4)$$

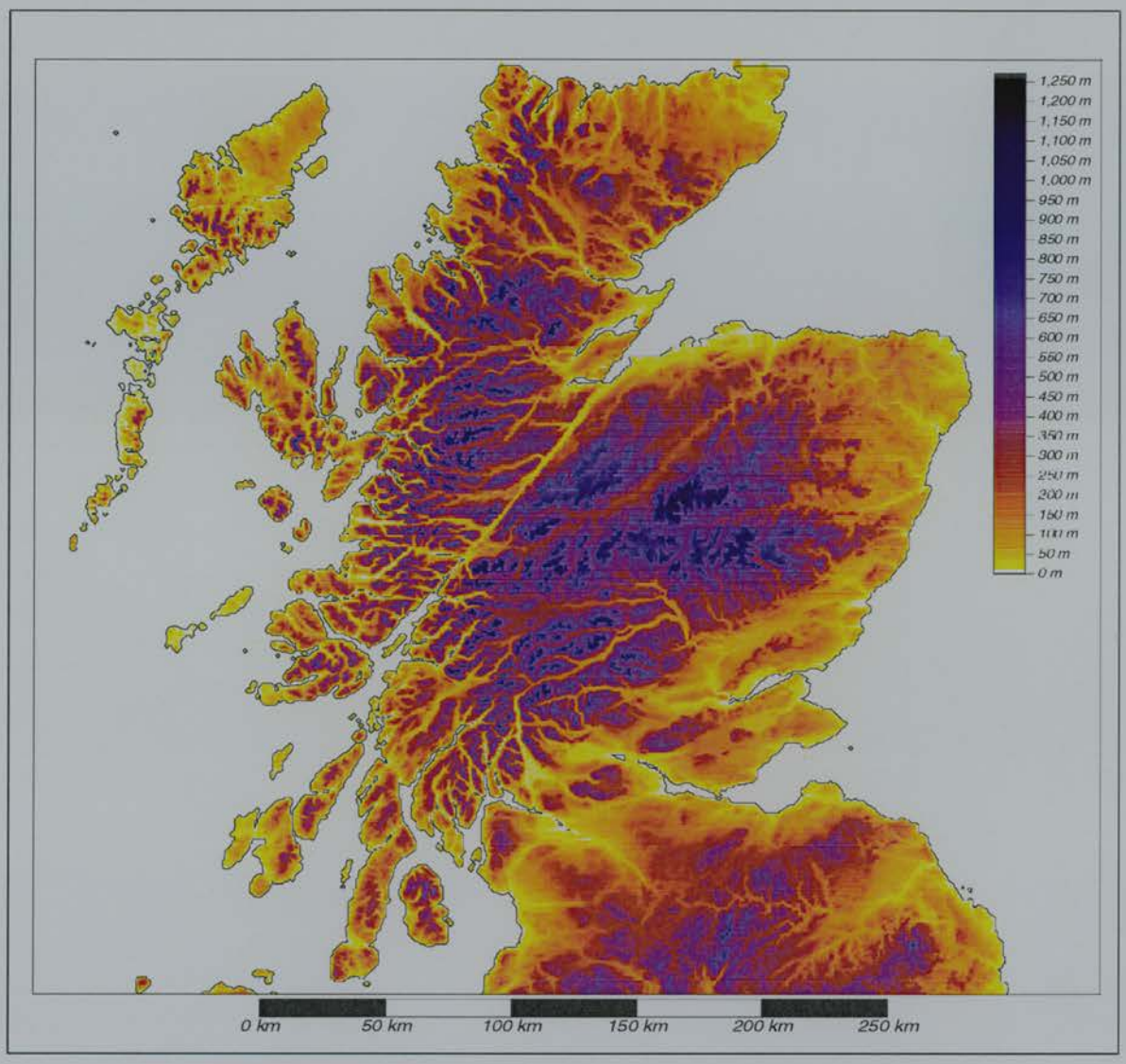

Fig. 5. *1 km digital elevation model of Scotland used as the basal topographic boundary condition.*

where τ' is the effective stress calculated from the second invariant of the stress tensor and U_b is the basal sliding component from Oerlemans (1989):

$$u_b = A_s H \tau_d^3(z_0) \quad (5)$$

where A_s is the sliding parameter and $\tau_d^3(z_0)$ is the basal shear stress calculated from equation III.

On computation of an initial estimate for longitudinal stress, the above three equations can be numerically relaxed using a straightforward iteration. On convergence, this scheme solves the vertically integrated internal stress/velocity field across the ice sheet for the given ice sheet geometry.

Mass Balance

The calculation of net mass balance (**b**) follows the method used by Payne and Sugden (1990) which relates the three quantities ablation (**Ab**), precipitation (**P**) and fraction of precipitation falling as snow, effectiveness (**Eff**):

$$b = P.Eff - Ab \quad (6)$$

Effectiveness is related to air temperature which is in turn related to surface elevation (**E**) and latitude (ϕ) using the following regression:

$$Eff = -0.698 + 0.014\phi + 0.224E \quad (7)$$

The variability of effectiveness is related to climatic change through the imposed annual isotherm shift at sea level associated with warming or cooling using a lapse rate fixed at 6.5°C km^{-1}. Ablation in the form of surface melt is calculated from a regression equation derived by Budd and Smith (1981), which predicts the present day distribution of ablation rates as a function of elevation and latitude in the form of:

$$\log_{10}Ab = 1/m(E - E) \quad (8)$$

July Temperature (T_{July}) is related to the mean annual temperature (T_{annual}) depression through the following equation:

$$\nabla T_{July} = \nabla T_{annual} / f \quad (9)$$

where **f** = 2.571 and present July temperature is taken as 17.0°C. Hence, annual temperature depression is taken to be c. 2.5 times greater than the July temperature depression, reflecting the greater seasonal amplitude associated with cooling.

The final variable required for the mass balance model is the mean annual precipitation for which the present day spatial distribution is taken as an initial base estimate (Fig. 4a). The initial distribution is subsequently adjusted for the model experiments by introducing enhanced south-north and west-east gradients through the following algorithm:

$$P_{LLS} = P_{present} x(WE_{size} - WE_{position})x(G\%_{WE}/WE_{size}) \quad (10)$$

where P_{LLS} is the Loch Lomond Stadial precipitation at each grid cell, $P_{Present}$ is the present day precipitation, WE_{size} = 250, and is the grid array size in the west/east direction, $WE_{position}$ is the position of the grid cell (0 in the west, 250 in the east) and $G\%_{WE}$ is percentage of imposed precipitation reduction. The algorithm for calculating the south to north enhanced precipitation reduction follows identical form where SN_{size} = 200. By adjusting the gradients $G\%_{WE}$ and $G\%_{SN}$ the magnitude and pattern of precipitation across Scotland can be modified. Modification of the Loch Lomond Stadial mass balance across Scotland is therefore possible through the tuning of the precipitation variables and the imposed temperature depression through time.

MODEL CALIBRATION AND SENSITIVITY

Flow and Sliding Parameters

The aim of the calibration runs was to validate the choice of sliding (A_s) and flow (A_d) parameters and investigate the sensitivity of the model to systematic changes in them. This was achieved by growing the ice sheet using the present day precipitation pattern and a single, stepped temperature depression (∇T_{annual}) of variable magnitude until the ice sheet achieved an equilibrium state in the western Lochaber region which matched the limits reconstructed from field mapping by Green (1995) (Fig. 2). On matching the ice limits, Green's trimline reconstructions for Loch Linnhe provide

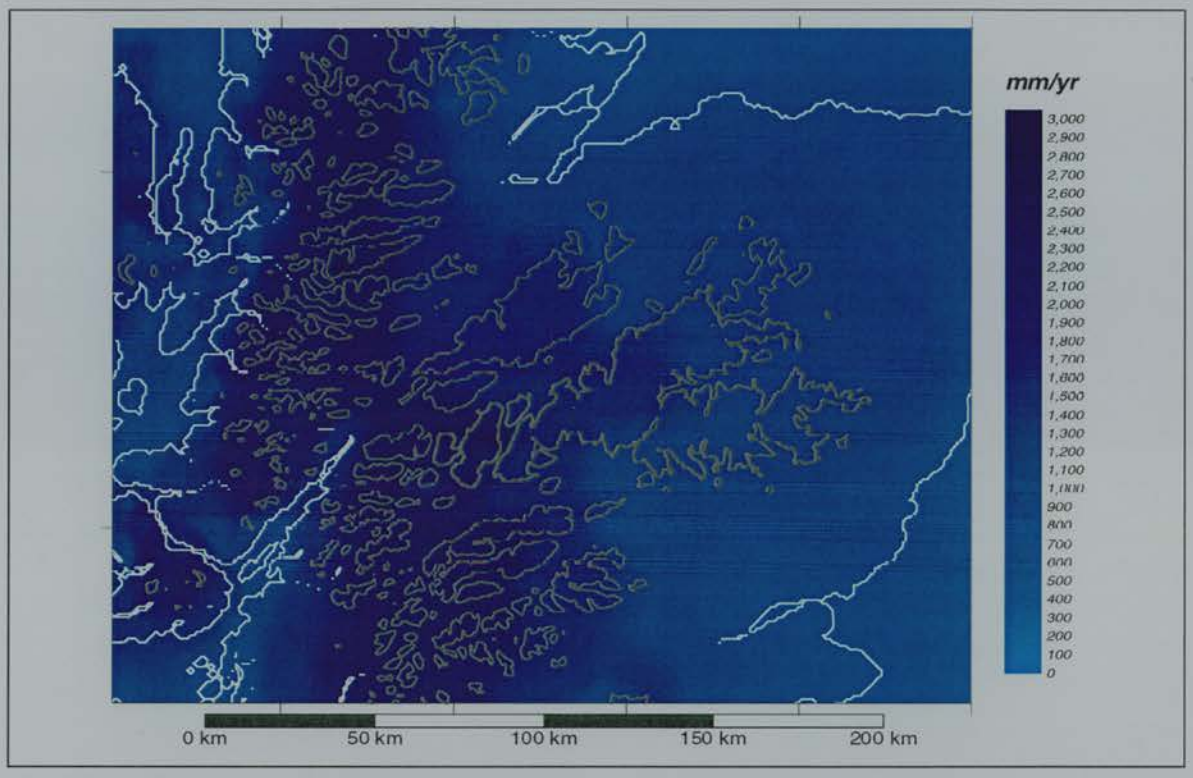

Fig. 4a. *The present day precipitation pattern across Scotland used as the initial distribution for the calculation of the net mass balance.*

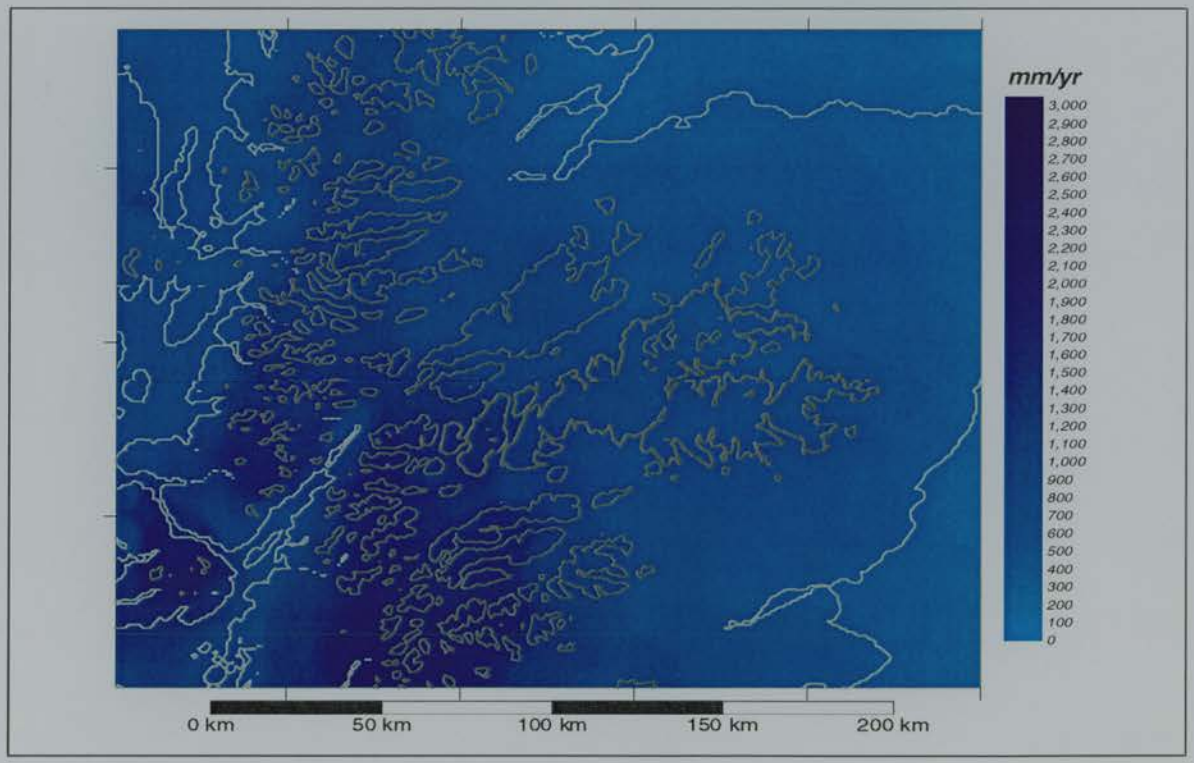

Fig. 4b. *The reconstructed precipitation pattern across Scotland for the early stages of the Younger Dryas based on the distribution of the maximum limits of glaciers in Skye, Mull and Lochnagar. The optimum model fit corresponds to* $\nabla T_{annual} = -7^{\circ}C$ *(*2.571) and* $G\%_{WE} = 40\%$ *and* $G\%_{SN} = 50\%$ *for the climatic parameters.*

an indicator of the correct longitudinal profile of the Loch Lomond Stadial ice sheet and comparison with the modelled profile provides evaluation of the flow and sliding parameters which control the effective viscosity of the modelled ice sheet.

Under the present day precipitation regime, modelled glaciers form on Ben Nevis with a mean annual temperature decrease ($-\nabla T_{annual}$) of 2.5°C. However, the minimum mean annual temperature forcing required to advance the ice sheet to Green's reconstructed limits was (∇T_{annual}) of -5°C. Comparison of observed trimline reconstructions with the modelled ice sheet profile for Loch Linnhe reveals that the values for A_s and A_d given in the previous section provide a good match (Fig. 5). Systematically varying the parameters by up to an order of magnitude in either direction makes little appreciable difference to the modelled ice profile. In addition, the initial choice of the parameters results in a glacier flow regime partitioned equally between deformation and sliding, giving a maximum surface velocity of c.160 ma^{-1}. Although there is no empirical data validating this result, the abundance of ice/bed contact (erosional) features across this region of the Western Highlands associated with the Loch Lomond Stadial ice sheet indicates that an appreciable component of basal sliding must have been taking place. Furthermore, varying A_s and A_d in opposing directions tends to cancel the overall effect as each parameter compensates for the other. This is due to the equations describing basal sliding and internal deformation taking similar form with an identical τ_d^3 term. These results suggest that the flow model is reasonably insensitive to changes in A_s and A_d. Furthermore, the good level of agreement between the modelled and observed longitudinal profiles in western Lochaber indicates that the model is functioning adequately.

MODEL RESULTS

Climatic Tuning

The climatic tuning runs aim at isolating the envelope of possible combinations of temperature depression and precipitation distribution across Scotland during the Loch Lomond Stadial. Over 40 model runs were initiated; in each run the climatic variables were varied systematically. The present day precipitation distribution was modified by introducing west to east and south to north gradients through $G\%_{WE}$ and $G\%_{SN}$ and cooling was simulated through a single, stepped temperature depression of varying magnitude (∇T_{annual}). The first experiment was configured in such a way that the model output was required to reproduce ice limits based on empirical studies. Modelled ice extent was compared against limits based on field reconstruction in the outlying glacierised areas of Mull, Skye, Lochnagar and the Cairngorms (Fig. 2). Deviation from or convergence with the required match allowed the climatic variables to be tuned more finely for each successive run.

Precipitation Distribution

In order to constrain the Loch Lomond Stadial precipitation distribution, locations were chosen outside the margin of the main Loch Lomond Stadial ice mass where small, independent and isolated ice caps or cirque glaciers existed and where their limits had been investigated in detail in the field. These sites have the advantage that they minimise the effects of the ice-elevation/mass balance feedback and therefore provide a good fix on the regional precipitation pattern. Thus, it is possible to investigate the required climatic forcing necessary to simulate these known limits.

The Isle of Skye (Ballantyne, 1989, Ben et al 1992) and Mull (Thorpe, pers. comm.) on the west coast and the Cairngorm massif (Brazier et al., 1995) in the east provided ideal case sites. The Loch Lomond Stadial limits at these areas have been investigated in detail in the field and their longitudinal and latitudinal spread allows an effective analysis of the precipitation gradients during the stadial. Implicit in this experiment are four assumptions; that the ice masses obtain their maximu limits simultaneously, that they are sensitive responders to climatic change, that those in the coastal locations of Skye and Mull do not become climatically decoupled through the process of calving, and that the imposed temperature depression is uniform across Scotland. Kerr (1993) concludes that maritime ice masses characterised by large mass balance fluxes

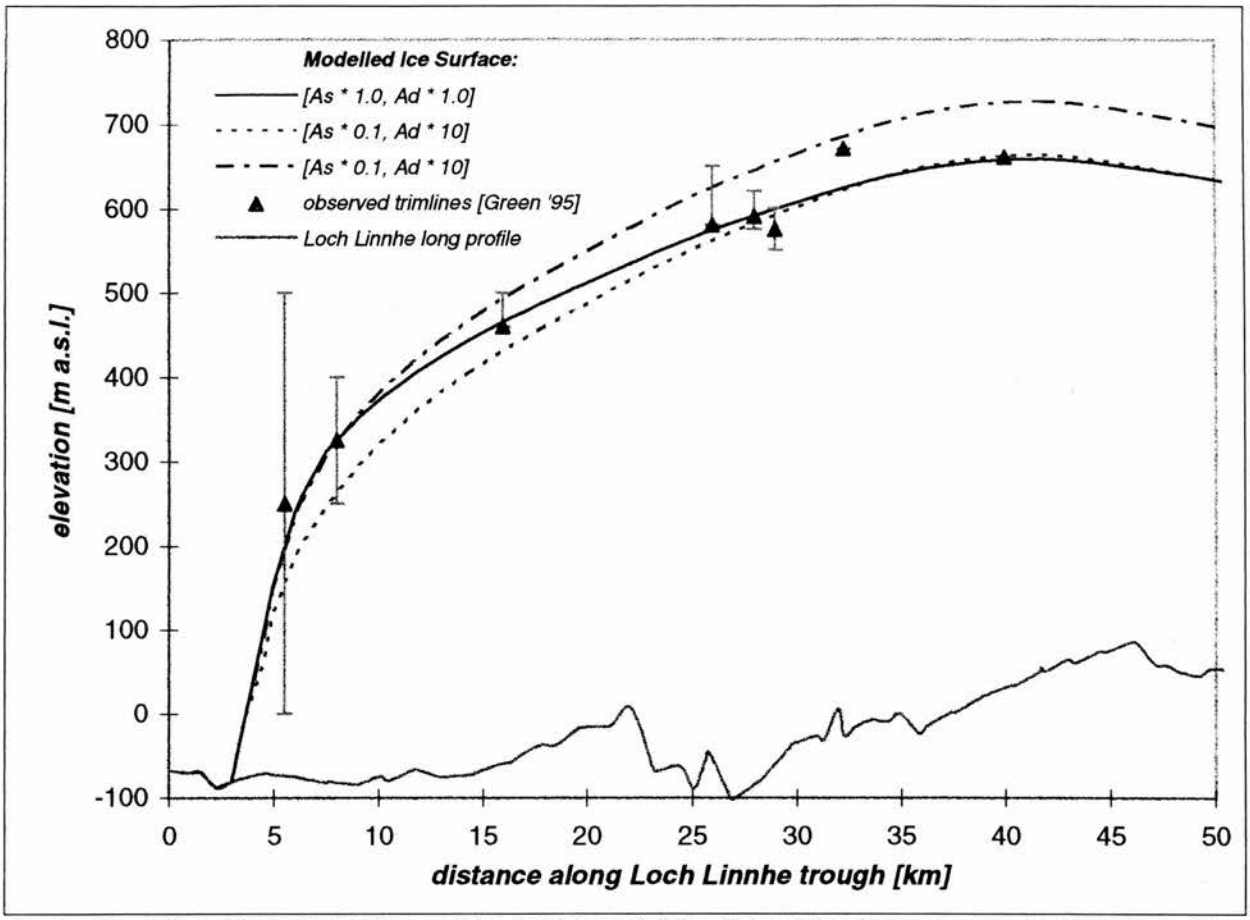

Fig. 5. *Fine tuning and sensitivity of the model to the values of sliding (As) and flow (Ad) parameters by comparison of the simulated Loch Linnhe outlet glacier long profile to mapped trimlines (Green, 1995). Order of magnitude perturbations in the parameters reveal the model is relatively insensitive to variations in these parameters.*

are extremely sensitive to climatic change and there is no reason to assume that such small ice masses did not behave synchronously. The third assumption concerning calving is difficult to justify. However, modelling indicates that calving does not become the significant mode of ablation in the case of Skye and Mull until expansion takes place beyond the Loch Lomond Stadial limits. Geomorphological evidence from the Cairngorms (Brazier et al., 1995) indicate that no significant ice mass built up in this area during the Loch Lomond Stadial. Hence, in eastern Scotland the requirement was for the modified climatic variables to result in local cirque type glaciers only.

Modelled limits of the Skye and Mull ice masses after 500 simulated years with ∇ $\mathbf{T}_{annual}$ = -7°C (*2.571) and $\mathbf{G\%}_{WE}$ = 40% and $\mathbf{G\%}_{SN}$= 50% gave the 'optimum-fit' with limits based on glacial geomorphological reconstruction. The reproduction of these limits required the introduction of enhanced south to north and west to east gradients to the present day precipitation distribution. Existence of permanent snow patches near the summit of Cairngorm today suggests the area is susceptible to ice build up as a result of a small deterioration in the present day climate. Introduction of a strongly enhanced west to east gradient reducing overall precipitation to c. 25% of present day over the Cairngorm massif was necessary to suppress ice expansion there. In addition, a south to north gradient of 50% was required between Mull and Skye in order to retard rapid ice build-up in Skye and the north (Fig. 4b).

Temperature Depression

A second series of climate tuning experiments involved reproducing the surface geometry of the main ice sheet and comparing it with empirical ice surface reconstructions based on trimline studies and limits. Thorp (1984) and Green (1995) indicate a number of separate, independent ice centres based on Rannoch Moor, Ben Nevis, Ailort, and Torridon which form part of the main ice sheet. Using the precipitation pattern isolated in the previous experiment and varying the magnitude of the stepped cooling $\nabla\mathbf{T}_{july}$, the model runs simulate the ice sheet form within the broad time scale of the stadial and yield further constraints on temperature depression during the Loch Lomond Stadial. With the precipitation variables $\mathbf{G\%}_{WE}$ = 40% and $\mathbf{G\%}_{SN}$= 50% these experiments revealed that ice builds up on the Ben Nevis massif when July temperatures ($-\nabla\mathbf{T}_{july}$) fall by as little as 3.5°C. With model runs forced by July temperature depression ($\nabla\mathbf{T}_{july}$) set between -3.5 and -6.5°C, it is apparent that the Lochaber massif undergoes ice build-up which dominates the whole of the Loch Lomond Stadial ice sheet. The magnitude of cooling is not strong enough to allow the ELA to drop sufficiently in other highland areas, thus preventing the growth of the independent ice centres reconstructed by empirical studies. A stepped July cooling ($-\nabla\mathbf{T}_{July}$) of at least 7°C is required before other highland areas initiate their own local, independent ice centres which eventually coalesce to form an ice sheet which reproduces that indicated by empirical reconstructions (Fig. 2).

GRIP Simulation

Armed with the mass balance parameterisations from the two climate experiments described above, the GRIP temperature curve was locally calibrated for amplitude and used to force the model over a full Younger Dryas simulation. The palaeoclimate curve reconstructed from oxygen isotope analysis of the Greenland Summit ice core was scaled so that the maximum cooling of the stadial corresponded to a July temperature depression of 8°C (Fig. 1c). This figure agrees with the results of the climatic experiment above and is also in accordance with Coope's palaeoecological estimate (Fig. 1a). The model was driven from initial ice-free conditions at the sheet were taken at various time-slices in its evolution (Fig. 6a-j).

Model results indicate that ice builds up rapidly on the onset of climatic deterioration. Within 100 years a large outlet glacier has flowed northwards off the Ben Nevis Massif and spread out into the great Glen into the Fort William locality (Fig. 6a). An effective elevation/mass-onset of the stadial and snapshots of the resulting ice

Fig. 6a: 100 years.

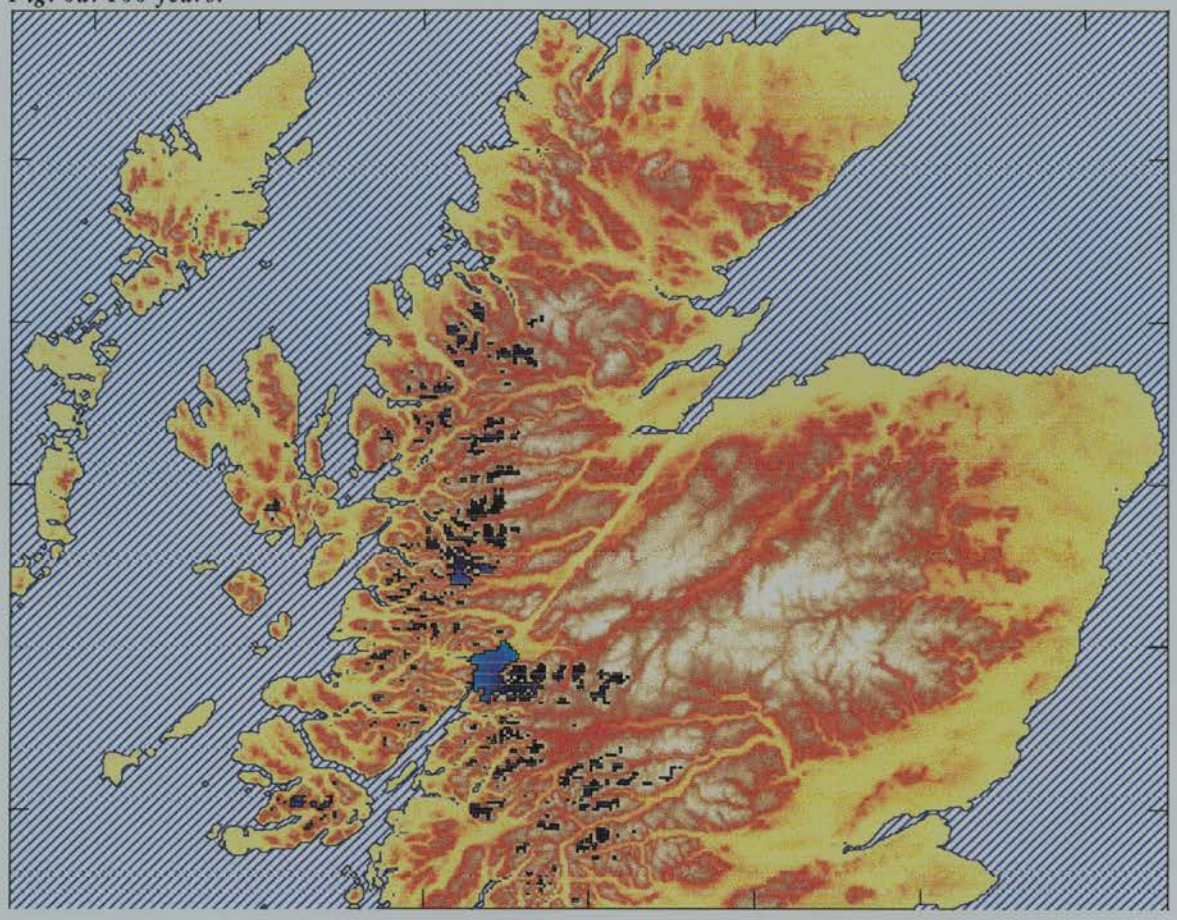

Fig. 6b: 150 years.

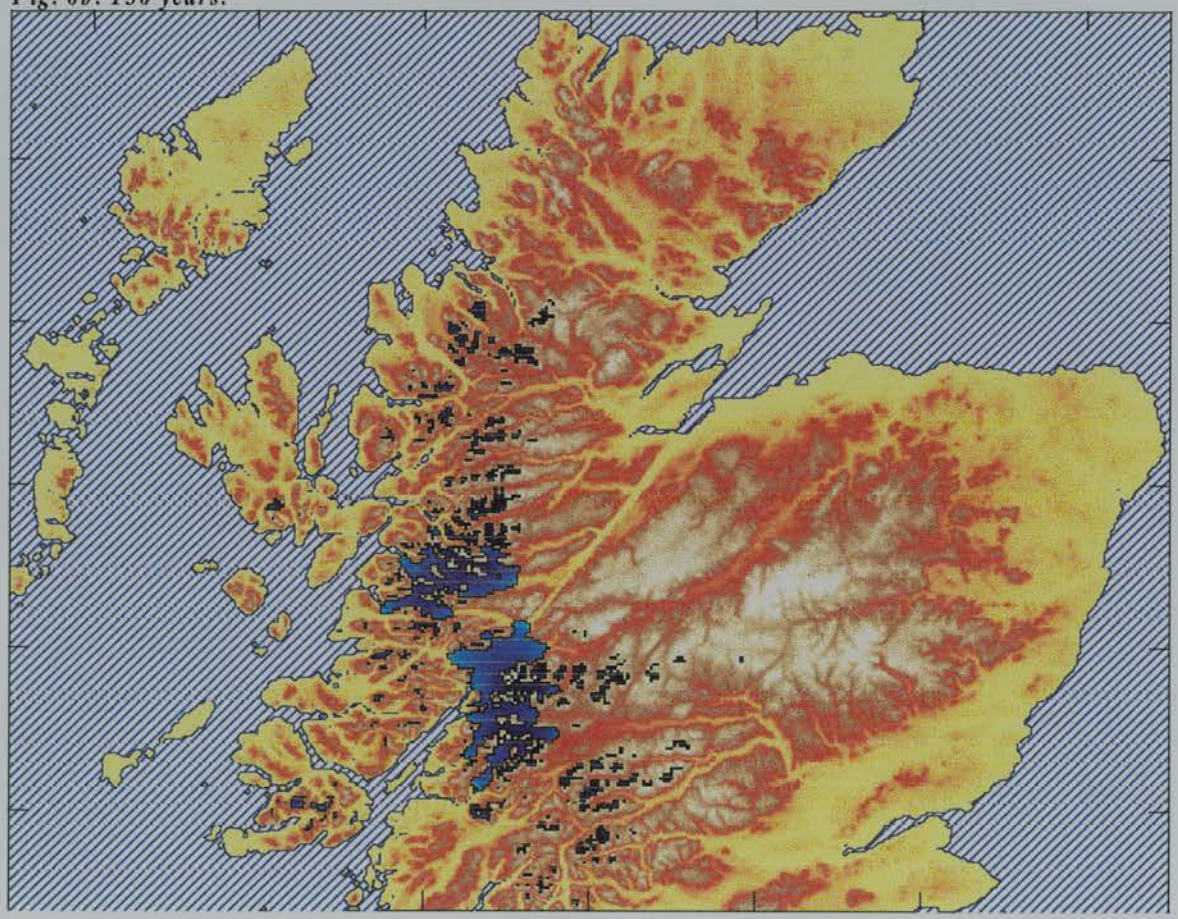

Figs. 6a-j. Modelled advance of the Younger Dryas ice sheet across Scotland from 100 - 550 years in time-slices of 50 years.

Fig. 6c: 200 years.

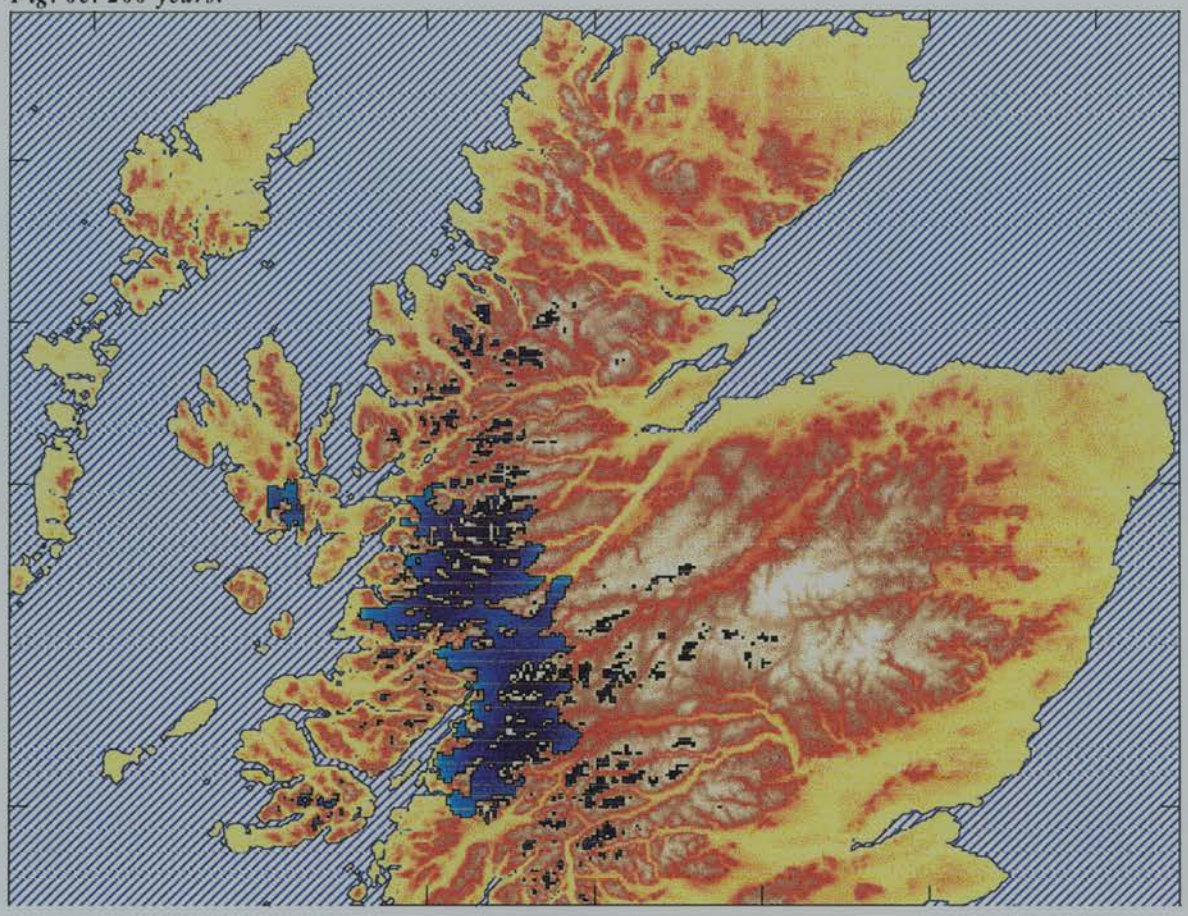

Fig. 6d: 250 years.

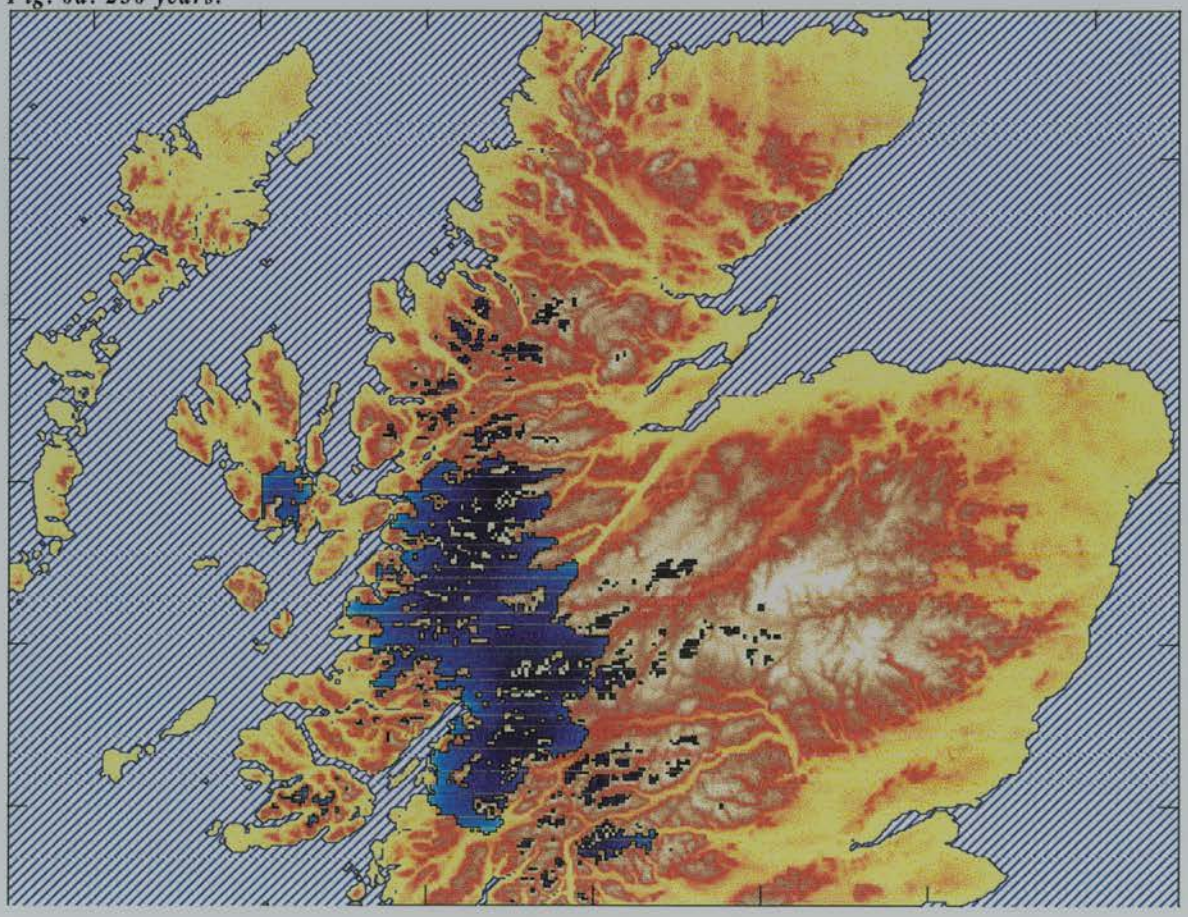

Fig. 6e: 300 years.

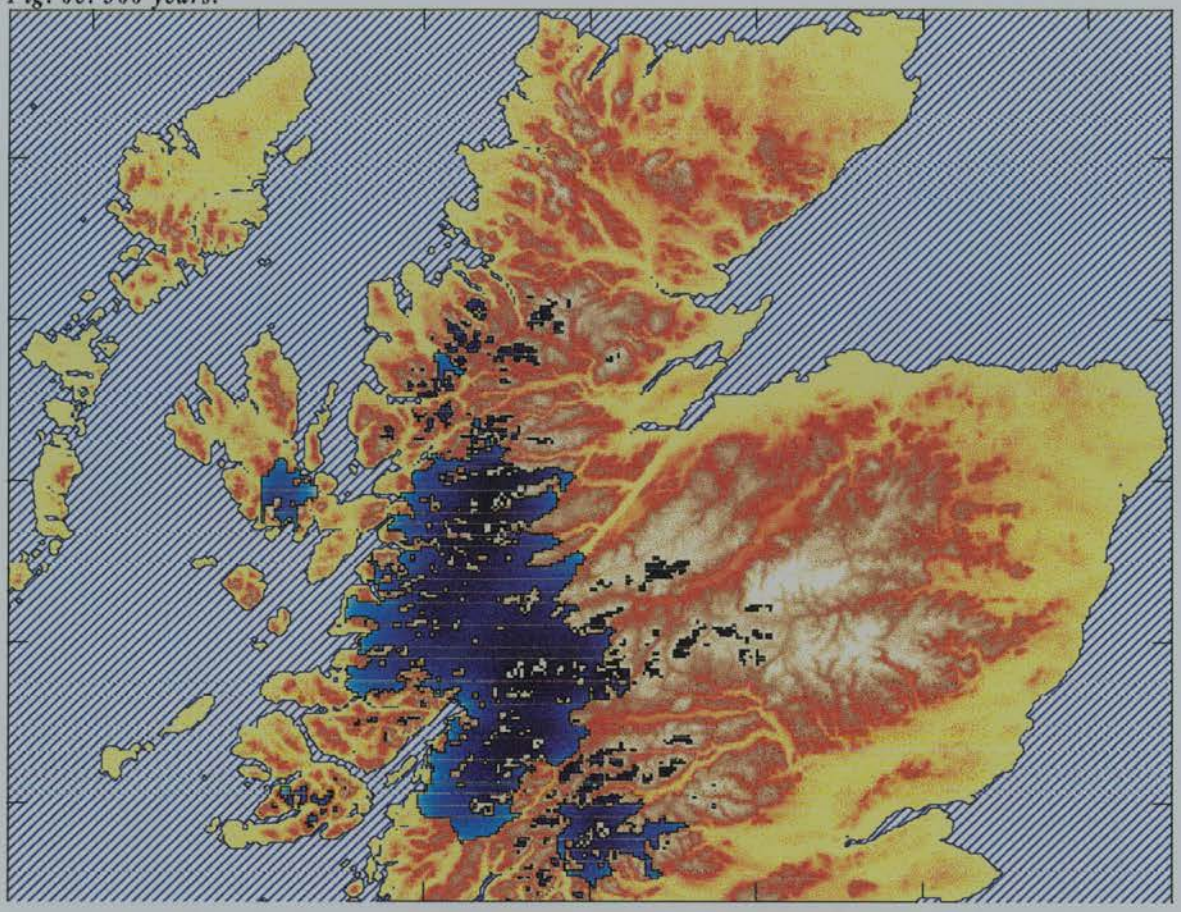

Fig. 6f: 350 years.

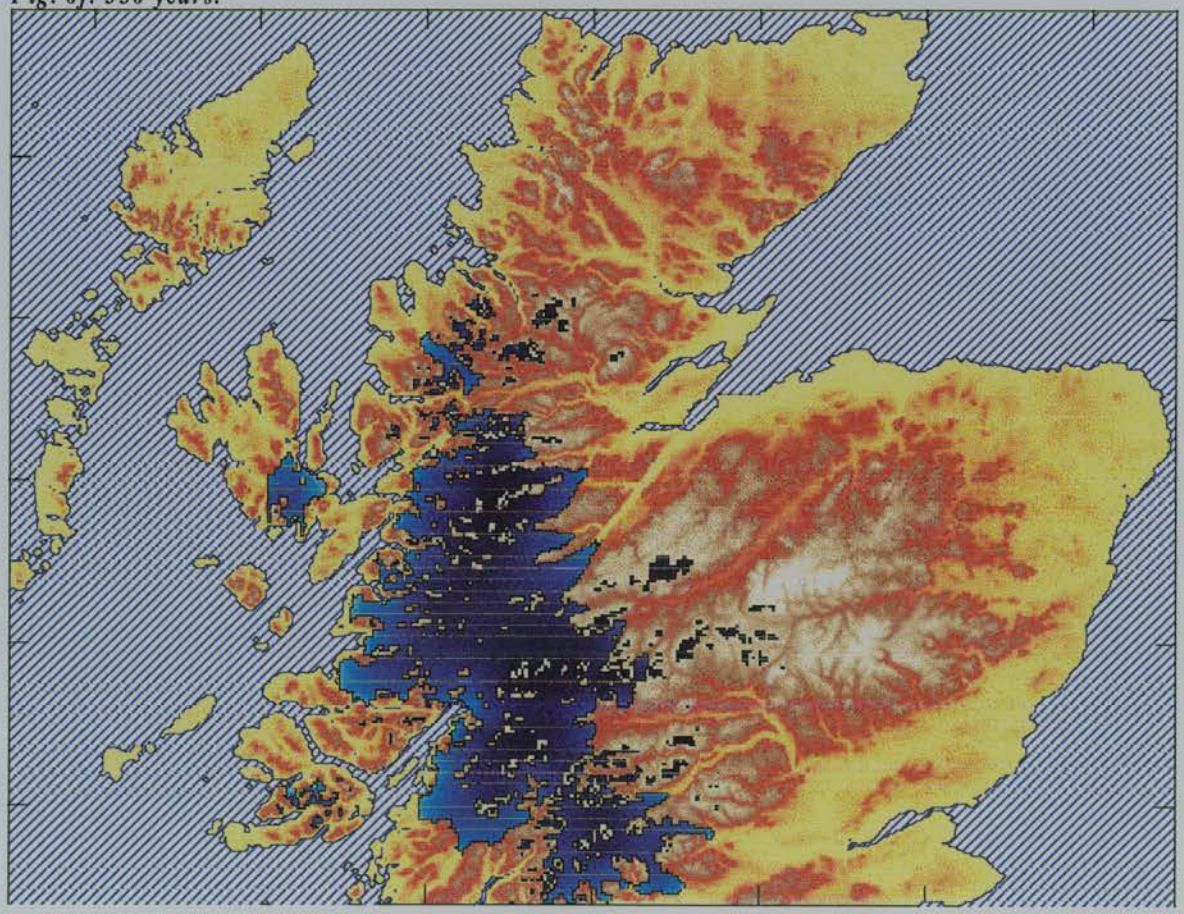

Fig. 6g: 400 years.

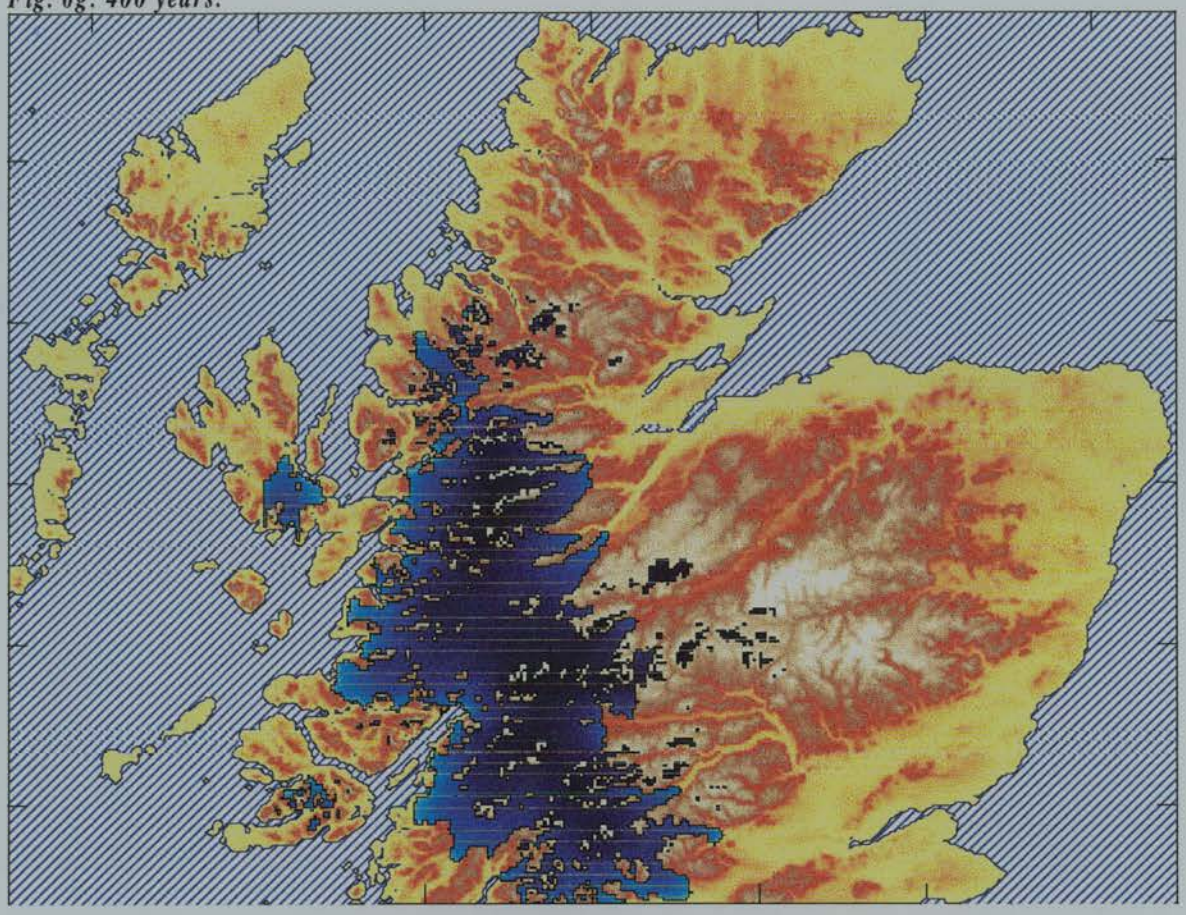

Fig. 6h: 450 years.

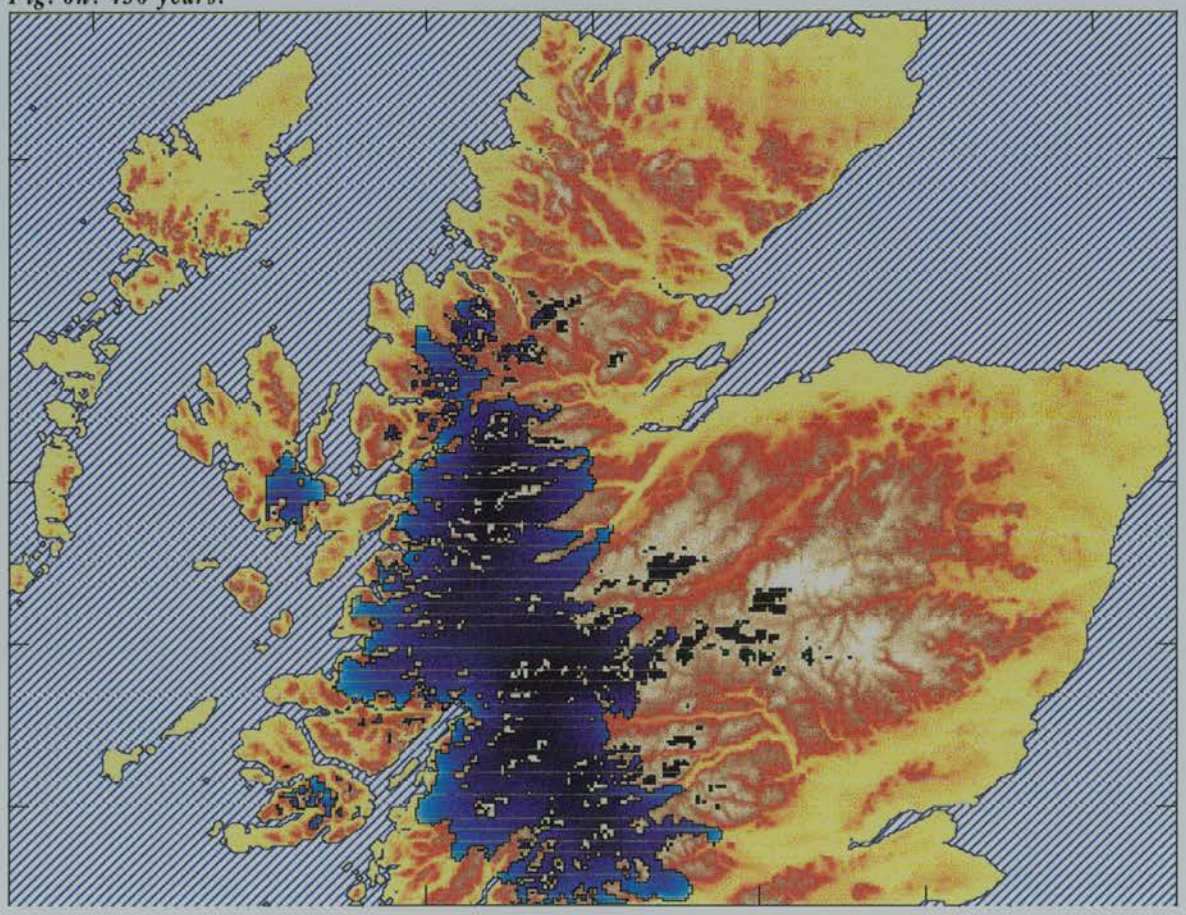

Fig. 6i: 500 years.

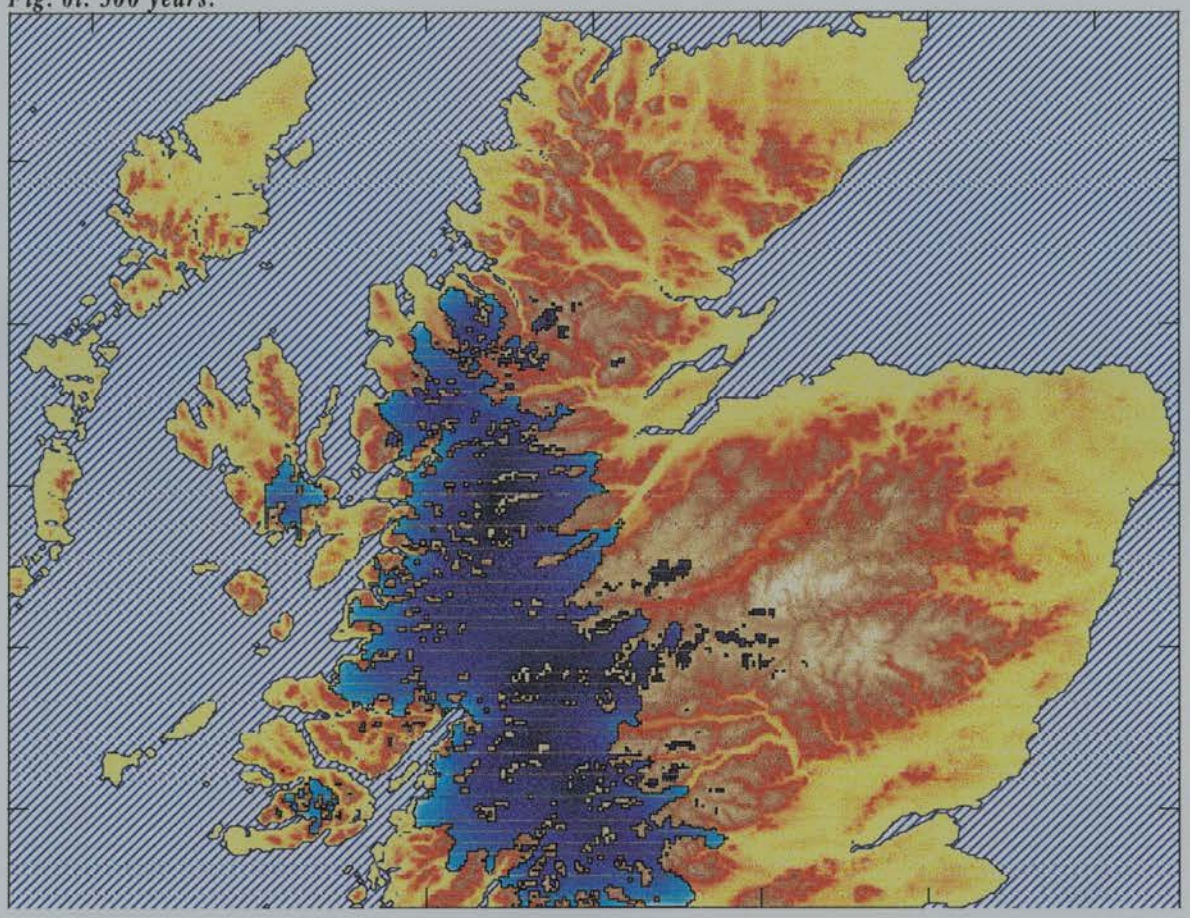

Fig. 6j: 550 years - 'optimum fit'

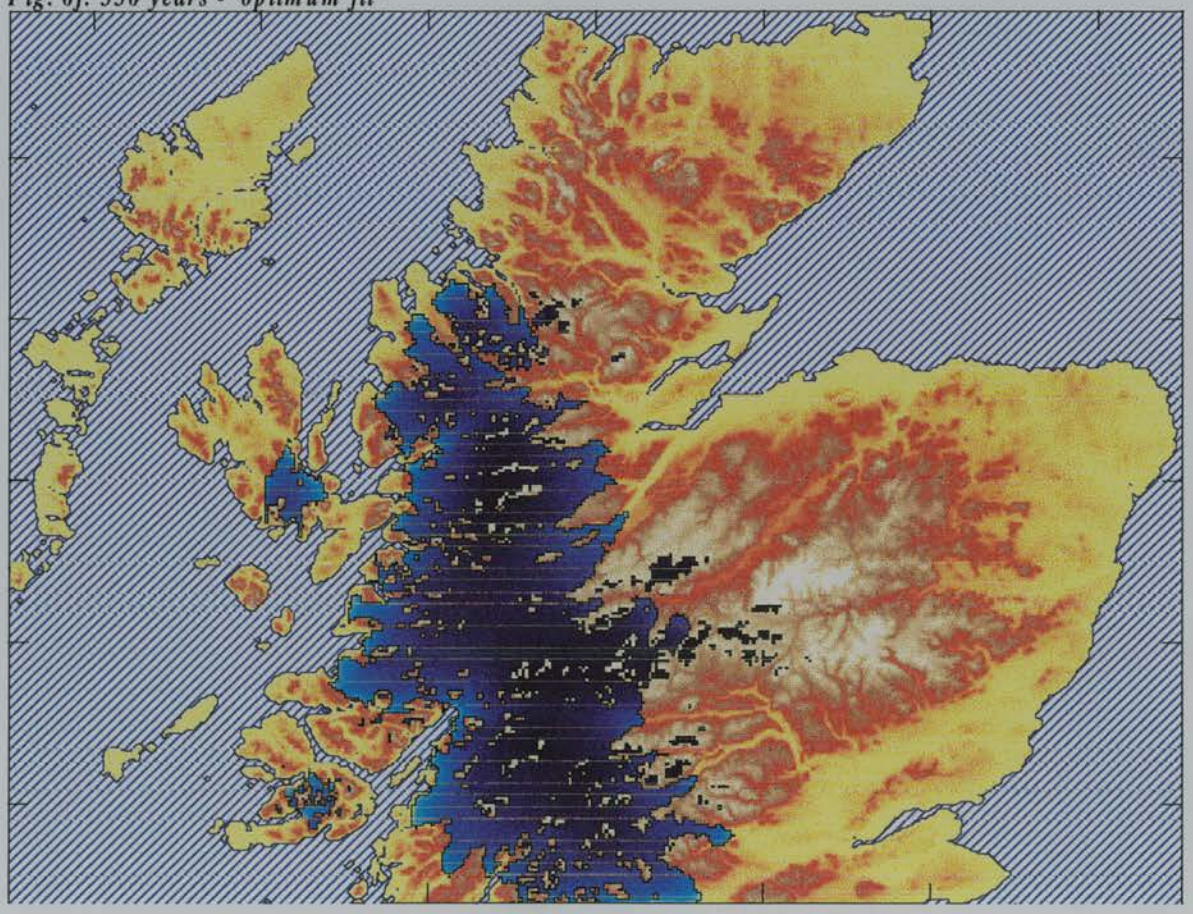

balance feedback in this area gives rise to rapid expansion of the ice lobe in the Great Glen. The expansion of the ice sheet area lying above the ELA as the ice sheet grows leads to further advance to the SW and NE along the Great Glen (Fig. 6b-e). During this time another large ice mass begins to expand north of the Great Glen and cirque glaciers are building up at high elevations in Mull, Skye and throughout the western Highlands (Fig. 6b). Once the two main individual ice masses of Torridon and Lochaber coalesce (Fig. 6d), rapid expansion of the western Highland ice sheet follows and is accompanied by the growth of local ice sheets in Skye, Applecross, Mull and isolated highland areas in the far North (Fig. 6f). A large ice mass also builds up in the SW Grampians which becomes incorporated into the main ice sheet within 350 years (Fig. 6f). Expansion of the ice sheet on all sides ensues but mostly to the north and south, the eastward expansion being curtailed by high ablation rates due to aridity; to the west the ice sheet is kept in check by increased calving rates as outlet glaciers advance out of their individual lochs and calving fronts expand (Fig. 6g-j). The optimum fit between the modelled ice sheet geometry and the limits reconstructed from empirical studies (Fig. 2) occurs after 550 years (Fig. 6j).

DISCUSSION

The required pattern of precipitation for the optimum-fit of 40% and 50% reduction to the east and north respectively (Fig. 4b), is in accordance with the empirical studies by Sissons (1980) and Ballantyne (1994). They suggested a more southerly track of incoming anti-cyclones during the Loch Lomond Stadial. Sissons used the high altitude of reconstructed former glaciers to suggest that stadial precipitation over the Cairngorms was as low as 500 - 600 mm. Whilst in the SW Grampians precipitation was similar to that of the present day at 3000 - 4000 mm/yr. Ballantyne used periglacial evidence to support the notion of a dry NE Scotland. Using the altitudinal distribution of protalus ramparts on Jura he calculates Loch Lomond Stadial precipitation not to have exceeded 800 - 1250 mm/yr (50 - 87% of present); for Coire Beanaidh in the Cairngorm estimates imply a figure of 350 - 550 mm/yr (19 - 27% of present day). Thus, he concludes that whilst calculations support the general pattern of precipitation decline they also suggest that Sissons may have overestimated stadial precipitation, particularly in assuming that it was similar to the present day in the mountains of the SW Grampians. Despite uncertainties, these empirical estimates do confirm that there was a steep south-west to north-east precipitation gradient across the Scottish Highlands during the Loch Lomond Stadial. Ballantyne notes that the likely cause of these enhanced gradients is the scavenging effect of the ice field that occupied the Western Highlands; cooling of moist air that was forced to rise over the icefield must have caused heavy precipitation on the windward side, whilst the lee side of the icefield to the northeast experienced marked aridity.

It is difficult to infer absolute estimates of precipitation values from model results since there are no definitive constraints on the chronology of the stadial. A reduction in the rate of growth of the simulation can be achieved through an overall reduction in the absolute precipitation distribution. The contrary also holds; that an increase in absolute precipitation rates would result in a more rapid ice sheet advance and hence, reduce the time taken to achieve maximum extent. However, what is important is that the spatial pattern of the modelled distribution remains unchanged, independent of the simulation run time. One implication of these results is support for the view of Sissons that, for an effective Loch Lomond Stadial advance lasting 500 years, precipitation patterns in the SW Scotland must have indeed been similar to present. For example, a somewhat slower modelled ice build up can only be achieved with a further reduction in overall precipitation leading to even further aridity in the northeast. A reduction of overall precipitation distribution by a further 25% increases the simulated time required to obtain Loch Lomond Stadial limits from 550 years to 750 years.

The fact that the Ben Nevis massif is close to glaciation has a wide significance in estimating the magnitude of cooling involved. 50 years of a July cooling ($-\nabla T_{july}$) of 3.5°C results in a large glacier forming on Ben Nevis and advancing into the Great Glen. Essentially, the topographic configuration of the Lochaber region coast,

coupled with the high precipitation rates (3,000 - 4,000 mm) makes this area sensitive to the onset of glacial conditions. The total domination of the Lochaber ice centre in all of the modelled ice sheet simulations with a July forcing (∇T_{July}) less than -7°C gives a clear indication that the actual temperature depression associated with the Younger Dryas event in Scotland must have been in excess of this value. This is because it must have been sufficiently cold to allow glaciers to build up over the lower mountain centres to the north and south. Assuming that the ice sheet required at least 450 years to achieve its maximum limits, then modelling results suggest that the actual mean magnitude of the July cooling was in the order of 8°C. However, this is not to say that there could not have been short fluctuations which may have been of considerably greater magnitude.

The requirement for rapid and large cooling is contrary to the steady decline lasting 2,000 years leading to the culmination of the Loch Lomond Stadial indicated by Coope's (1975) curve (Fig. 1a). Although model results are in good agreement with the absolute magnitude of July cooling of 8°C, a steady decline in temperature over any period in excess of 250 years would give rise to a scenario in which Lochaber ice quickly inundates most of the western Highlands. The mismatch of such a Lochaber centred ice sheet with the field evidence suggests that this did not occur. Rather, the optimum-fit model run indicates a short sharp jump into extreme cold conditions.

Forcing by the GRIP curve results in a modelled ice sheet after 550 years that bears a close resemblance to reconstructed limits based on empirical evidence. A high degree of fit is seen across the calving western ice limits, margins and isolated ice masses to the north (Ballantyne, pers. comm., 1995) and the southern margins. The only notable discrepancy is with Bennett and Boulton's (1993) reconstructed limits in the northwest at Achnashean. However, extensive laminated, silty deposits in this area associated with the Loch Lomond Stadial lend support for the existence of a large ice damned lake, the effect of which has not been modelled and would considerably alter the actual ice sheet dynamics in this area.

A considerable problem with the GRIP experiment is the perpetuation of ice sheet advance, after 550 years, beyond the optimum-fit Loch Lomond Stadial limits. Using the optimum precipitation pattern and continuing to force the model with the GRIP-calibrated curve results in a modelled ice sheet that greatly exceeds the limits for Loch Lomond Stadial. This result, suggesting that the Loch Lomond Stadial ice sheet failed to achieve equilibrium with its climate is contrary to empirical evidence. The existence of large moraines marking the Loch Lomond Stadial maximum limits which indicate that the ice sheet margins were stable for some extended period of time. The implication here is that either the timing of the GRIP curve is wrong for Scotland or that at some stage during the stadial precipitation is considerably overestimated. One tentative explanation lending support for the latter view would involve a migration of the position of the atmospheric polar front south of Scottish latitudes which would lead to reduced atmospheric activity. After some 400 or so years into the stadial, a shift in the circulation pattern could enhance aridity, starving the ice sheet and thereby halting its further expansion. Benn et al, (1992) support this line of reasoning suggesting that the prolonged initial phase of retreat, marked by still-stands and minor readvances, can be interpreted as representing a decline in snowfall during the latter part of the stadial rather than any marked thermal improvement.

Finally, of crucial importance to the dynamics and geometry of the Loch Lomond Stadial ice sheet is the role of Loch Linnhe as a sump for the large ice flux which accumulates in the Lochaber massif. Once ice has advanced into coastal waters, the model is especially sensitive to calving rates. This is indicated by the results of further calibration experiments conducted using the GRIP-forced run where calving was altered by changing the parameter $\mathbf{C_d}$ by an order of magnitude in either direction. Decreasing the calving rate resulted in rapid expansion of the ice sheet down the Great Glen, with the Lochaber ice centre almost exclusively dominating the whole ice sheet. Furthermore, the

modelled ice sheet is considerably larger with limits extending much further out of the glens on the west coast into deeper water before they calve away. The implication is that the morphology and dynamics of the ice sheet are highly sensitive to calving in Loch Linnhe.

CONCLUSIONS

- Scotland is susceptible to glaciation. An annual cooling of just 2.5°C with the present day precipitation regime is sufficient to form glaciers which flow off Ben Nevis within 100 years.

- The high precipitation and accumulation in western Scotland permit the rapid expansion of localised glaciers to form an ice sheet within 200 years.

- Comparison of modelled ice extent with empirically reconstructed limits for discrete outlying glaciers reveals that a enhanced southwest to northeast precipitation gradient occurred during the Loch Lomond Stadial. The Cairngorms receiving 25% and Skye receiving 75% of their present day precipitation totals respectively. In the southwest Grampians, precipitation was similar to that of today.

- A large, stepped mean annual July cooling of 8°C with steeper precipitation gradients is required for the optimum fit between modelled ice sheet and empirical reconstructions. A cooling of this magnitude is in agreement with Coope's estimate based on palaeoecological data but contradicts the view of prolonged and slow decline in temperature throughout the stadial. The rapidity of the cooling required lends strong support for a GRIP shaped temperature curve affecting Scotland during the Younger Dryas.

- A model experiment forced with a calibrated GRIP time series reveals that Loch Lomond Stadial maximum limits were obtained within 550 years of onset of glacial conditions. The modelled ice sheet continues to expand under these climatic conditions, a result which is in disagreement with empirical studies which indicate a sustained period of stability of the ice sheet at its maximum position. This suggests that during the latter part of the stadial the precipitation regime became significantly more arid throughout Scotland. This could have been associated with reduced atmospheric moisture due to a southerly shift of the Atmospheric Polar Front.

COMPARISON OF A THREE-DIMENSIONAL MODEL FOR GLACIER FLOW WITH FIELD DATA FROM HAUT GLACIER D'AROLLA, SWITZERLAND

ABSTRACT

A three dimensional, finite difference model based on a first order solution of the ice flow equations is applied to Haut Glacier d'Arolla, Switzerland. The numerical model successfully converges at horizontal resolutions down to 70 m, so a number of detailed comparisons with field data can be made. Modelled surface velocities with no basal sliding component are compared with surface velocities observed on the glacier over 4 different time periods. The best fit is achieved with over-winter surface velocities (R^2 = 0.75) using a rate factor, A, in Glen's flow law of 0.063 a^{-1} bar^{-3}. Surface zones of maximum computed effective stress display a high level of coincidence with observed crevassing, the orientation of which is successfully predicted by the direction of the tensile component of the computed principal surface stress. Comparison of the relative magnitude and direction of computed principal stresses with principal strains measured at the ice surface also correspond closely. In an attempt to simulate the observed annual velocity distribution within a cross-section of the glacier tongue, we incorporate two basal motion patterns into the model. By treating net annual ice motion as a time-weighted composite of three separate flow situations; normal sliding, enhanced sliding and no sliding, we are able to reproduce the key features of the observed cross-sectional ice and basal slip velocity distributions. These experiments indicate there may be substantial decoupling taking place along an elongated narrow zone at the bed of Haut Glacier d'Arolla, and that this decoupling interacts in a complex manner with the englacial stress and strain field.

INTRODUCTION

Glacier movement is commonly divided into internal deformation and basal motion, the latter comprising basal sliding and bed deformation. These components, however, are not mutually exclusive because stresses within an ice mass continuously adjust to, and feed back into, temporal and spatial variations in basal motion. This dynamic pattern, in turn, directly influences the forces driving basal motion. For these reasons, a clear insight into the processes governing a glacier's internal rheology plays an essential role in the understanding of its associated dynamics. As the stress and strain pattern within a glacier is difficult to measure, particularly at the bed, ice flow models have been developed to attempt to simulate these patterns.

This study aims to evaluate the applicability and potential of a first order solution of the equations of ice motion, developed by Muller (1991) and extended to three dimensions by Blatter (1995), for the computation of the three dimensional stress and strain fields within grounded ice masses. In contrast to previous finite difference solutions, this model successfully incorporates terms for the computation of longitudinal deviatoric stresses. These stresses become increasingly important at the high resolutions involved in valley glacier modelling, where tensile and compressive stresses are induced by gradients at the glacier surface, bed, and in the basal motion pattern (Kamb and Echelmeyer, 1986). Despite these merits, the computational efficiency, performance and ability of Blatter's (1995) model at simulating glacier flow have yet to be tested against field data. Here, we apply the model in three dimensions to Haut Glacier d'Arolla, Switzerland, both to perform such a test and to provide a basic insight into the processes of glacier dynamics. Specifically we:

i) test the computational performance and stability of the three dimensional first order model at horizontal resolutions down to 70 m.

ii) compare modelled ice surface velocities with no basal motion against velocities measured at the glacier over four periods to test general model applicability and the contention that the winter flow regime is predominantly composed of internal deformation with a negligible basal motion component.

iii) determine the rate factor, A, used in the flow law for ice (Glen, 1958) which best reproduces the observed patterns.

iv) compare the magnitude and orientation of modelled principal surface stresses with crevasse patterns on the glacier.

v) compare the magnitude and orientation of modelled principal surface stresses with strain patterns derived from repeat surveys of surface strain diamonds.

vi) attempt to model an observed distribution of annual velocity within a cross-section of the glacier tongue by treating the annual flow regime as a time-weighted composite of three contrasting basal motion

scenarios: no sliding, 'normal summer' sliding, and enhanced 'spring-event' sliding along an elongated decoupled zone.

It should be noted that we do not specifically attempt to model real patterns of basal motion. In the absence of sufficient high-resolution information on basal conditions, the simulation of actual sliding patterns is considered beyond the scope of the present study. However, long-term field investigations do enable us to make some tentative assumptions regarding basal sliding patterns, which we do explore. First, observations at predominantly temperate-based valley glaciers indicate that basal sliding velocities decrease significantly during the winter season (Hooke and others, 1989, 1992; Gudmundsson, 1994; Willis, 1995). Large decreases in measured mid-winter surface velocities at Haut Glacier d'Arolla suggest major basal sliding suppression relative to other periods. We investigate this observation through comparing velocities measured over four different periods with surface velocities modelled with no associated basal motion.

Second, repeat inclinometry of a transect of boreholes provides us with site-specific information on local strain and sliding patterns at Haut Glacier d'Arolla. The distinctive feature of the annual velocity distribution in cross-section is the low internal strain experienced within an, 80 m-wide zone dominated by enhanced basal motion, whereas internal strain contributes significantly to total movement elsewhere (Harbor and others, 1997). This feature is observed in fast flowing ice streams where much of the high velocity is attributed to basal motion, but is also confirmed for small valley glaciers, where sliding patterns vary over spatial scales that are comparable with the local ice thickness. We attempt to reproduce the observed cross-sectional velocity distribution by applying the model under contrasting basal boundary configurations. We do not consider these configurations as precise simulations of the velocity field, but rather as a gauge that the observed strain pattern could potentially result from basal decoupling along a longitudinally linear zone within a field of lower background sliding.

FIELDSITE AND METHODS

Haut Glacier d'Arolla is located in the western Pennine Alps at the head of the Val d'Hérens, Valais, Switzerland (Fig. 1). The glacier is approximately 4 km long and has an elevation range of 2560 to 3500 m a.s.l.. It has an area of 6.3 km^2, comprising two firn basins that combine to feed a main glacier tongue. The glacier is currently retreating at approximately 25 ma^{-1} and has receded by more than 720 m since 1967. It has a maximum depth of approximately 180 m (Sharp and others, 1993) and a maximum surface velocity of about 15 ma^{-1}. The glacier therefore has a relatively simple geometrical configuration, a small areal extent and a relatively large ice flux, all of which make it well suited as a field test site for high resolution flow modelling.

Field Data

A 5 m-resolution digital elevation model of the glacier surface in September 1994 was generated by aerial photogrammetry conducted in collaboration with Grande Dixence, S.A. (Willis and others, 1996), and a 20 m-resolution digital elevation model of the glacier bed was generated from radio-echo sounding data (Sharp and others, 1993). Crevasse fields were mapped from the original aerial photographs and layered onto the digital elevation model (Fig. 1).

Ice velocity data were obtained by standard ground surveying, using a Geodimeter 410 Total Station, of an extensive network of velocity markers drilled into the glacier surface in 1994 and 1995. In June 1994, 2 independent marker arrays were installed: a glacier-wide set of 4 transects consisting of 7 or 8 markers each was established to provide data on overall dynamics, and a further 4 staggered transects consisting of 5 markers were established within the ablation zone of the glacier, to provide high resolution strain data (Fig. 1). Each marker housed a permanent reflector prism and, weather permitting, was surveyed twice daily from each of two survey stations. The position of each marker was thus based on four individual co-ordinate readings. During each survey, regular checks were made to three stable ground references to provide control data and permit correction for changing atmospheric conditions. Surveys of the stake network were carried out between June 13 and September 3, summer 1994, between February 3 and 8, winter 1995, and June 22 and August 27, summer 1995. The February visit enabled the glacier surface displacement to be divided into the four periods which we used to constrain the flow model; summer 1994 (13/6/94 to 3/9/94), fall/winter 1994/95 (3/9/94 to 3/2/95), winter 1995 (3/2/95 to 8/2/95) and summer 1995 (22/6/95 to 27/8/95). Each period is assumed to be characterised by a different motion regime reflecting some change in

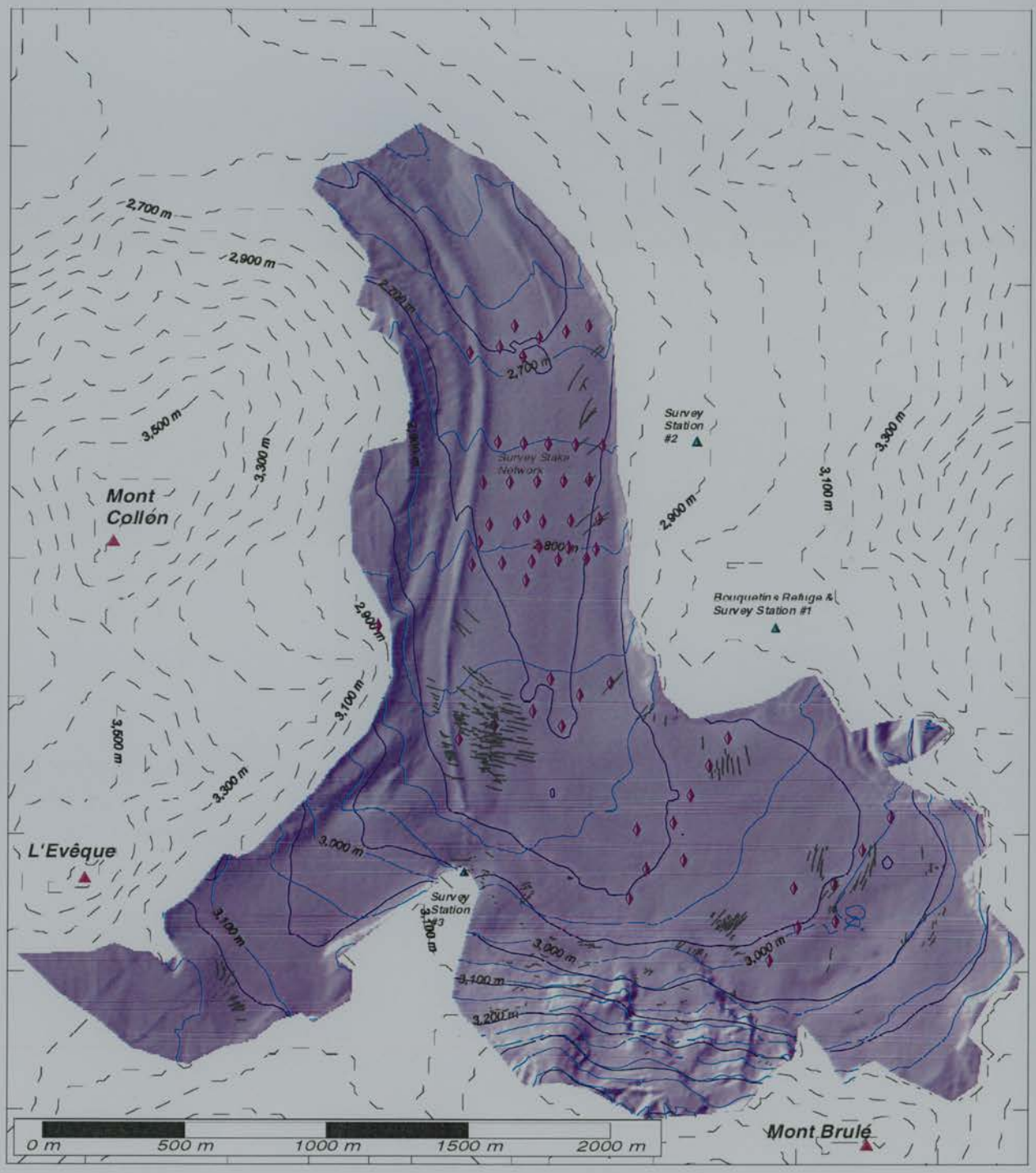

Fig. 1. *Surface and bed topography of Haut Glacier d'Arolla and its catchment showing the main summits, velocity survey stake network and associated survey stations.*

the balance between internal ice deformation and basal sliding and/or bed deformation as the subglacial drainage system evolves.

The magnitude and orientation of principal surface strains were derived, following Ramsay (1967), from the motion of multiple suites of surface strain triangles. The annual, cross-sectional velocity distribution was determined through repeat inclinometry profiling of a transect of boreholes drilled to the glacier bed between August 1995 and August 1996. Repeat surveys of the tops of these boreholes enabled calculation of annual surface velocities at each point, permitting isolation of the net annual basal motion pattern across the transect (Harbor and others, 1997).

MODEL BOUNDARY CONDITIONS

A detailed description of the derivation and numerical solution of the first order algorithm in three dimensions is given in Blatter (1995). However, to understand the limitations imposed through the convergence criterion of the model, a synopsis of the main procedures and iteration scheme are presented.

The numerical model solves the equations of force balance and the stress-strain relations that are bounded by a prescribed velocity distribution at the glacier bed and a vanishing shear traction at the surface. A second order Runge-Kutta integration scheme shoots vertically from the glacier bed for zero shear traction at the ice surface. The unknown basal shear traction is modified through a fixed point iteration scheme based on the computed shear traction at the surface:

$$\tau_b^{new} = \tau_b^{old} - \beta.\tau_s^{old} \qquad (1)$$

where τ_b and τ_s denote the basal and surface shear tractions respectively and β ($0 < \beta < 1$) is an iteration parameter. The convergence radius of this iteration is defined by the aspect ratio of the ice mass and the chosen horizontal grid resolution. Higher resolution (decreasing grid size) requires smaller values of β, which reduces the progress of the iteration step within the scheme and thus increases the overall number of iterations required to satisfy convergence ($\tau_s < 0.001$ kPa). This ultimately places limits on the horizontal resolution that can be obtained for a given glacier geometry.

For application of the numerical model in three dimensions, six inputs must be specified: bed and surface slopes, ice thickness, the basal motion field and Glen's flow law rate factor and exponent. Ice thickness at each grid node was generated by subtracting the bed from the surface elevation models which were spline interpolated (Keckler, 1995) to the required resolution. The local bed and surface gradients were generated at each node through central 2^{nd} order differencing and single-sided 2^{nd} order differencing at the margins.

We apply the model under three contrasting basal motion configurations. In the first experiment, the basal velocity distribution is set to zero for comparison with measured surface velocities. The second experiment attempts to simulate the annual velocity distribution within the glacier cross-section, which we treat as a composite of three different basal motion configurations reflecting seasonal changes: non-sliding conditions during 'winter', normal sliding conditions during 'normal summer' melt-season and locally enhanced sliding within a background of normal sliding during a proposed 'spring event' (Harbor and others, 1997). The weights of each scenario on the overall modelled annual velocity distribution should be defined by the contribution of each scenario over the year.

Defining the 'normal summer' and the enhanced 'spring event' basal motion distributions are extremely problematic since information on internal velocity and sliding is only available across a small transect of the glacier tongue and is averaged over a year. This precludes any attempt at isolating actual basal motion distributions since within sliding areas the surface velocity may be defined almost totally by sliding, whereas in zones of no or small sliding velocities the surface velocity may be increased by faster sliding in neighbouring zones. Hence, at any time, local basal velocity may actually lie anywhere between zero and the surface velocity. Although differences between seasonal velocities cannot be directly attributed to variations in sliding, in the absence of any more rigorous method we derive the normal melt-season basal motion distribution from the residual of the observed summer minus the observed winter surface velocities at each survey marker and, with the glacier margins defined at zero, use a three dimensional kringing algorithm (Keckler, 1995) to interpolate the resulting velocity field glacier wide.

The enhanced 'spring-event' sliding distribution is based on the 'normal summer' distribution but with a

narrow zone down the eastern margin of the glacier tongue defined by a sliding value equal to the peak local ice surface velocity. This elongated zone of artificially enhanced sliding, 1 grid cell wide by 15 cells long, coincides with the location of a subglacial channel or variable pressure axis (VPA), characterised by significant melt-season diurnal water-pressure variations, peak values of which often exceed ice overburden pressure (Sharp and others, 1993; Hubbard and others, 1995). The justification for an enhanced sliding scenario lies in the fact that maximum surface velocities recorded during a 'spring event' in early July 1995 were substantially greater than both annually-averaged and summer-averaged velocities and were centred over the proposed channel (Hubbard and others, 1995). Furthermore, repeat borehole inclinometry reveals considerably larger sliding rates within this narrow c. 80 m zone relative to the remainder of the glacier cross-section (Harbor and others, 1997).

The rate factor, A, in Glen's flow law for ice is strongly dependent on ice temperature and water content. The model incorporates the flexibility to define A at each node, therefore permitting the approximation of cold, wet and polythermal glaciers. However, since Haut Glacier d'Arolla is a predominantly temperate glacier, the rate factor is held constant and a value of 3 is used for the flow law exponent, n.

RESULTS

The model with zero basal motion was successfully applied to the geometry of Haut Glacier d'Arolla at resolutions of 250, 150, 100, 75 and 70 m. All runs provided consistent results, characterised by smooth surface velocity distributions displaying classic transverse parabolic profiles characterised by high velocities close to the glacier centreline rapidly decreasing to zero at the margins (e.g. Fig. 2). Computed basal traction varies to a maximum value of c. 160 kPa and at all resolutions the longitudinal deviatoric stress component was significant and on the same order of magnitude as the computed basal traction. Model runs at resolutions below 70 m were attempted but failed to converge, even with values of b < 0.0002 which was the cutoff limit before machine precision round-off errors dominated the numerical scheme. The maximum resolution of 70 m used an optimum value of b = 0.001 and required c. 12,000 iterative steps to achieve convergence. The geometry of Haut Glacier d'Arolla at 70 m resolution corresponds to an array of 40 x 52 horizontal cells and required 40 levels to provide the vertical stability necessary for convergence. Since this represents the maximum practicable resolution, all calculations and comparisons reported in the remainder of this paper refer to this 70 m geometry.

Comparison of modelled and measured surface velocities

The predicted surface velocity pattern is characterised by a high level of spatial consistency, with smooth transitions from areas of maximum velocity into areas of lower velocity (Fig. 2). To assess the success of the first order model in simulating flow at Haut Glacier d'Arolla, the computed surface velocities are interpolated onto the co-ordinate positions of the surface survey markers using a linear algorithm (Keckler, 1995). These modelled velocities are plotted against observed surface velocities for the four periods defined above, revealing a good relationship with velocities measured over the winter 1995 period (R^2 = 0.75), but a poor relationship with summer 1994 (R^2 = 0.37), fall/winter 1994/95 (R^2 = 0.38), and summer 1995 (R^2 = 0.27) data (Fig. 3). A poor correspondence for the latter three periods is expected since zero motion is specified at the basal boundary in the model while these three periods all span at least part of the summer melt-season when extensive basal lubrication, and therefore motion, is expected. We interpret this result as an indication that winter motion of Haut Glacier d'Arolla is achieved primarily through internal deformation and that Blatter's (1995) first order model is capable of predicting valley glacier flow by internal deformation reasonably well.

Derivation of the rate factor

For a uniform rate factor, A, in Glen's flow law for ice the magnitude of modelled strains is proportional to A and the pattern of those strains is independent of A. Hence, using a subsequent multiplier, A', of the form:

$$A_{optimum} = A_{initial} \cdot A' \qquad (2)$$

it is possible to fine-tune the model to empirical data by calculating an optimum rate factor, $A_{optimum}$, without re-computing the stress field. Linear regression (constrained through the origin) of modelled surface velocities against those measured during the winter 1995 flow period results in a value for $A_{optimum}$ of 0.082 a^{-1} bar^{-3}. The best fit between these data, however, is achieved when the regression line intercepts the measured velocity axis at 1.63 ma^{-1}, yielding a value for $A_{optimum}$ of 0.063 a^{-1} bar^{-3} (R^2 = 0.75) (Fig. 4). While

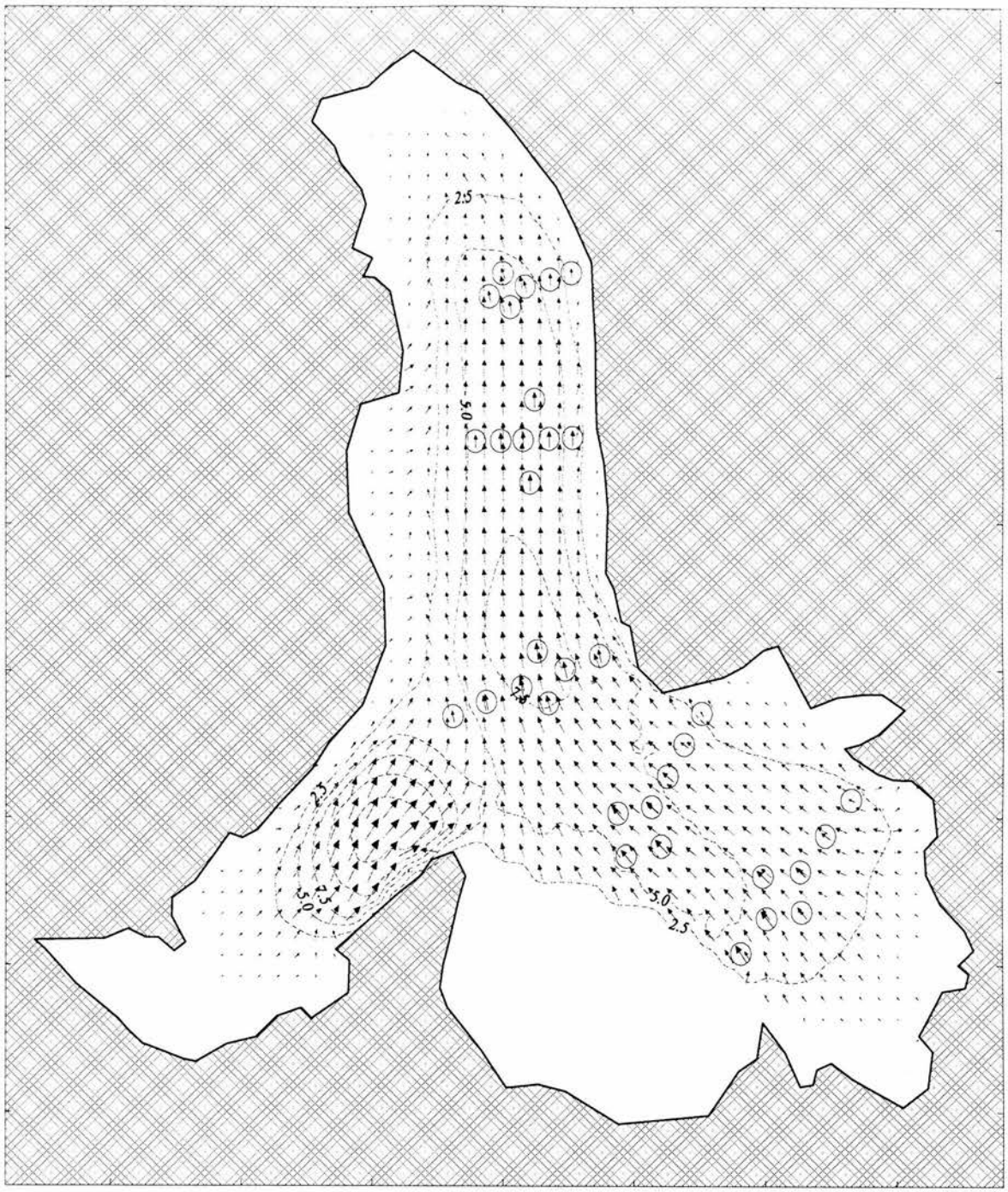

Fig. 2. Numerically modelled horizontal surface velocity field at Haut Glacier d'Arolla at 70 m resolution for n = 3 and A = 0.063 a-1 bar-3. Surface speed is contoured at 2.5 m a-1 intervals and measured winter 1995 velocity vectors (circled) are shown for comparison.

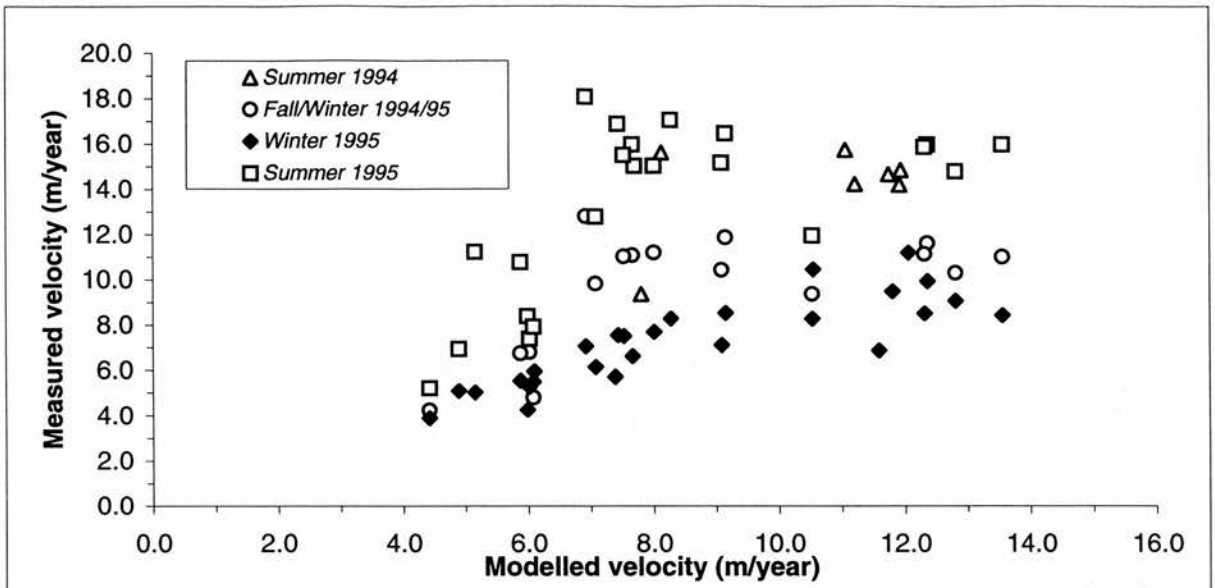

Fig. 3. Numerically modelled horizontal surface velocities at 70 m resolution for n = 3 and A = 0.1 a^{-1} bar^{-3} at survey marker locations at Haut Glacier d'Arolla plotted against surface velocities recorded at those markers for four periods of flow (see text).

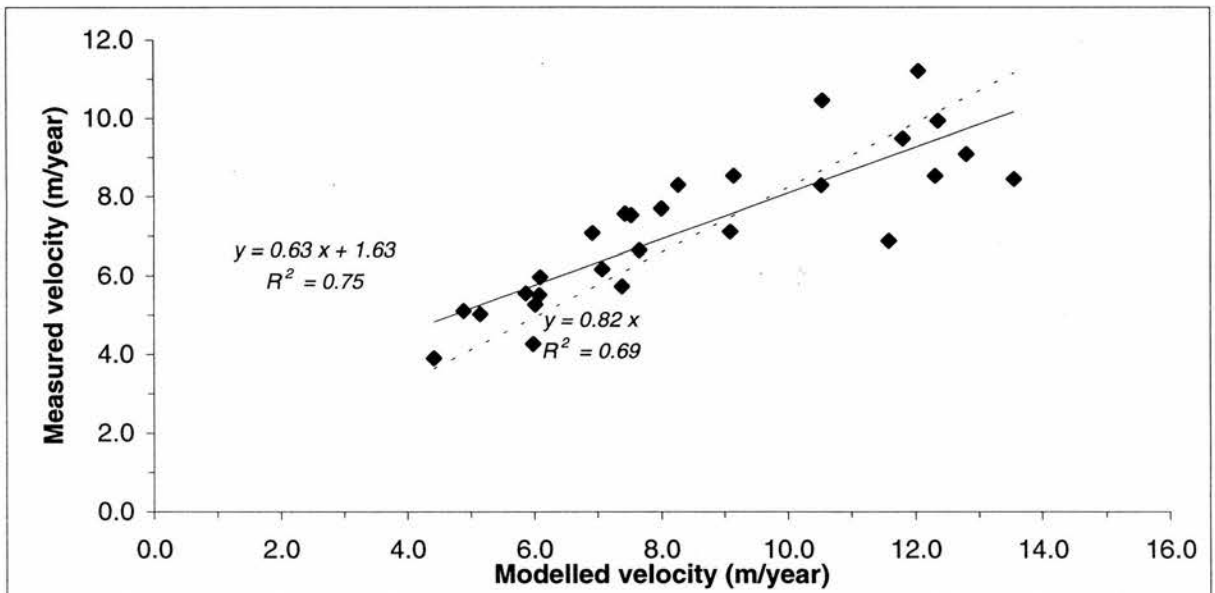

Fig. 4. Bivariate plot of numerically modelled ice velocities against observed winter 1995 velocities at survey marker locations at the surface of Haut Glacier d'Arolla. Best fit, least squares linear regressions are given (dashed line is constrained through the origin).

this value of A is about half that of the traditionally accepted value (e.g. Paterson, 1994), it is in general agreement with recent estimates of the flow law parameters based on finite element models of glacier flow. For example, Gudmundsson (1994) achieved a best fit with $A = 0.075\ a^{-1}\ bar^{-3}$ ($n = 3$) between surface velocities calculated using a three-dimensional finite element model and those measured at Unteraargletscher, Switzerland. It may be worth noting that the 'full stress' models predict a value for the rate factor that is somewhat less than the values traditionally presented for temperate ice (Paterson, 1994). One possible explanation could be the failure of previous, shallow ice models to account for the full stress field, leading to an underestimate of the effective stress in the flow law, resulting in a requirement for correspondingly 'softer ice'. However, without precise information on the internal flow regime and ice character (e.g. debris, gas and moisture content and crystal orientation) we can only conclude that the above value of A at Haut Glacier d'Arolla represents a best-fit, glacier-wide generalisation of what is likely to be variable on spatial and temporal scales.

Occurrence of Crevasses

Areas of potential ice-surface crevassing may be predicted on a glacier by application of the von Mises criterion, which is based on the premise that ice can support only a limited octahedral stress before failure (Vaughan, 1993). This criterion is most readily expressed as a limiting value on the second invariant, I_s, of the deviatoric stress tensor, derived from the components of the principal stresses, σ_s:

$$\sigma_t^2 > I_s^2 = \sigma_{s1}^2 + \sigma_{s2}^2 - \sigma_{s1}\,\sigma_{s2}, \qquad (3)$$

where σ_t^2 is the tensile strength of the ice (Vaughan, 1993). Vaughan (1993) successfully matched this criterion, derived from measured strain rates, with crevassing on a number of ice masses. Significantly, application of Blatter's model permits generation of both the magnitude of I_s and the orientation of the principal stresses directly from the computed surface stress field. Comparison of these data with observed crevassing may thereby serve as a check on the accuracy of the model as applied to Haut Glacier d'Arolla. If the model calculates the three dimensional stress field accurately and at a sufficiently fine resolution, then regions of the glacier surface corresponding to maximum values of I_s will correspond with areas of glacier crevassing, and the orientations of those crevasses will correspond with the principal tensile stress directions.

Comparison of areas of maximum I_s determined from the first order model with no basal sliding (Fig. 5) with the actual distribution of crevassing across Haut Glacier d'Arolla (Fig. 1) reveals a high level of correspondence. The directions of the principal tensile stresses in these zones also generally match the orientations of observed crevasses. The most extensive zone of crevassing occurs at the confluence of the southwest tributary and the main glacier, and corresponds with a zone of maximum I_s. The directions of the modelled principal stresses in this region indicate flow-parallel extension, which is consistent with the transverse orientation of the observed crevasses. The occurrence and direction of longitudinally-orientated crevasses at the top of the southwest tributary along with a zone of transverse crevasses on the lower eastern margin of the glacier tongue are also successfully predicted, providing validation both of the model and of the application of the von Mises criterion to crevasse prediction.

Comparison of modelled principal stresses and measured principal strains

As the relative patterns of the modelled stress and strain fields are independent of the rate factor A, a direct comparison of modelled principal stresses with measured principal strains is also permitted. The principal strains were derived from the displacement of a dense strain network established across a small area of the glacier tongue between 3 September, 1994 and 27 August, 1995 (Fig. 1). In this limited study area, the modelled stress field with no basal motion successfully reproduces the general pattern of measured principal strains (Figs. 6a & b) showing relatively low vector magnitudes along the glacier centreline, with steadily increasing magnitudes towards the eastern glacier margin. There is also strong agreement between the orientation of the modelled principal stresses and derived principal strains. This is particularly evident from the centreline to the eastern side of the study area. At the glacier centreline within the comparison area, compressive and tensile vectors are aligned perpendicular and parallel to the direction of glacier flow, respectively. Towards the eastern margin, vectors progressively turn through 45° such that the compressive vector is orientated so as to oppose tranverse drag and intercepts the margin obliquely. Towards the west of the area, there is greater discrepancy between the

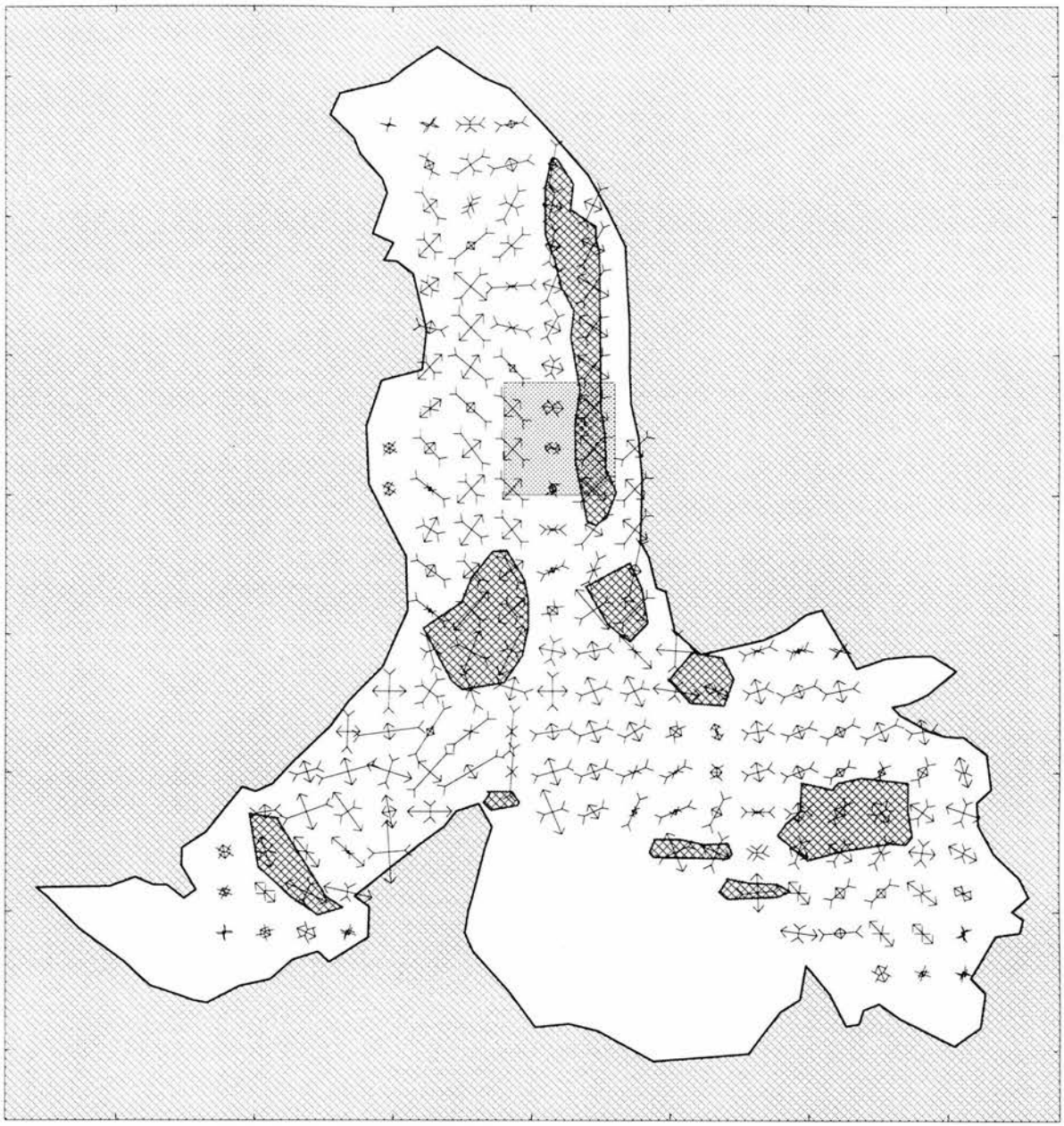

Fig. 5. The magnitude and direction of modelled surface-parallel principal stresses at Haut Glacier d'Arolla (every second node has been omitted). Inward arrows indicate compression, and conversely. The enclosed contours represent zones of maximum computed Is (2nd invariant of the surface stress tensor) and indicate regions most likely to fail as defined by the von Mises criterion. The shaded square indicates the region of the high density strain diamond network shown in Fig. 6.

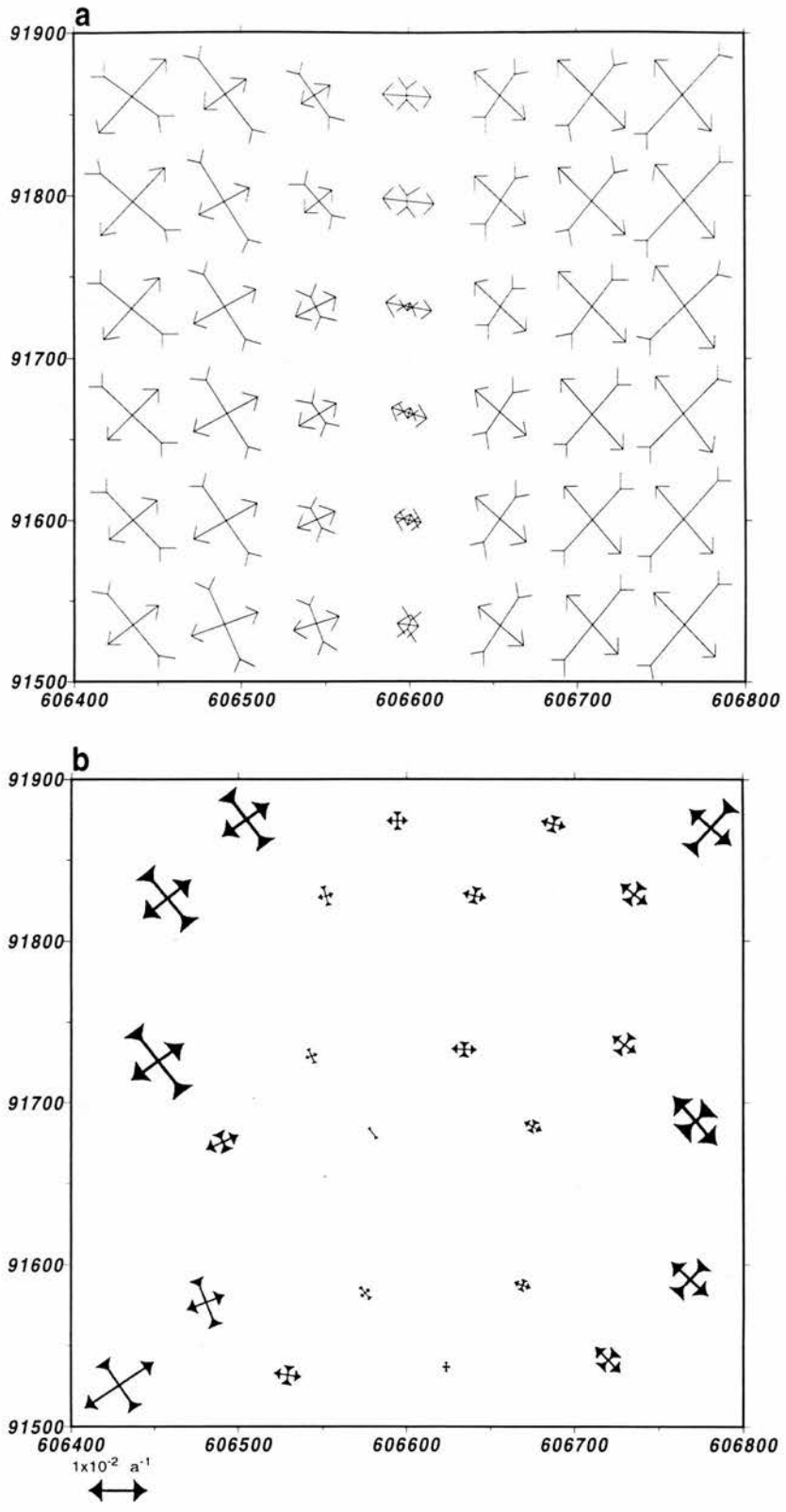

Fig. 6. Magnitude and orientation of surface-parallel (a) modelled principal stresses and (b) measured principal strains in the region of the strain diamond network at the glacier tongue.

orientations of measured and modelled vectors. A possible explanation here maybe that much of the western area of the glacier consists of almost stagnant, ice-cored moraine which may be significantly less dynamic in reality than the model is capable of predicting with a spatially uniform rate factor. It should also be noted that the principal stresses are calculated from the model run with no basal motion component, whereas the period over which the surface strains were observed covers much of the summer melt-season when a substantial component of basal sliding would be expected. For the most part however, strong correspondence is apparent between these modelled and measured quantities, providing further validation of the model.

Simulation of the annual velocity distribution in cross-section

Two further model runs were initiated at 70 m resolution to obtain stress and velocity fields under the two basal motion scenarios described above (Figs. 7a & b). The resulting cross-section distributions of modelled velocity and basal traction, along with the no sliding results, reveal several interesting features. Given the asymmetric geometry of the glacier cross-section, the 'winter' and 'normal summer' sliding scenarios display a notable symmetry in their flow and stress regimes (Figs. 8a & b). For the 'winter' no sliding configuration, computed basal traction varies little around 120 kPa over much of the cross-section and the resulting vertical velocity distribution displays the classic vertical profile with peak surface velocities of 7.5 ma^{-1} coinciding with the zone of maximum ice thickness at Easting 606580, somewhat to the east (true right) of the glacier centreline (Fig. 8a).

As expected, introducing the 'normal summer' sliding distribution (Fig. 7a) results in generally increased surface velocities relative to 'winter' velocities (Fig. 8b). However, this summer velocity increase is also accompanied by a small decrease in net internal deformation rates. This decrease may be understood in terms of the role of reduced basal drag in relieving basal shear traction. For instance, where the bed at Easting 606600 experiences the maximum imposed sliding of c. 7 ma^{-1}, the computed basal traction declines by 20 kPa. A similar reduction in basal traction occurs across the central 400 m zone of the glacier and is compensated for by increased values of modelled basal traction (up to 70 kPa at Easting 606870) towards the margins (Fig. 8b). Thus, under conditions of reduced basal drag, transverse stresses come into play, transferring the component of basal shear traction required to stabilise the glacier away from the decoupled zone.

Under conditions of enhanced sliding along the inferred subglacial channel (Fig. 7b), transverse stress/strain field effects become considerably more pronounced. Within the decoupled zone at the proposed subglacial channel, computed values of basal traction become negligible. Here, slip is essentially providing the whole component to surface movement effectively enabling the overlying ice to move as a vertical column over its bed. The basal velocity perturbation diffuses laterally across and upward through the transect and its effects, increased velocity at the glacier surface, are evident up to 300 m to the west. Strong associated transverse coupling effects are also observed, consequently enhancing basal drag across the bed with maximum basal traction of 160 kPa apparent immediately west of the decoupled zone.

Various configurations of the three modelled scenarios were time-weight averaged and combined on a systematic basis in an attempt to reproduce the observed annual velocity distribution within the cross-section at the glacier tongue (Fig. 9a). Weights of 20/52 'winter' no sliding, 20/52 'normal summer' sliding and 12/52 enhanced 'spring event' sliding results in a composite velocity distribution in cross-section (Fig. 9b) which represents a compromise between a realistic weighting and a best-fit to the observed data. Given the limits imposed by the operating resolution, the modelled and observed surface and basal velocity patterns across the transect show a good likeness (Figs. 9a and 9b). Peak surface velocities in both modelled and observed distributions rise to nearly 10 ma^{-1} directly above the decoupled zone and remain high to within 100 m of the eastern margin. Throughout the transect, modelled velocities do not deviate more than 0.5 ma^{-1} from measured velocities. The composite modelled velocity pattern across the glacier bed is also similar to the pattern inferred from observations, varying between 5 and 6 ma^{-1} over most of the transect and rising to 8 ma^{-1} at the location of the proposed subglacial channel. Both the observed and the composite modelled distributions also correspond in the area of maximum down-glacier velocity at 9.5 ma^{-1} occurring over the inferred subglacial channel as 'plug flow'. However, despite the many similarities, the two cross-section velocity patterns differ significantly in the lateral diffusion of the

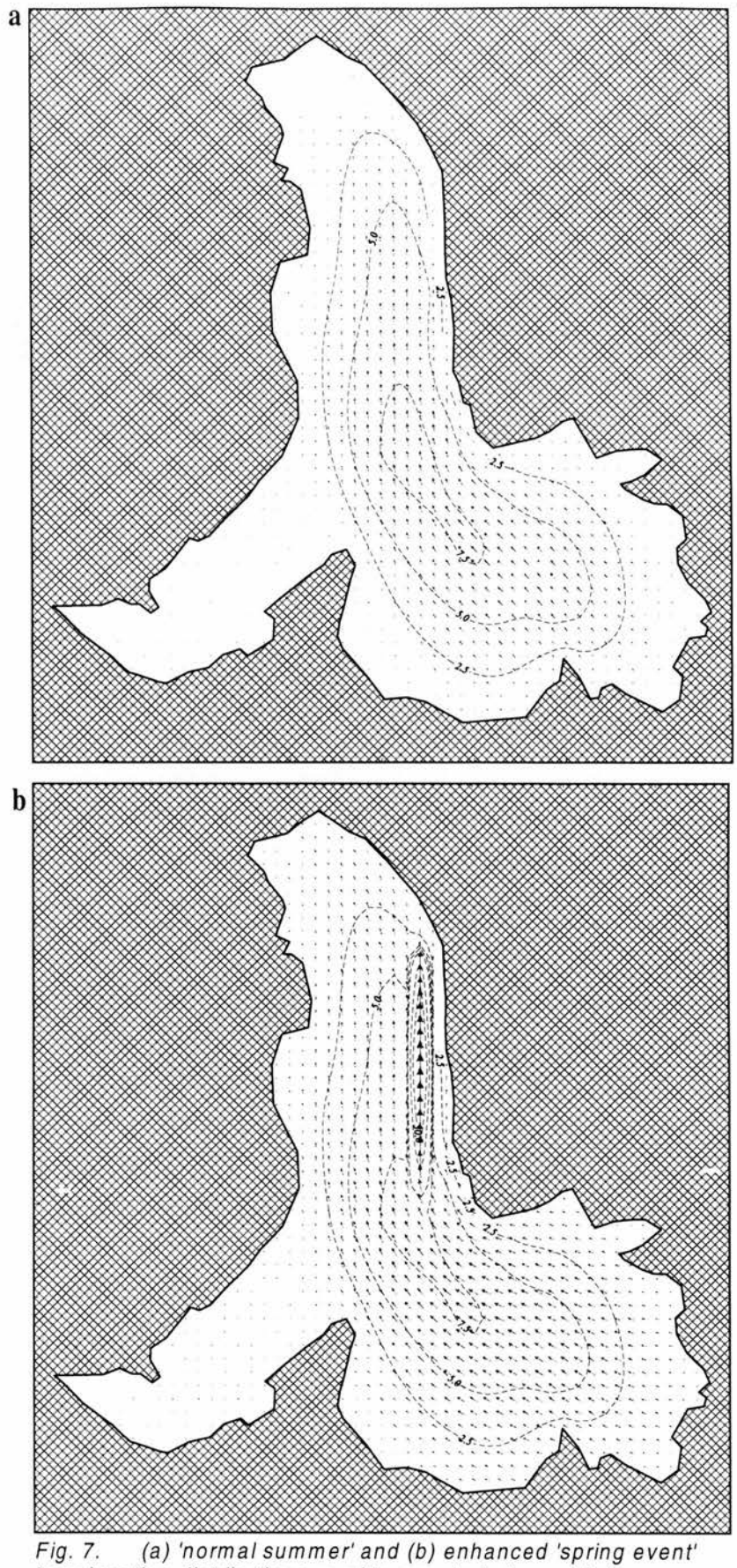

Fig. 7. (a) 'normal summer' and (b) enhanced 'spring event' basal motion distributions used to constrain the model.

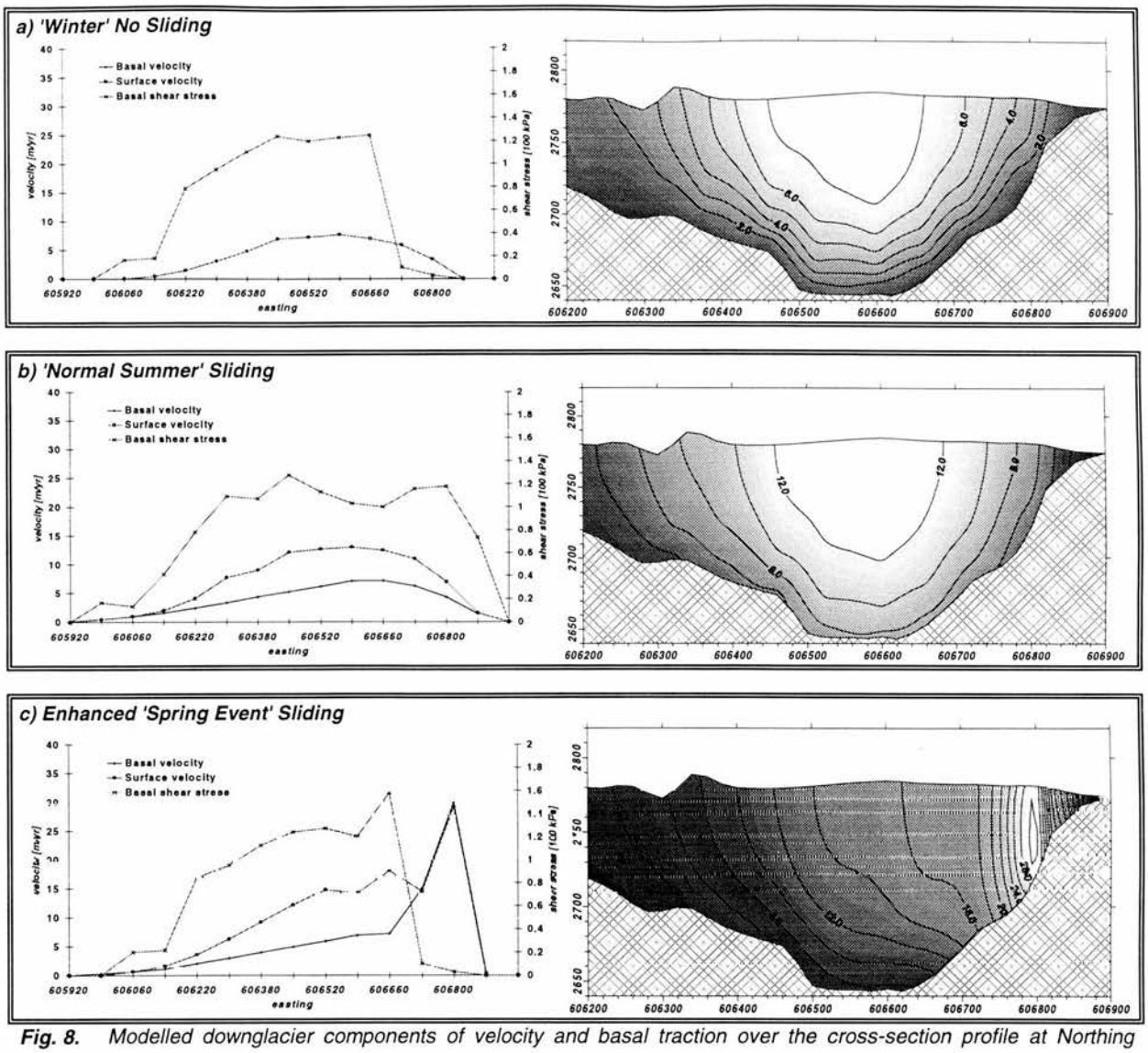

Fig. 8. *Modelled downglacier components of velocity and basal traction over the cross-section profile at Northing 91700 under (a) 'winter' no sliding, (b) 'normal summer' sliding, and (c) enhanced 'spring event' sliding scenarios.*

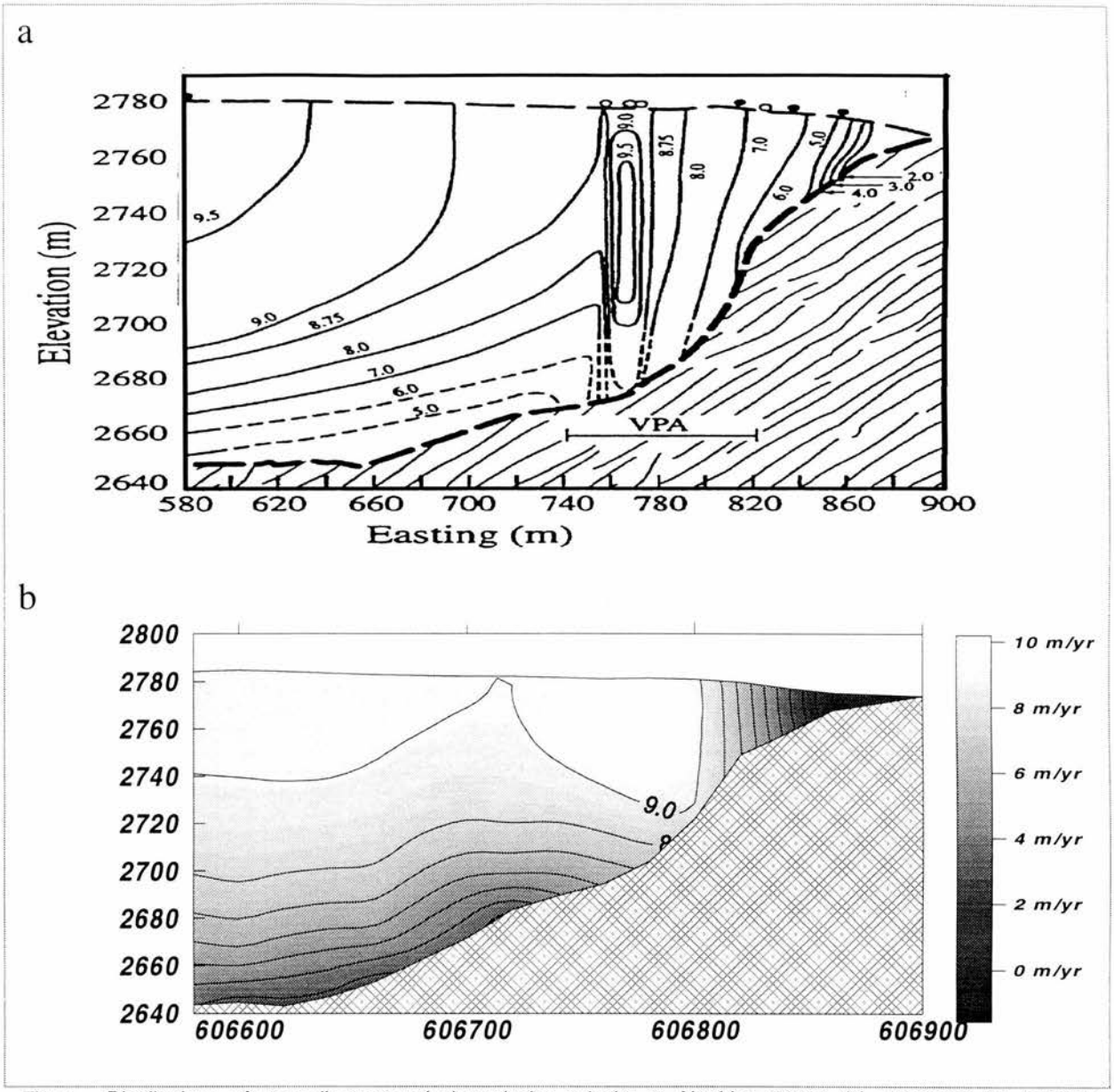

Fig. 9. *Distributions of annually-averaged downglacier velocity at Northing 91700 (a) measured by borehole deformation studies and (b) modelled as a composite, time-weighted average of 20 weeks 'winter' no sliding, 20 weeks 'normal summer' sliding and 12 weeks enhanced 'spring event' sliding. The measured velocity distribution is adapted from Harbor and others (1997) and indicates the inferred location of the variable pressure axis (VPA). Solid contours are well-constrained by borehole data, dashed contours are extrapolated from boreholes that did not reach the bed. Circles indicate positions of the tops of boreholes used in constructing the velocity profile. Solid circles are boreholes with data reaching close to the bed, open circles are boreholes with data extending at least 50% of ice depth, but not to the bed.*

basal velocity perturbation. In contrast to the modelled composite, the observed velocity pattern displays a well defined boundary between the decoupled column and the adjacent ice over the whole glacier thickness. However, the failure of the model to delimit such a boundary may well be a shortcoming of its limited 70 m operating resolution.

DISCUSSION AND CONCLUSIONS

Blatter's (1995) model (based on a finite difference solution in three dimensions of the first order approximation of the flow equations for ice) has been applied successfully to a valley glacier at high spatial resolution. Comparison of model predictions with field data from Haut Glacier d'Arolla, Switzerland, reveals that the model is flexible and accurate, and does not compromise the quality of results, as have previous finite difference solutions.

Least squares linear regression of modelled surface velocities with no basal motion component against measured surface velocities for various time periods indicates a good match for winter (1995) flow. For this period the optimum value for the flow parameter, A, in Glen's flow law for ice (with $n = 3$) is 0.063 a^{-1} bar^{-3}. This best-fit relationship, however, does not pass through the origin but intercepts the observed velocity axis at 1.63 ma^{-1}, suggesting that there may be a basal motion component of this magnitude in the winter flow regime. Comparison of modelled and measured velocities for other periods indicates a poorer correspondence characterised by basal motion patterns that are non-uniform in space and time.

The computed three dimensional stress field at 70 m resolution successfully predicts, through the application of von Mises criterion for failure, observed zones of crevassing across the glacier surface. The direction of the tensile component of the computed principal stress field within these zones also correctly matches the orientation of the observed crevasses. Comparison of the direction and relative magnitude of the computed principal stresses with principal strains derived from annual survey of a network of strain diamonds over part of the glacier surface shows a high level of coincidence and provides further validation for the model and the survey techniques employed at Haut Glacier d'Arolla.

Inclusion of generalised basal motion approximations into the first order model of Haut Glacier d'Arolla provides a first step towards realistic modelling of melt-season dynamics and enables us to reproduce the key features of the annual downglacier velocity distribution within a cross-section of the glacier tongue. Applying a hypothetical basal motion distribution based on subtracting mean winter from mean summer surface velocities results in moderate amendment of the modelled internal stress and strain fields as transverse stress gradients come into operation. Prescribing enhanced basal velocities along an elongated zone down the eastern margin results in total decoupling of the glacier from its bed. Negligible shear strain rates are experienced in the immediately overlying column of ice, and strong transverse coupling gives rise to an increase in computed basal drag in adjacent zones and associated enhanced strain rates as the basal perturbation is dissipated upwards and across the section. Time-weight averaging the internal velocity field modelled using the three basal motion scenarios of 'winter' no sliding, 'normal summer' and enhanced 'spring event' sliding gives a cross-sectional velocity distribution that reproduces well the main features of the observed annual velocity profile. This experiment confirms that the site of the inferred subglacial channel is probably characterised by strong decoupling for some period of time. That the required weighting of enhanced 'spring event' sliding in the overall modelled distribution is somewhat longer (12 weeks) than that observed, suggests that there may be enhanced basal motion taking place within this zone over an extended part of the year and that it is not only associated with 'spring event' basal conditions. That the modelled distribution shows considerable dissipation of the basal motion perturbation throughout the glacier cross-section whilst the observed distribution shows remarkably sharp flow regime boundaries may be a product of the relatively coarse operating resolution of the model. We cannot however, discount an inconsistency in the composite approach used to simulate the inclinometry profile nor errors associated with the derivation of the observed distribution (Harbor and others, 1997). Despite this, and given the limitations imposed by the maximum operating resolution of the model, the observed and simulated annual cross-section velocity distributions compare well and illustrate that the first order model is capable of successfully solving the internal stress and strain fields associated with complex configurations of basal motion.

REFERENCES

Alley, R. 1996. 'Towards a Hydrologic Model for Computerised Ice-Sheet Simulations', *Hydrological Processes Special Issue*, in press.

Arnold, N. & Sharp, M. 1992. 'Influence of glacier hydrology on the dynamics of a large Quaternary ice sheet', *Journal of Quaternary Science,* **7**(2), 109 - 124.

Atkinson, T., Briffa, K. & Coope, G. 1987. 'Seasonal Temperaures in Britain during the last 22,000 years, reconstructed using beetle remains', *Nature,* **325,** 587 - 593.

Ballantyne, C. 1989. 'The Loch Lomond Readvance on the Isle of Sky, Scotland: Glacier reconstruction and palaeoclimatic implications', *Journal of Quaternary Science,* **4,** 95 - 108.

Ballantyne, C. 1994. 'The tors of the Cairngorms', *Scottish Geographical Magazine,* **110,** 54 - 59.

Ballantyne, C. 1996. *Past and present Periglacial Environments.*

Ballantyne, C. & Gray, J. 1984. 'The Quaternary geomorphology of Scotland: The research contirbution of J. Sissons', *Quaternary Science Review,* **3,** 259 - 289.

Benn, D., Lowe, J. & Walker, M. 1992. 'Glacier response to climate change during the Loch Lomond Stadial and early flandrain: Geomorphological and palynological evidence from the Isle of Skye, Scotland', *Quaternary Science Review,* **11,** 781 - 799.

Bennett, M. 1991. *Scottish 'hummocky moraine': Its implications for the deglaciation of the North West Highlands during the Younger Dryas,* Ph.D. thesis, University of Edinburgh.

Bennett, M. & Boulton, G. 1993. 'The deglaciation of the Younger Dryas ice field in the Northern Highlands, Scotland', *Journal of Quaternary Science,* **8,** 133 - 145.

Bentley, M. 1996. 'The Role of Lakes in the formation of moraines in the Lake District, Southern Chile', *Earth Surface Processes and Landforms,* in press.

Blatter, H. 1995. 'Velocity and stress fields in grounded glaciers: A simple algorithm for including deviatoric stress gradients', *Journal of Glaciology,* **41**(138), 333 - 343.

Brazier, V., Gordon, J., Hubbard, A. & Sugden, D. 1995. 'The Geomorphological Evolution of a Dynamic: Landscape: The Cairngorm Mountains, Scotland', in **J. McConnell & J. Conroy** (Eds), *Environmental History of the Cairngorms,* Edinburgh University Press, Edinburgh.

Budd, W. F. & Jenssen, D. 1975. 'Numerical modelling of glacier systems'. *IAHS Publication,* **104,** 257-291.

Budd, W., Jenssen, D. & Smith, N. 1984. 'A three-dimensional time-dependent model of the West Antarctic Ice Sheet', *Annals of Glaciology,* **5,** 29 - 36.

Budd, W. & Smith, I. 1981. 'Large Scale Numerical Modelling of the Antarctic Ice Sheet', *Annals of Glaciology,* **3,** 42 - 49.

Campos, H., Steffen, W., Aguero, G., Parra, O. & Zuniga, L. 1992. 'Limnological studies of Lake Rupanco', *Arch. Hydrobiol./Suppl.*, **90**, 85 - 113.

Campos, H., Steffen, W., Aguero, G., Parra, O. & Zuniga, L. 1989. 'Estudios Limnologicos en el Lago Puyehue', *Medio Ambiente*, **10**(2), 26 - 53.

Clapperton, C. 1993. *The Quaternary in South America*, Elsevier, Amsterdam.

CLIMAP project members 1984. *Journal of Quaternary Research,* **21,** 123 - 224.

Coope, G. 1975. 'Climate fluctuation in Northwest Europe since the last interglacial', in **A. Wright & F. Moseley** (Eds), *Ice Ages: Ancient and Modern,* Steel House Press, Liverpool, 153 - 168.

Dansgaard, W., White, J. W. C. & Johnsen, S. J. 1989. 'The abrupt termination of the Younger Dryas climate event', *Nature,* **339,** 532 - 536.

Denton, G. 1993. 'Chronology of the late Pleistocene Glaciation near Lake Llanquihue', in **C. Villagran** (Ed), *The Quaternary of the Lake District of Chile: Field Guide for the International Workshop,'Quaternary of Chile',* University of Chile, Santiago, 53 - 63.

Glen, J. W. 1955. 'The creep of polycrystalline ice'. *Proc. R. Soc. Lon., Ser. A,* **228**(1175), 519-538.

Glen, J. W. 1958. 'The flow law of ice', *International Association of Scientific Hydrology Publication,* **47**, 169 - 170.

Gray, J. 1982. 'The last glaciers (Icoh Lomond Advance) in Snowdonia, North Wales', *Geological Journal,* **17,** 111-133.

Gray, J. & Coxon, P. 1991. 'The Loch Lomond Glaciation in Britain and Ireland', in **J. Ehlers, P. Gibbard & J. Rose** (Eds) *Glacial depositis in Great Britain and Ireland,* Balkema, Rotterdam, 89-105.

Green, D. 1995. *The glacial geomorphology of the Loch Lomond Advance in Lochaber.* Ph.D. thesis, University of Edinburgh.

Greuell, W. 1992. 'Hintereisferner, Austria: mass-balance reconstruction and numerical modelling of the historical length variations', *Journal of Glaciology.* **38**, 233 - 244.

Greuell, W. 1989. *Glaciers and Climate.* Ph.D. thesis, Rijksuniversiteit Utrecht.

Gudmundsson, G. H. 1994. *Converging Glacier Flow - a case study: The Underaarglacier,* VAW Mitteilungen 131, Zurich.

Häberli, W. 1994. 'Fluctuations of mountain glaciers and climate change detection - operational elements of a world-wide monitoring strategy', *European Geophysical Society Newsletter,* **50**, 120.

Hambrey, M. & Alean, J. 1992. *Glaciers,* Cambridge University Press, Cambridge

Harbor, J., Sharp, M., Copland, L., Hubbard, B., Nienow, P. and Mair, D. 1997. 'The influence of subglacial drainage conditions on the velocity distribution within a glacier cross section'. *Geol.* **25**(8), 739 - 742.

Heusser, C. 1974. 'Vegetation and climate of the Southern Chilean Lake District during and since the last Interglaciation', *Quaternary Research,* **4**, 290 - 315.

Heusser, C. 1989. 'Southern Westerlies during the Late Glacial Maximum', *Quaternary Research,* **31**, 423 - 425.

Hindmarsh, R. 1993. 'Modelling the dynamics of ice sheets', *Progress in Physical Geography,* **17**(4), 291 - 412.

Holmlund, P. & Fastook, J. 1995. 'A time dependent glaciological model of the Weichselian ice sheet', *Quaternary International,* **27**.

Holmlund, P. & Fastook, J. 1993. 'Numerical modelling provides evidence of a Baltic Ice Stream during the Younger Dryas', *Boreas,* **22**, 77 - 86.

Hooke, R.LeB., Calla, P., Holmund, P., Nilsson, M. and Stroeven, A. 1989. 'A 3 year record of seasonal variations in surface velocity, Storglaciaren, Sweden'. *J. Glaciol.*, **35**(120), 235-247.

Hooke, R.LeB., Pohjola, V.A., Jansson, P. and Kohler, J. 1992: 'Intra-seasonal changes in deformation profiles revealed by borehole studies, Storglaciaren, Sweden'. *J. Glaciol.*, **38**(130), 348-358.

Hubbard, A. 1996. 'Modelling Climate, Topography and Palaeo-Glacier Fluctuations in the Chilean Andes', *Earth Surface Processes and Landforms,* in press.

Hubbard, B., Sharp, M., Willis, I. C., Nielsen, M. K. and Smart, C. C. 1995. 'Borehole water-level variations and the structure of the subglacial hydrological system of Haut Glacier d'Arolla, Valais, Switzerland'. *J. Glaciol.,* **41**(139), 572-583.

Hughes, T. 1987. 'Ice dynamics and deglaciation models when ice sheets collapsed', in **W. Ruddiman & H. Wright** (Eds) *North America and Adjacent Oceans during the Last Deglaciation: The Geology of North America, K-3,* Geology Society of North America, Boulder, Colorado.

Hulton, N., Sugden, D., Payne A. and Clapperton, C. 1994. 'Glacier modelling and the Climate of Patagonia during the Last Glacial Maximum', *Quaternary Research,* **42,** 1 - 19.

Hutter, K. 1983. *Theoretical Glaciology: Material science of ice and the mechanics of glaciers and ice sheets,* D. Reidel Publishing Co., Dordrecht.

Huybrechts, P. 1986. *A three-dimensional time-dependent numerical model for Polar ice sheets: Some basic testing with a stable and efficient finite difference scheme, Report 86-1,* Geografisch Instituut, Universiteit Brussel.

Huybrechts, P. 1992. 'The Antarctic ice sheet and environmental change: a three-dimensional modelling study', *Reports on Polar Reseach,* **99,** 1-241.

Huybrechts, P., De Nooze, P. & Decleir, H. 1989, 'Numerical modelling of Glacier d'Argentiere and its historic front variations', in: **J. Oerlemans** (Ed) *Glacier Fluctuations and Climatic Change,* Kluwer Academic Publishers, Dordrecht,

Huybrechts, P. & Oerlemans, J. 1988. 'Evolution of the East Antarctic ice sheet: A numerical study of thermo-mechanical response patterns with changing climate', *Annals of Glaciology,* **11,** 52 - 59.

Jóhannesson, T., Raymond, C. & Waddington, E. 1989a. 'A simple method for determining the response time of glaciers', in **J. Oerlemans** (Ed) *Glacier Fluctuations and Climatic Change,* Kluwer Academic Publishers, Dordrecht, 343 - 352.

Jóhannesson, T., Raymond, C. & Waddington, E. 1989b. 'Time-Scale for adjustment of glaciers to changes in mass balance', *Journal of Glaciology,* 35(121), 355 - 369.

Kamb, B. and Echelmeyer, K. A. 1986. 'Stress-gradient coupling in glacier flow: IV. Effects of the "T" term'. *J. Glaciol.,* **32**(112), 342-349.

Keckler, D. 1995. *Surfer for Windows Operating Manual.* Golden Software Inc., Colorado.

Kerr, A. R. 1993. 'Topography, Climate and ice masses: A review', *Terra Nova,* **5,** 332 - 342.

Kerr, A. & Sugden, D. 1994. 'The sensitivity of the southern Chilean snowline to climatic change', *Climatic Change*, **28**, 255 - 272.

Lliboutry, L. 1971. 'The Glacier Theory', *Advances in Hydroscience*, **7,** 81 - 167.

Mahaffy, M. 1976. 'A numerical three dimensional ice flow model', *Journal of Geophysical Research,* **81,** 1059 - 1066.

Mercer, J. 1976. 'Glacial history of southernmost South America', *Quaternary Research*, **6**, 126 - 166.

Moreno, H. & Varela, J. 1985. 'Geologia, volcanismo y sedimentos piroclasticos cuaternarios de la region central y sur du Chile', in **J. Tosso** (Ed) *Suelos volcanicos de Chile*, Institutio de Investigaciones Agropecuarias-INIA, Santiago, Chile, 495 - 526.

Moreno, P. 1995. 'Vegetation and Climate near Lago Llanquihue in the Chilean Lake District between 20,200 and 9500 yrs BP', *Quaternary Research*, in press.

Morland, L. W. 1984. 'Thermo-mechanical balances of ice sheet flows', *Geophys. Astrophys. Fluid Dyn.,* **29,** 237 - 266.

Morland, L. W. & Shoemaker, E. M. 1982. 'Ice sheet balances', *Cold Reg. Sci. Technol.,* **5**(3), 235 - 251.

Muller, H.C. 1991. *Une méthode iterative simple pour résoudre les équations de mouvement d'un glacier.* (Mémoire de Diplôme en Mathematique, Université de Genève.)

Nienow, P. 1995. *Hydrological influences on basal flow dynamics in valley glaciers,* Interim report on NERC Research Fellowship GTS/93/AAPS/1, University of Edinburgh.

Nye, J. F. 1953. The flow law of ice from measurements in glacier tunnels, laboratory experiments and the Jungfraufirn borehole experiment. *Proc. R. Soc. London, Ser. A,* **219** (1139), 477 - 213.

Nye, J. F. 1957. 'The distribution of stress and velocity in glaciers and ice sheets', *Proc. R. Soc. London, Ser. A,* **239,** 113 - 133.

Nye, J. F. 1963. 'The response of a glacier to changes in the rate of nourishment and wastage', *Proc. R. Soc. London, Ser. A,* **275**(1360), 87 - 112.

Nye, J. F. 1960. 'The response of glaciers and ice sheets to seasonal and climate changes', *Proc. R. Soc. London, Ser. A,* **256**(1287), 559 - 584.

Nye, J. F. 1965. 'The frequency response of glaciers', *Journal of Glaciology*, **5**(41), 567 - 587.

Oerlemans, J. 1986. 'An attempt to simulate historic front variations of Nigardsbreen, Norway', *Theoretical & Applied Climatology,* **37**, 126 - 135.

Oerlemans, J. 1988. 'Simulatation of historic glacier variations with a simple climate-glacier model', *Journal of Glaciology,* **34**, 333 - 341.

Oerlemans, J. 1989. 'On the Response of Valley Glaciers to Climatic Change', in **J. Oerlemans** (Ed) *Glacier Fluctuations and Climatic Change,* Kluwer Academic Publishers, Dordrecht, 353 - 372.

Oerlemans, J. 1992. 'Climate sensitivity of glaciers in southern Norway: Application of an energy-balance model to Nigardsbreen, Hellstugubreen and Alforbreen', *Journal of Glaciology,* **38**, 223 - 232.

Oerlemans, J. 1993 'Evaluating the role of climate cooling in iceberg production and the Heinrich events', *Nature,* **364**, 783 - 785.

Paterson, W. S. B. 1994. *The Physics of Glaciers,* 3rd edition, Pergamon, Oxford.

Payne, A. 1995. 'Limit cycles in the basal thermal regime of ice sheets', *Journal of Geophysical Research.*

Payne, A. & Sugden, D. 1990. 'Topography and ice sheet growth', *Earth Surface Processes and Landforms*, **15**, 625 - 639.

Porter, S. 1981. 'Pleistocene glaciation in the southern Lake District of Chile', *Quaternary Research*, **16**, 263 - 639.

Press, W., Flannery, B., Teukolsky, S. & Vetterling, W. 1986. *Numerical Recipes.* Cambridge University Press, Cambridge.

Ramsay, J. G. 1967. *The folding and fracturing of rocks*, New York, McGraw-Hill.

Roberts, B. 1991. 'Modelling the Cordilleran ice sheet', *Géographie physique et Quaternaire,* **45**(3), 287 - 299.

Ruddiman, W. F. & McIntyre, A. 1981. 'The North Atlantic Ocean during the last deglaciation', *Palaeogeography, Palaeoclimatology and Palaeoecology,* **35,** 145 - 214.

Sharp, M. J., Richards, K. S., Willis, I. C., Nienow, P., Lawson W. and Tison J-L. 1993. 'Geometry, bed topography, and the drainage system structure of Haut Glacier d'Arolla, Switzerland', *Earth Surface Processes and Landforms,* **18**(6), 557 -571.

Sissons, J. 1979. 'The Loch Lomond Advance in the British Isles', *Nature,* **278,** 518 - 521.

Sissons, J. 1980. 'The Loch Lomond Stadial in the British Isles', *Nature,* **280,** 199-203.

Stroeven A. 1996. 'The robustness of one-dimensional time dependent ice-flow models: A case study from Storglaciaren, Sweden', *Geografisca Annaler,* in press.

Sugden, D. 1970. 'Landforms of deglaciation in the Cairngorms, Scotland', *Transactions of the I.B.G.,* **51,** 201 - 219.

Sutherland, D. 1984. 'The Quaternary deposits asnd landforms of Scotland and the neighbouring shelves: A review', *Quaternary Science Review, **3,*** 157 - 234.

Thorp, P. W. 1984. *Glacial geomorphology of part of the western Grampians with specific reference to the limits of the Loch Lomond Advance*, Ph.D. thesis, City of London Polytechnic.

Thorp, P. W. 1986. 'A mountain ice field of Loch Lomond Stadial age, western Grampians Scotland', *Boreas,* **15,** 83 - 97.

Thorp, P. W. 1991. 'The glaciation and glacial deposits of the western Grampians', in **J. Ehlers, P.L. Gibbard & J. Rose** (Eds) *Glacial depositis in Great Britain and Ireland,* Balkema, Rotterdam, 89-105.

van de Wal, R.S. & Oerlemans, J. 1995. 'Response of valley glaciers to climatic change and kinematic waves: A study with a numerical ice-flow model', *Journal of Glaciology,* **41**(137), 142 - 152.

van der Veen, C.J. 1987. 'Longitudinal Stresses and Basal Sliding: A Comparative Study', in **C. van der Veen & J. Oerlemans** (Eds) *Dynamics of The West Antarctic Ice Sheet.* Kluwer, Dordrecht, 223 - 248.

van der Veen, C. J. & Whillans, I. M. 1990. 'Flow laws for glacier ice: Comparisons of numerical predictions and field measurements', *Journal of Glaciology,* **36,** 324 - 339.

Vaughan, D. 1993. 'Relating the occurrence of crevasses to surface strain rates', *Journal of Glaciology,* **39**(132), 255-266.

Willis, I.C. 1995: Intra-annual variations in glacier motion: a review. *Progress in Physical Geography* **19**(1), 61-106.

Willis, I., Arnold, N., Sharp, M., Bonvin, J.-L. & Hubbard, B. 1996. 'Mass Balance and Flow Variations of Haut Glacier d'Arolla, Switzerland calculated using Digital Terrain Modelling Techniques', In **S.N Lane, J.H. Chandler and K.S. Richards,** (Eds) *Landform Modelling, Monitoring and Analysis.* Wiley

APPENDIX A

DERIVATION OF THE PLANE-STRAIN SCHEME FOR THE CALCULATION OF LONGITUDINAL DEVIATORIC STRESSES

Adapted from van der Veen (1987), equation numbers refer directly to the original text.

For quasi two-dimensional plane flow along a flowline with the x-axis horizontal in the direction of ice flow and the z-axis vertically upwards the constitutive relation for ice flow may be written:

$$\frac{\partial u}{\partial x} = A\left[\tau'^{2}_{xx} + \tau^{2}_{xz}\right]\tau'_{xx}, \qquad (6)$$

$$\frac{\partial u}{\partial z} = 2A\left[\tau'^{2}_{xx} + \tau^{2}_{xz}\right].\tau_{xz}, \qquad (7)$$

where **u** is the horizontal velocity (positive in the x-direction), τ_{xz} the basal shear stress and τ'_{xx} the longitudinal deviatoric stress. The shear stress, based on the driving stress and correction term is given by:

$$\tau_{xz}(z') = -\rho g(h-z')\frac{\partial h}{\partial x} + 2\frac{\partial}{\partial x}\int_{z'}^{h}\tau'_{xx}\,dz. \qquad (8)$$

where **h** is the ice surface, **z'** is elevation and ρ is the density of ice and **g** is gravity. Replacing τ'_{xx} with its vertical mean $\overline{\tau'_{xx}}$ and substituting the equation for driving stress: $\frac{\tau_d}{H} = -\rho g\frac{\partial h}{\partial x}$ yields:

$$\tau_{xz} = \frac{(h-z)}{H}\tau_d + 2\frac{\partial}{\partial x}\int_{z'}^{h}\overline{\tau'_{xx}}\,dz;$$

$$\tau_{xz} = \frac{(h-z)}{H}\tau_d + 2\frac{\partial}{\partial x}\left[\overline{\tau'}_{xx}\,z\right]_{z}^{h}$$

$$\tau_{xz} = \frac{(h-z)}{H}\tau_d + 2\frac{\partial}{\partial x}\left[\overline{\tau'}_{xx}\,(h-z)\right] \qquad (9)$$

substituting $\tau_1 = \tau_d + D$,

where:

$$D = 2H\frac{\partial}{\partial x}\left(\overline{\tau'_{xx}}\right) \qquad (11)$$

equation 9 becomes:

$$\tau_{xz} = \frac{h-z}{H}\tau_1 + 2\overline{\tau'}_{xx}\frac{\partial}{\partial x}(h-z). \qquad (10)$$

Inserting this equation for shear stress into equation (7) yields:

$$\frac{\partial u}{\partial z} = 2A\left[\begin{array}{l}\tau_1\overline{\tau'}_{xx}^{\,2}\dfrac{h-z}{H} + 2\overline{\tau'}_{xx}^{\,3}\dfrac{\partial(h-z)}{\partial x} + \\ \tau_1^{\,3}\left(\dfrac{h-z}{H}\right)^3 + 8\overline{\tau'}_{xx}^{\,3}\left(\dfrac{\partial(h-z)}{\partial x}\right)^3 + \\ 6\overline{\tau'}_{xx}\tau_1^{\,2}\left(\dfrac{h-z}{H}\right)^2\dfrac{\partial(h-z)}{\partial x} + \\ 12\tau_1\overline{\tau'}_{xx}^{\,2}\dfrac{h-z}{H}\left(\dfrac{\partial(h-z)}{\partial x}\right)^2\end{array}\right] \qquad (12)$$

By analogy to deleting terms of order $O(\varepsilon^2)$ in Blatter's (1995) first order approximation, van der Veen (1987) eliminates a number of terms from the above equation. He argues that since the glacier surface slope is typically << 1, then the following inequalities hold:

$$8\overline{\tau'}_{xx}^{\,3}\left(\frac{\partial(h-z)}{\partial x}\right) << 2\overline{\tau'}_{xx}^{\,3}\frac{\partial(h-z)}{\partial x},$$

and

$$12\tau_1\overline{\tau'}_{xx}^{\,2}\frac{h-z}{H}\left(\frac{\partial(h-z)}{\partial x}\right)^2 << \tau_1\overline{\tau'}_{xx}^{\,2}\frac{h-z}{H}.$$

In this way the terms on the left-hand side may be neglected from equation (12). Using Leibnitz' rule van der Veen proceeds to integrate of the various terms in the reduced equation (12) from the base to some height z':

$$\int_{h-H}^{z'} \frac{\partial(h-z)}{\partial x}dz = \frac{\partial}{\partial x}\left[\int_{h-H}^{z'}(h-z)dz\right] -$$

$$(h-z')\frac{\partial z'}{\partial x} + H\frac{\partial(h-H)}{\partial x}$$

$$= H\frac{\partial h}{\partial x} - (h-z')\frac{dh}{dx},$$

and

$$\int_{h-H}^{z'}(h-z)^2\frac{\partial(h-z)}{\partial x}dz = \frac{1}{3}\int_{h-H}^{z'}\frac{\partial(h-z)^3}{\partial x}dz$$

$$= \frac{1}{3}\frac{\partial}{\partial x}\int_{h-H}^{z'}(h-z)^3dz - \frac{1}{3}(h-z')^3\frac{\partial z'}{\partial x} + \frac{1}{3}H^3\frac{\partial(h-H)}{\partial x}$$

$$= \frac{1}{3}H^3\frac{\partial h}{\partial x} - \frac{1}{3}(h-z')^3\frac{\partial h}{\partial x}.$$

Yielding from equation (12) an expression for the horizontal velocity u(z'):

$$u(z') = A\tau_1\overline{\tau}_{xx}'^2\left[H - \frac{(h-z')^2}{H}\right] +$$

$$4A\tau_1^2\overline{\tau}_{xx}'\left[H - \frac{(h-z')^3}{H^2}\right]\frac{\partial h}{\partial x} +$$

$$\frac{1}{2}A\tau_1^3\left[H - \frac{(h-z')^4}{H^3}\right] + \qquad (13)$$

$$4A\overline{\tau}_{xx}'^3[H-(h-z')]\frac{\partial h}{\partial x} + U_s$$

where U_s is the basal sliding boundary condition.

Integrating equation (13) from the bed to the surface, yields the following expression for the ice flux:

$$u_h = AH\tau_1\overline{\tau}_{xx}'^2 + 4AH\tau_1^2\overline{\tau}_{xx}'\frac{\partial h}{\partial x} +$$

$$+\frac{1}{2}AH\tau_1^3 + 4AH\overline{\tau}_{xx}'^3\frac{\partial h}{\partial x} + U_s$$

Integrating equation (13) again, from the bed to the surface, the following expression for the ice flux is obtained:

$$HU = \frac{2}{3}AH^2\tau_1\overline{\tau}_{xx}'^2 + 3AH^2\tau_1^2\overline{\tau}_{xx}'\frac{\partial h}{\partial x} +$$

$$\frac{2}{5}AH^2\tau_1^3 + 2AH^2\overline{\tau}_{xx}'^3\frac{\partial h}{\partial x} + HU_s \qquad (15)$$

The first term on the right-hand side can be identified with the ice flux due to internal deformation, Hu_d. Writing the deformational velocity as:

$$U_d = AH\tau^2\tau_d, \qquad (2)$$

it follows from (15) and (11) that the effective stress τ is given by

$$\tau^2 = \frac{2}{5}\tau_d^2 + (3\overline{\tau}_{xx}'\frac{\partial h}{\partial x} + \frac{6}{5}D)\tau_d +$$

$$\left(\frac{2}{3}\overline{\tau}_{xx}'^2 + 6D\overline{\tau}_{xx}'\frac{\partial h}{\partial x} + \frac{6}{5}D^2\right) + \qquad (16)$$

$$\left(\frac{2}{3}D\overline{\tau}_{xx}^2 + 3D^2\overline{\tau}_{xx}'\frac{\partial h}{\partial x} + \frac{2}{5}D^3 + 2\overline{\tau}_{xx}'\frac{\partial h}{\partial x}\right)/\tau_d$$

Since we still have not arrived at an equation for $\overline{\tau}_{xx}'$, we continue our journey through this algebraic jungle a little further. Differentiating (15) with respect to x yields